TRAUMATIC BRAIN INJURY BIOMARKER DISCOVERY USING MASS SPECTROMETRY IMAGING OF 3D NEURAL CULTURES

A Thesis
Presented to
The Academic Faculty

by

Daniel Olivero

In Partial Fulfillment
of the Requirements for the Degree
Master of Science in the
School of Mechanical Engineering

Georgia Institute of Technology
August 2011

TRAUMATIC BRAIN INJURY BIOMARKER DISCOVERY USING MASS SPECTROMETRY IMAGING OF 3D NEURAL CULTURES

Dr. Peter Kottke, Co-Advisor
George W. Woodruff School of Mechanical Engineering
Georgia Institute of Technology

Dr. Michelle LaPlaca, Co-Advisor
Wallace H. Coulter Department of Biomedical Engineering
Georgia Institute of Technology

Dr. Andrei Fedorov
George W. Woodruff School of Mechanical Engineering
Georgia Institute of Technology

Dr. Peter Hesketh
George W. Woodruff School of Mechanical Engineering
Georgia Institute of Technology

Date Approved: May 5, 2011

To my parent Luis and Patricia Olivero

ACKNOWLEDGEMENTS

I would like to thank everyone that has helped me complete this thesis and has been there for me over the past two years. I would like to thank foremost, both of my advisors, Dr. Michelle LaPlaca and Dr. Peter Kottke. The both of you have been invaluable throughout this entire process and without your advice, constant motivation and endless support I would not be where I am today. I am grateful for the knowledge and skills you have provided me. The both of you have helped to make me a better engineer.

I would also like to thank my parents, Luis and Patricia Olivero, for all of the support they have given me. They have always pushed me to challenge myself and told me to never give up even when things get tough. The both of them have always believed in me and always told me to follow my dreams.

Special thanks to my fiancée Michelle, who has always been there to push me to do a good job with my work. She has always there to calm me down and bring me back to reality whenever I was super stressed.

My fellow graduate students, JT Shoemaker, Brock Wester, and Brian Rooney have always been there to answer random questions and have also been a great distraction whenever I needed a break from work. Special thanks to JT who was indispensible when it came to helping me with the in-vitro experiments. Without JT I would have never been able to get such great cell culture results and images. In addition I would like to thank Jelena Vukasinovic for all of the great brainstorming sessions for the cell culture chambers. Finally, I would also like to Dr. Fedorov and Dr. Hesketh for serving on my thesis committee.

TABLE OF CONTENTS

	Page
ACKNOWLEDGEMENTS	iv
LIST OF TABLES	viii
LIST OF FIGURES	ix
LIST OF SYMBOLS	xiii
LIST OF ABBREVEIATIONS	xvi
SUMMARY	viii
CHAPTER	
1 INTRODUCTION	1
1.1. Purpose and Motivation	1
1.2. Background	2
1.2.1. Traumatic Brain Injury and Biomarkers	2
1.2.2. Mass Spectrometry	6
1.2.3. Electrospray Ionization and nano-Electrospray Ionization	7
1.2.4. Time of Flight Mass Spectrometry	10
1.2.5. Cell Cultures and In-Vitro Modeling of TBI	14
1.2.6. Sampling – Typical Methods and State-of-the Art	15
1.3. Conclusions	17
2 MICRODIALYSIS-NANO-ESI MS	19
2.1. Microdialysis	19
2.1.1. Microdialysis Assembly	19
2.1.2. Microdialysis Theoretical Analysis	20
2.1.3. Microdialysis Theoretical Model Results	26

2.2. Microdialysis Testing 27

2.2.1. Microdialysis Experimental Assembly 27

2.2.2. Microdialysis Experimental Results 27

2.3. MD nano-ESI Experiments 31

2.3.1. MD Bruker ESI Analyte Retention Experiments 32

2.3.2. Microdialysis Experimental Results 35

2.3.3. Microdialysis Experimental Results 36

2.4. Discussion 42

3 SAMPLING PROBE AND 3-D CELL CULTURE MODEL OF LOCALIZED INJURY 43

3.1. Local Marker Release Injury Model 43

3.2. Local Marker Release Model Theory 45

3.2.1. Theoretical Model 46

3.2.2. Model Results 49

3.3. Injury Model and Probe Experiments 52

3.3.1. Dye Injection Study 53

3.3.2. Experimental Assembly 57

3.3.3. Experimental Assembly 57

3.4. Matrigel Experimental Results 61

3.5. In-Vitro Probe Placement and Sampling 63

3.5.1. Cell Culture Local Injection Experimental Results 67

3.6. Discussions 68

4 CONCLUSIONS AND RECOMMENDATIONS 70

4.1. Conclusions 70

4.2. Recommendations for Future Work 75

APPENDIX A: CYLINDRICAL MODEL INJURY CHAMBER ASSEMBLY PROTOCOL 78

APPENDIX B: PLANAR MODEL INJURY CHAMBER ASSEMBLY PROTOCOL 83

REFERENCES 87

LIST OF TABLES

	Page
Table 3.1.: Modelinjury conditions and dimensions	50
Table 4.1.: Final design parameters for MD-nano-ESI MS	71
Table 4.2.: Final experimental MS settings	72

LIST OF FIGURES

Page

Figure 1.1.: Cell death mediated by complex cascades post TBI 5

Figure 1.2.: Dynamic events post TBI 5

Figure 1.3: Conceptual Illustration of generic MS analysis 6

Figure 1.4.: Pictorial description of ESI 7

Figure 1.5.: Pictorial description of a Coulombic explosion 8

Figure 1.6.: Pictorial description of the Charge Residue Model 9

Figure 1.7.: Pictorial description of the Ion Evaporation Model 9

Figure 1.8.: Linear TOF schematic 11

Figure 1.9.: Schematic of a reflectron 13

Figure 1.10.: Illustration of an orthogonal acceleration TOF 14

Figure 1.11.: Diagram of protein identification methods 16

Figure 2.1.: Schematic of MD unit 20

Figure 2.2.: Illustration of the mass transfer of species *s* from Media A to Media B through a membrane 22

Figure 2.3.: Cross section of the MD unit 24

Figure 2.4.: Theoretical MD performance with respect to ζ at various values of $\frac{\dot{Q}_{media}}{A_s \bar{h}_m}$ 26

Figure 2.5.: Experimental MD performance with respect to a varying buffer flow rate 28

Figure 2.6.: Experimental MD performance with respect to a varying sample flow rate for a length of 1cm 29

Figure 2.7.: Experimental MD performance with respect to a varying sample flow rate for a length of 3cm 29

Figure 2.8.: Experimental MD performance with respect to a varying MD unit length 30

Figure 2.9.: Spectrum of 20 µM Cyt-C in a 10% methanol, 1% acetic acid buffer using the bruker ion source with no MD 33

Figure 2.10.: Spectrum of 20 μM Cyt-C in a 10% methanol, 1% acetic acid buffer using the bruker ion source with off-line MD. 33

Figure 2.11.: Comparison between the pre-MD and post-MD MS analysis 34

Figure 2.12.: Schematic of in-line MD-nano-ESI 35

Figure 2.13.: MD nano-ESI 20 μM Cyt-C in a 10% methanol 1% acetic acid solution with no added salt 36

Figure 2.14.: A sample of 20 μM Cyt-C in a 500 mM NaCl solutions was flowed through the in-line MD nano-ESI device without any dialysis buffer flowing 37

Figure 2.15.: A sample of 20 μM Cyt-C in a 250 mM NaCl solution with in-line MD 37

Figure 2.16.: Schematic of nano-ESI with a perpendicular low pressure nebulizer gas cross flow of nitrogen 38

Figure 2.17.: Experiment with intermittent low pressure nebulizer gas cross flow application 39

Figure 2.18.: 20 μM Cyt-C in a 250 mM NaCl solution with a MD unite length of 2.4cm and the use of a nebulizer cross flow 39

Figure 2.19.: 20 μM Cyt-C in a neuronal cell culture media solution with no MD 40

Figure 2.20.: 20 μM Cyt-C in a neuronal cell culture media solution with a MD unit length of 2.4 cm and the use of a nebulizer cross flow 40

Figure 2.21.: Typical performance of a MD-nano-ESI device 42

Figure 3.1.: Model cell culture chamber constructed out of an extruded polycarbonate cylinder with NanoPorts and silica capillaries affixed to it 44

Figure 3.2.: Schematic of the model cell culture connected in-line with the MD-nano-ESI device 45

Figure 3.3.: Schematic demonstrating the coordinate system for the model cell culture 49

Figure 3.4.: C/C_f with respect to axial position in a chamber filled with 0.6% agarose porous matrix at various time points 51

Figure 3.5.: C/C_f with respect to time for a 8 μL injection of Cyt-t into 0.6% agarose porous matrix at a fixed distance of 1.4mm downstream of the injection point 52

Figure 3.6.: Schematic of the planar chamber 53

Figure 3.7.: Dye injection experiments 54

Figure 3.8.: Image of an air bubble released before dye exited the injection capillary 55

Figure 3.9.: Image of dye at 8.5 minutes after initial introduction 56

Figure 3.10.: Schematic of model injury chamber with the sampling probe offset by 1.4mm downstream of the injection capillary 58

Figure 3.11.: MS chromatograms and spectra from continuous in-line analysis with MD-nano-ESI of 8 μL injections of 30 μM Cyt-C 59

Figure 3.12.: MS chromatograms and spectra from continuous in-line analysis with MD-nano-ESI of 8 μL injections of 5 μM Cyt-C 60

Figure 3.13.: MS chromatogram and spectra from continuous in-line analysis with MD-nano-ESI of 8 μL injection of 30 μM Cyt-C in a Matrigel filled chamber 62

Figure 3.14.: Four day old mixed neural cultures in Matrigel plated in a model cell culture with no probe or perfusion 64

Figure 3.15.: Four day old mixed neural cultures in Matrigel plated in a model cell culture with probe and no perfusion 65

Figure 3.16.: Four day old mixed neural cultures in Matrigel were perfused with fresh NeruoBasal media for 15 minutes and liquid was allowed to flow through the sampling probe 66

Figure 3.17.: MS chromatogram and spectra from continuous in-line analysis with MD-nano-ESI of 8 μL injection of 30 μM Cyt-C in a chamber filled with mixed neural 3-D cell cultures 67

Figure A.1.: Aligned and offset hole configuration 78

Figure A.2.: NanoPort attached to the top of a cylinder using Quick Set 79

Figure A.3.: Cylinder with two NanoPorts attached to the top and bottom of the cylinder 79

Figure A.4.: Small dab of Quick Set at the tip of a silica capillary 80

Figure A.5.: Inserted silica capillary affixed with Quick Set 81

Figure A.6.: Assembly with both capillaries affixed with Quick Set. 81

Figure B.1.: Dimensions for the bottom of the chamber 83

Figure B.2.: Dimensions for the top of the chamber 83

Figure B.3.: Highlighted surface of the bottom part to apply thin layer of SYLGARD 186 84

Figure B.4.: Top and bottom assembly with all four sides aligned and pressed together 84

Figure B.5.: Nanoport affixed to the top of the chamber with Quick Set 85

Figure B.6.: Assembly with silica capillaries inserted into the sides 86

Figure B.7.: Inserted silica capillary affixed with Quick Set into the bottom hole 87

LIST OF SYMBOLS

m/z	Mass to charge ratio
$\boldsymbol{F}$	Force
m	Mass
$\boldsymbol{a}$	Acceleration
Q	Ion charge
$\boldsymbol{E}$	Electric field
$\boldsymbol{v}$	velocity
$\boldsymbol{B}$	Magnetic Field
z	Number of elementary charges
e	Elementary charge
$E_{electric}$	Electric Potential
U_{accel}	Accelerating potential
KE	Kinetic Energy
t_{flight}	Time of flight
s	Drift region length
Re	Reynolds Number
u_m	Mean fluid velocity
φ_h	Hydraulic Diameter
v	Kinematic viscosity
$x_{fd,h}$	Hydrodynamic entry length
L	MD unit length
n_s''	Mass flux across a membrane
h_m	Mass transfer coefficient

$C_{s,A}$	Concentration of species s in media A
$C_{s,B}$	Concentration of species s in media B
n_s	Total rate of species transfer
A_s	Surface Area
d	Membrane diameter
$\Delta C_{s,lm}$	Log mean concentration difference
$\dot{Q}$	Volume Flow rate
$\bar{h}_m$	Overall mass transfer coefficient
h_i	Interior average mass transfer coefficient
h_o	Outer average mass transfer coefficient
R_m	Resistance to mass transfer from membrane
Sh_i	Interior Sherwood Number
Sh_o	Outer Sherwood Number
$\varphi_{o,fiber}$	Fiber outer diameter
$\varphi_{i,Teflon}$	Teflon tube inner diameter
φ_{insert}	Capillary insert outer diameter
$\varphi_{i,fiber}$	Fiber inner diameter
$\overline{Sh}_D$	Overall Sherwood number
D_s	Diffusion coefficient of species *s*
α_m	Available volume fraction to analytes
ζ	Ratio of media volume flow rate to buffer volume flow rate
t_{media}	Media contact time with the fiber
t_{buffer}	Dialysis buffer contact time with the fiber
τ	Ratio of t_{media} to t_{buffer}
$\boldsymbol{j}$	Mass flux

D	Diffusion Coefficient
C	Mass concentration
r	Spherical radial coordinate
t	Time
s	Source Density
α	Porosity (Volume Fraction)
V	Entire volume
V_o	Void volume
D^*	Diffusion coefficient in a porous matrix
λ	Tortuosity
$\boldsymbol{v}^*$	Velocity in a porous matrix
b	Radius of liquid sphere within the void space
U	Volume
u	Velocity
η	Coordinate system transformation
z	Cylindrical axial coordinate
ρ	Radial axial coordinate
C_f	Initial concentration
Pe	Péclet Number
L_s	Characteristic Length
Sc	Schmidt Number
u_e	Equivalent velocity
A	Cross sectional area

LIST OF ABBREVIATIONS

TBI	Traumatic Brain Injury
MD	Microdialysis
nano-ESI	Nano-Electrospray Ionization
MS	Mass Spectrometry
CNS	Central nervous system
GCS	Glascow Coma Scale
CT	Computed tomography
MRI	Magnetic resonance imaging
ICP	Intracranial pressure
CPP	Cerebral Perfusion pressure
NSE	Neuron Specific Enolase
GFAP	Glial fibrillary acidic protein
ESI	Electrospray ionization
TOF	Time of flight
ECM	Extracellular Matrix
LC	Liquid Chromatography
SDS	Sodium Dodecyl Sulfate
2D-PAGE	Two dimensional polyarcylamide gel electrophoresis
MSMS	Tandem mass spectrometry
SPE	Solid Phase Extraction
ID	Inner diameter
OD	Outer diameter
DI	Deionized

Cyt-C	Cytochrome-C
TIC	Total ion chromatogram
ECS	Extracellular space
Q-TOF	Quadrapole time of flight

SUMMARY

Biomarker research is of great interest in the field of traumatic brain injury (TBI), since there are numerous potential markers that may indicate central nervous system damage, yet the brain is normally well isolated and discovery is at its infancy. Traditional methods for biomarker discovery include time consuming multi step chromatographic mass spectrometery (MS) techniques or pre-defined serial probing using traditional assays, making the identification of biomarker panels limiting and expensive. In addition to the difficulty in identifying new biomarkers, clinical and animal studies contribute to added complexity. These shortfalls have motivated the development of a MS based probe that can be embedded into 3D neural cultures and obtain temporal and spatial information about the release of biomarkers.

This thesis presents the development and testing of a novel method to monitor chemical markers within a porous matrix. Using the high sensitivity MS ionization method of nano-electrospray ionization (nano-ESI) with an in-line microdialysis (MD) unit allows us to use MS to analyze low concentrations of TBI biomarkers from within cell cultures with no need for off-line sample manipulation.

The MD unit was examined both theoretically and experimentally, and a set of design variables were chosen to allow for continuous sampling and MS analysis directly from cell cultures. A model cell culture injury chamber was developed and also examined theoretically and experimentally. The chambers were constructed and filled with a porous matrix, and biologically relevant markers were locally injected into the chamber. The probe collected samples from within the matrix, which were analyzed in-line with the MD-nano-ESI MS probe. A model predicting the transport of the chemical markers within a porous matrix provided a basic understanding of what to expect experimentally. Experiments demonstrated the probe's capability to detect chemical markers within a

simple agarose matrix and a biologically complex matrix of Matrigel. In addition, cells experienced no adverse effects when cultured in chambers with the sampling probe. Samples were successfully collected through the probe in live neural cultures. Results demonstrated that this novel method of detecting biological samples using MS could potentially allow researchers to better understand the pathophysiological events of TBI.

CHAPTER 1

INTRODUCTION

The aim of this project is to develop and characterize a novel method for biomarker discovery. Although the specific motivation for this project is traumatic brain injury (TBI) biomarker discovery, the method lends itself to other areas of research. This novel method consists of a micro sampling probe, which is imbedded in neuronal cell cultures and is coupled to an in-line microdialysis (MD) nano-electrospray ionization (nano-ESI) source for mass spectrometry (MS) analysis. This system has the capability of detecting and identifying molecules released from cells within cell cultures with high temporal and spatial resolution. General theoretical principles, simulative models and experimental characterization all contributed to the development and characterization of the probe.

1.1. Purpose and Motivation

The study of biomarkers is of great interest to the TBI research community since the central nervous system (CNS) does not have a wide variety of well characterized markers available for analysis [1]. The generally accepted definition of a biomarker is that the marker can be objectively measured and evaluated as an indicator of normal biological processes, pathogenic processes, or pharmacological responses for therapeutic intervention [2]. Existing methods for TBI biomarker discovery include chromatographic MS techniques and the use of targeted assay kits. These methods offer limited temporal and spatial information with respect to complex chemical cascades that occur during or post injury. The desire to increase the capability of discovering TBI biomarkers and accessing detailed spatial and temporal information was a major motivation to develop a novel MS based sampling probe. The probe is based on in-line MD coupled with nano-

ESI MS, which has the capability of analyzing low concentrations of biomarkers in a quick and efficient manner without losing important temporal and spatial information.

1.2. Background

1.2.1. Traumatic Brain Injury and Biomarkers

TBI is a serious public health problem in the United States and is referred to as the "silent epidemic" due to its resulting complications. On average, approximately 1.7 million people sustain TBI annually and it is estimated that TBI contributes to 52,000 deaths and 270,000 hospitalized patients. It is estimated that TBI's direct medical costs and indirect costs, such as lost productivity, totaled $60 billion in the US in 2000 [3].

TBI is caused by an impact, blow or jolt to the head or a penetrating head injury that causes a disruption in the normal function of the brain. There are different ranges of TBI which include "mild" to "severe" injury which range from a brief change in mental status or consciousness to extended period of unconsciousness or amnesia after injury, respectively [3].

Methods for predicting the outcome in severe TBI patients have hardly changed over the last twenty years, and current diagnostic tools provide insufficient information for measuring the extent and severity of TBI [4]. TBI diagnosis can be attempted with a variety of approaches. These include use of the Glasgow Coma Scale (GCS), computed tomography (CT), magnetic resonance imaging (MRI), and neurointensive monitoring. The GCS is a neurological scale that provides an objective way of recording the conscious state of a person for initial and subsequent assessments post TBI. It has been shown that determining initial GCS in a repeatable and reproducible manner is difficult especially with the application of aggressive prehospital treatments of early sedation and intubation for some patients [5]. Cranial CT scan images can provide information regarding the extent and the prospective outcome of some injuries. The relatively low

sensitivity and poor specificity of CT scans limit its diagnostic capability for diffuse TBI [6]. MRI of the brain can provide information on the extent of diffuse injury with high sensitivity even when patients are fully sedated or intubated [7]. MRI is not ideal for routine emergency of TBI since it is not available in all hospitals and it is time consuming [8]. Neurointensive monitoring is used to obtain intracranial pressure (ICP), mean arterial blood pressure, and cerebral perfusion pressure (CPP). Out of these measurements ICP can best indicate the severity of primary injury. These parameters primarily reflect secondary injuries, and are only useful for the prognosis of extremely abnormal results, since not all TBI patients will have a probe inserted into the brain [9]. Due to the complexity of the brain and the multifaceted nature of TBI, there can be a disproportionate relation between traditional measures of TBI and the biochemical changes in the brain.

There are no biomarkers that have proven clinical utility for the diagnosis of brain injury [1]. This lack of markers is especially disadvantageous for specialists who treat head injuries. In many cases neurological deficits are not prominent, and biomarkers would advance the establishment of a proper diagnosis by providing valuable information regardless of whether or not there was detectable tissue damage. This would allow a physician to determine a specific treatment for the patient's unique trauma. There have been several markers which have shown clinical potential. Below is a summary of the generally accepted potential biomarkers.

S-100β is a calcium-binding protein with a molecular weight of 21 kDa with three known subtypes. It is secreted by glial cells and structural damage of these cells causes leakage of S-100β into the extracellular compartment and into the CSF [10]. Various studies have shown relationships between S-100β levels to both injury magnitude and patient outcome, S-100β has also been found in melanocytes, adipocytes, and chondrocytes [11, 12]. This limits S-100β's specificity to the brain and could provide incorrect clinical diagnosis.

Neuron Specific Enolase (NSE) is a glycolytic enzyme with a molecular weight of 78 kDa. Its γ-γ isoform is specific for neurons and the α-γ isoform is specific for neuroendocrine cells [13]. It is released into the extracellular space only during cell destruction and high levels can be found in the CSF [6]. NSE was thought to be strictly neuronal, but further research found NSE to also be present in red blood cells and platelets, which limits NSE value as a marker for TBI [14]. Clinical studies have demonstrated that NSE concentration in serum and/or CSF may be useful as a screening test for TBI outcome [15, 16].

Glial fibrillary acidic protein (GFAP) is a 52kDa intermediate filament protein found in astroglial cytoskeleton, and is not found outside of the CNS [17, 18]. In recent studies the determination of GFAP levels allowed researchers distinguish between severe disability and vegetative state versus good and moderate outcomes as evaluated by Glasgow Outcome Scale (GOS), and it has been show to predict mortality, although it has not been studied in mild and moderate injuries. GFAP has the potential to be a better marker candidate than S-100β, but this is dependent on the time point after trauma and the pattern of TBI [19].

The role of neuro-inflammatory cytokines in various CNS injuries has been shown in previous studies [20]. Cytokines are small cell signaling proteins that are secreted by glial cells that are found in the nervous system [21]. Various cytokines (IL-1β, TNF-α, IL-6, IL-8, and IL-10) levels were measured and compared to concentrations of S-100β within the CSF. Results were correlated to ICP and prognosis, and it was concluded that IL-1β could be useful as outcome predictors in cases of severe TBI [22].

Although there are many potential TBI biomarker candidates, a panel of useful markers has not been identified. Some marker candidates have been able to provide a general relationship between concentration levels and patient outcome, but none of the markers have been able to provide specific information regarding some of the complex processes which occur post TBI. The pathophysiological processes in TBI are very

complex and brain damage and death occur from both primary and secondary mechanisms. Figure 1.1 and Figure 1.2 outline the dynamic events post TBI.

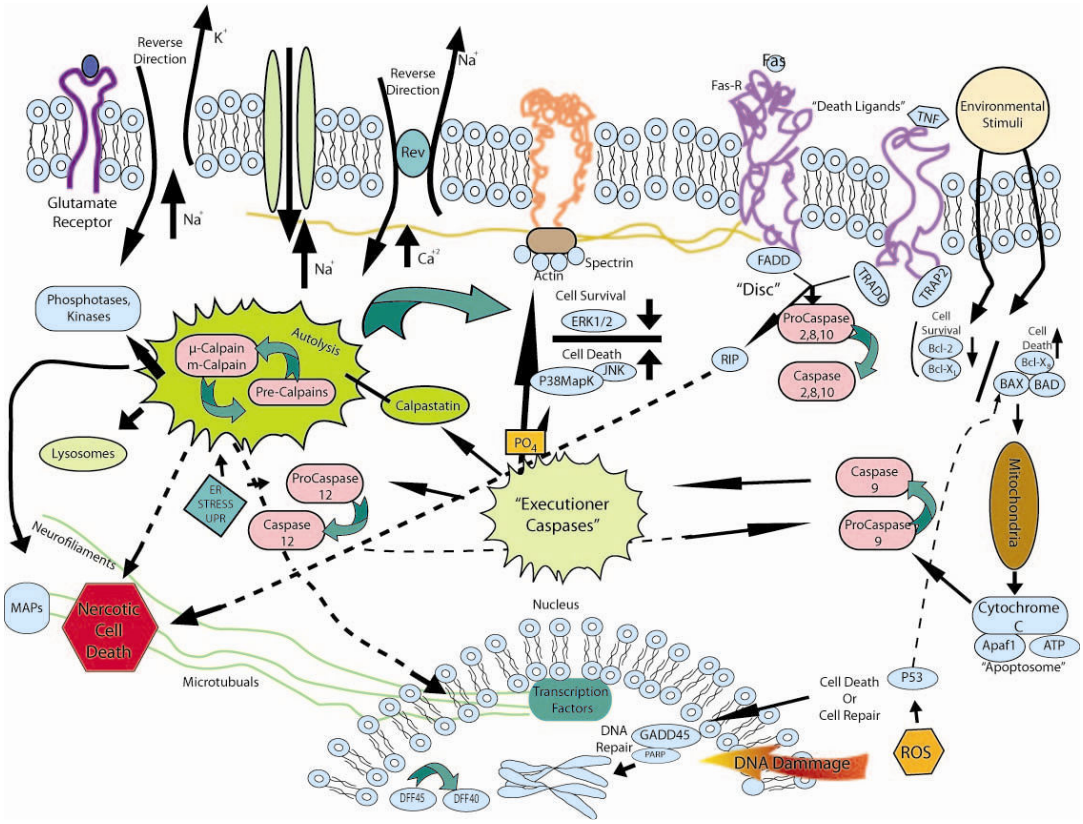

Figure 1.1. Cell death mediated by complex cascades post TBI [23].

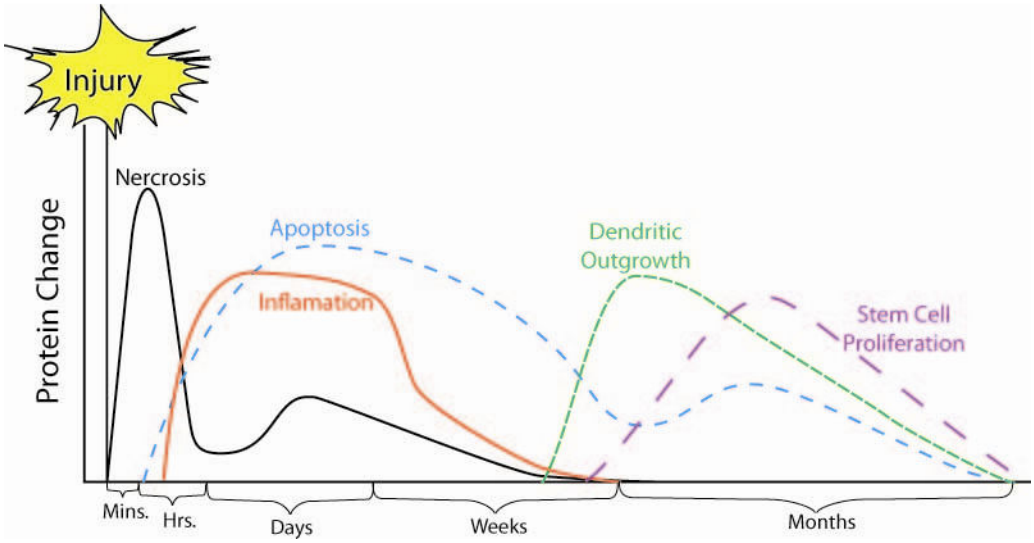

Figure 1.2. Dynamic events post TBI [23].

Treatment of patients would greatly improve if the pathophysiological events of TBI were better understood. Despite this limitation, there exists a need to improve methods for the detection of suspect TBI biomarkers in parallel with novel biomarker discovery and elucidation of the biochemical events post injury. A tool that could determine the time points of various secondary injury cascades and study the spatial effects of both acute and diffuse injuries would greatly benefit the TBI research community.

1.2.2. Mass Spectrometry

Significant advances in biomarker discoveries have been achieved with the help of the powerful analytical technique of MS. MS is an analytical technique that can be used to detect, identify and quantify analytes. MS works on the principle of manipulating ions, which are charged molecules, by using electric and magnetic fields, so that individual ions can be grouped according to their unique properties and moved from one point to another. Ions must be free from any other forms of matter to be analyzed, and therefore they are analyzed in a vacuum. This requires ions to be in the gas phase, so the MS can separate and detect them according to their mass-to-charge ratio (m/z). The mass component is the atomic weight of the analyte, and it is divided by the number of charges the ion possesses. Only ions are detected in MS and the m/z values are presented as a bar-graph spectrum (Figure 1.3) [24].

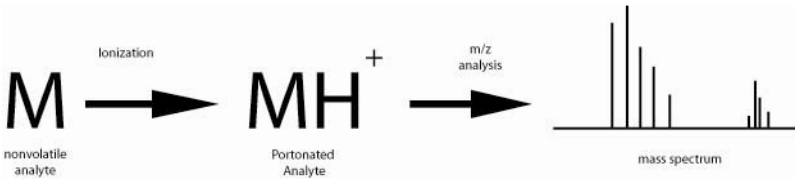

Figure 1.3. Conceptual illustration of generic MS analysis

1.2.3. Electrospray Ionization and nano-Electrospray Ionization

As previously discussed, for MS to function the analytes must be ionized. A popular and powerful method of ionizing nonvolatile molecules is electrospray ionization (ESI). This ionization method is especially useful for analyzing intact proteins. ESI is the process where an intense electric field disperses a sample liquid into a fine spray of highly charged droplets. These droplets evaporate and produce gas phase ions which are then analyzed by the MS. ESI is typically accomplished by flowing liquid through a small tube (needle), which is maintained at a significant electrostatic potential relative to an opposing counter-electrode. This potential difference between the needle and the counter-electrode creates a large external electric field which disperses the liquid as a fine spray of charged droplets as Figure 1.4 demonstrates [25].

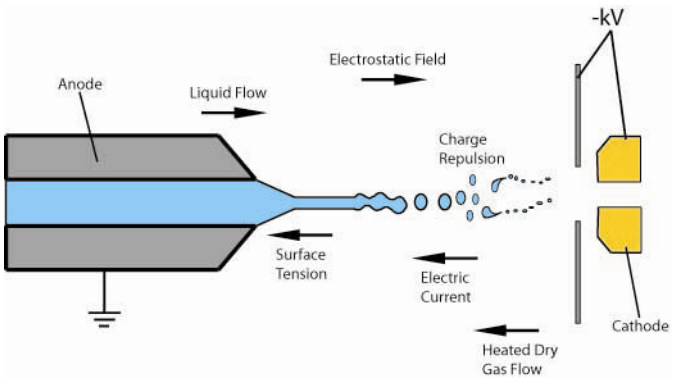

Figure 1.4. Pictorial description of ESI

Due to the electric field at the tip of the needle, the emerging liquid forms a 'Taylor Cone' [26]. For a metallic needle (the anode) which is in positive ion mode, anions near the surface of the cone liquid are driven toward the needle rim by the electrical field where they undergo an electro-chemical interaction with the needle surface. These anions deposit their excess charge on the surface of the needle. In the case of a non-metallic needle, which cannot absorb charge in the positive mode, i.e. a silica needle, this same reaction occurs where the liquid is in contact with an electrode, which

is the source of positive potential. The discharge of anions occurs at any electron-accepting surface with which the liquid is in contact. In ESI, the high field at the needle tip removes positive ions from the tip and directs them towards the surface of the liquid, and produces the Taylor Cone [26]. After a short flight path, the jet spreads into a plume of fine droplets. These droplets contain an excess of positive charges, when in the positive mode, and they diminish in size due to evaporation of the solvent. As the droplets shrink the repulsive forces between the cations increase and the droplet reaches its Rayleigh limit where a "Coulombic explosion" occurs as seen in Figure 1.5 [25].

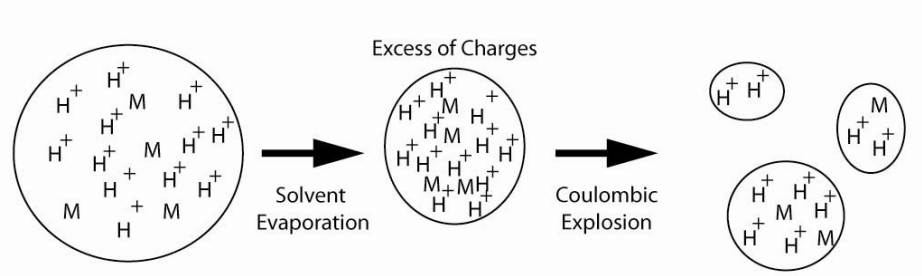

Figure 1.5. A microscopic droplet containing analyte and an excess of positive charges. The droplets undergo solvent evaporation and reach their Rayleigh limit and undergo a Coulombic explosion.

As the droplets continue to shrink and the solvent has evaporated, the analyte molecules gain residual charges and are ionized. There are two competing models describing how analytes become ionized, and they both rely on the increase in surface charge due to the evaporation of solvent.

The Charge Residue Model (Figure 1.6) states that due to solvent evaporation the surface charge increases because of the higher concentration of charges. As the droplets undergo Coulombic explosions, smaller charged droplets are produced. As the solvent further evaporates the analytes that remain eventually have an ion attach to it [27, 28].

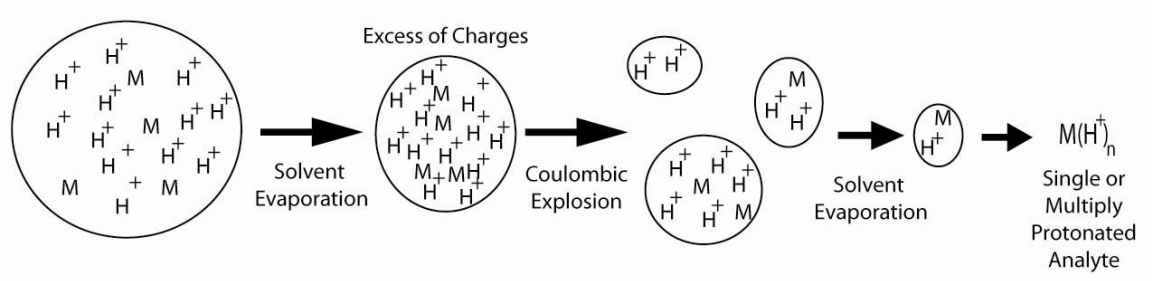

Figure 1.6. Pictorial description of the Charge Residue Model

The Ion Evaporation Model (Figure 1.7) similarly states that as droplet size diminishes, the surface charge density increases [29, 30]. Some of the ions migrate to the surface of the droplet and this is known as a partition process. The analyte molecules in the smaller droplets compete for the few charges that are still available after a Coulombic explosion. Once analyte molecules become charged, they are pushed away from the droplet and can "evaporate", i.e. jump off of the droplet, at different rates due to the electrical field.

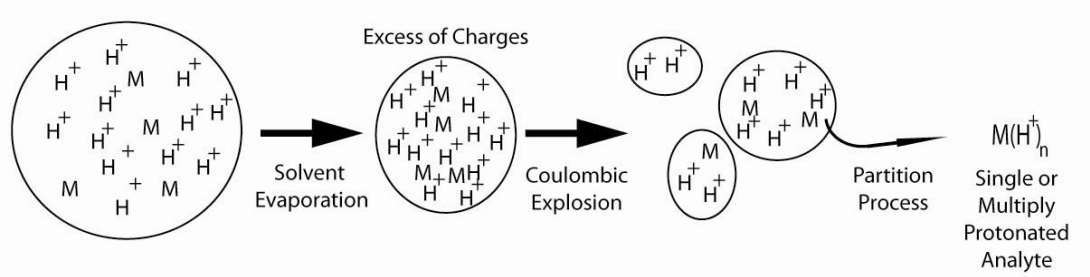

Figure 1.7. Pictorial description of the Ion evaporation Model

Both of these models are valid depending on the type of analyte. It is widely agreed upon that the Charge Residue Model applies to very large molecules or multiply charged molecules [31-34]. There is still active debate of whether small ions are purely ionized by the Ion Evaporation Model [31].

The efficiency of ESI is dependent on various variables. Miniaturization of the ESI device is one method of increasing ionization efficiency [26]. The miniaturization of ESI is called nano-ESI, and the advantages arise due to its ability to produce much smaller droplets at the needle tip. This means that fewer Coulombic explosions are

needed to expose the analyte to detection by the mass spec, which means lower concentrations can be detected with a MS [24]. In addition to lower detection limits, nano-ESI has been shown to increase the ability to detect analytes in 0.1M NaCl solutions [26]. The ability of nano-ESI to operate in the nL min^{-1} flow rate, allows for small sample consumption.

1.2.4. Time of Flight Mass Spectrometry

Time of flight mass spectrometry TOF MS is a method in which ions m/z is determined by a time measurement. In TOF MS, ions are first accelerated through ion optics in the acceleration region. The acceleration of ions in an electric field are governed by Lorentz force law (1.1) and Newton's second law (1.2)

$$\boldsymbol{F} = Q(\boldsymbol{E} + \boldsymbol{v} \times \boldsymbol{B}) \tag{1.1}$$

$$\boldsymbol{F} = m\boldsymbol{a} \tag{1.2}$$

where $\boldsymbol{F}$ is the force applied to the ion, m is the mass of the ion, $\boldsymbol{a}$ is the acceleration, Q is the ion charge, $\boldsymbol{E}$ is the electric field, and $\boldsymbol{v} \times \boldsymbol{B}$ is the vector cross product of the ion velocity and magnetic field. Once charged particles start moving in the applied electric field there is a non-zero induced magnetic field, but it can be considered negligible. Data are presented in MS by the dimensionless term *m/z,* where *z* is the number of elementary charge on the ion ($Q=ze$). Equating the two equations together gives:

$$F = m\boldsymbol{a} = ze \cdot \boldsymbol{E} \tag{1.3}$$

Therefore,

$$\boldsymbol{a} = \frac{z}{m}\boldsymbol{E}e \tag{1.4}$$

Assuming the ions of similar m/z have no initial velocity before entering the acceleration region, they will have been accelerated to the same velocity when entering the drift region (Figure 1.8).

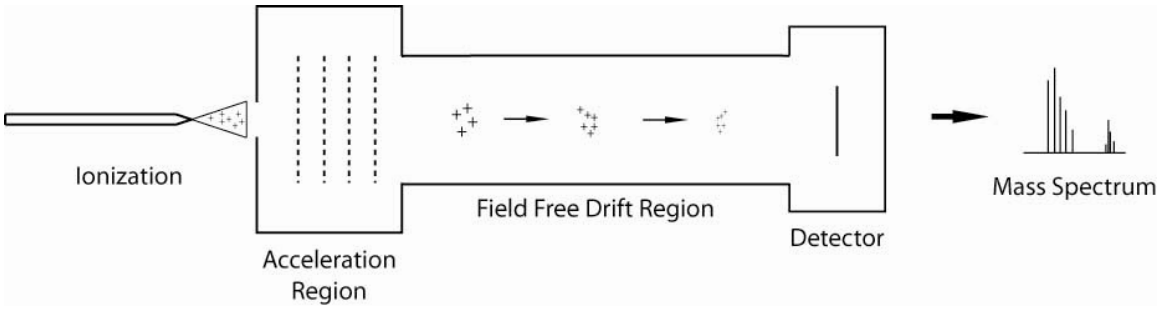

Figure 1.8. Linear TOF schematic

During the instantaneous acceleration, all ions of the same m/z receive the same specific kinetic energy (i.e. speed). Due to their different m/z values, ions correspondingly have different velocities. As ions traverse the field free region, they separate into packets according to their velocity, which is a function of their m/z value. The amount of time it takes an ion to traverse this distance is measured and its m/z value is calculated. Using the ion's equations for electrical potential (1.5) and its kinetic energy (1.6), the m/z value can be calculated,

$$E_{electric} = e \cdot z \cdot U_{accel} \tag{1.5}$$

where U_{accel} is the accelerating potential between the accelerator plates.

$$KE = \frac{1}{2} m \cdot v^2 \tag{1.6}$$

Therefore

$$v = \sqrt{\frac{2ezU}{m}} \tag{1.7}$$

Time of flight is then,

$$t_{flight} = \frac{s}{v} \tag{1.8}$$

Rearranging the terms gives,

$$m/_z = \frac{{t_{flight}}^2 \cdot 2eU}{s^2} \tag{1.9}$$

The resolving power of a TOF m/z analyzer is dependent on flight-tube length, acceleration voltage, and the spatial and velocity distributions of the initial velocity packet. A reflectron, which is an ion mirror, can be used to increase the flight-tube length and remove excess kinetic energy, which ions may have before being introduced into the acceleration area. The principles of the reflectron can be seen in Figure 1.9 where three ions of the same m/z are in the TOF, but each one has a different kinetic energy. When they enter the opposing electric field of the reflectron the ion with the highest kinetic enters first and goes the furthest because of its higher velocity. The ions decelerate until their velocity reaches zero, and they are accelerated in the opposite direction. They leave the reflectron with the same kinetic energy that they previously had,

but ions with the higher kinetic energy had to travel a longer distance, therefore all of the ions of the same m/z reach the detector at the same instance.

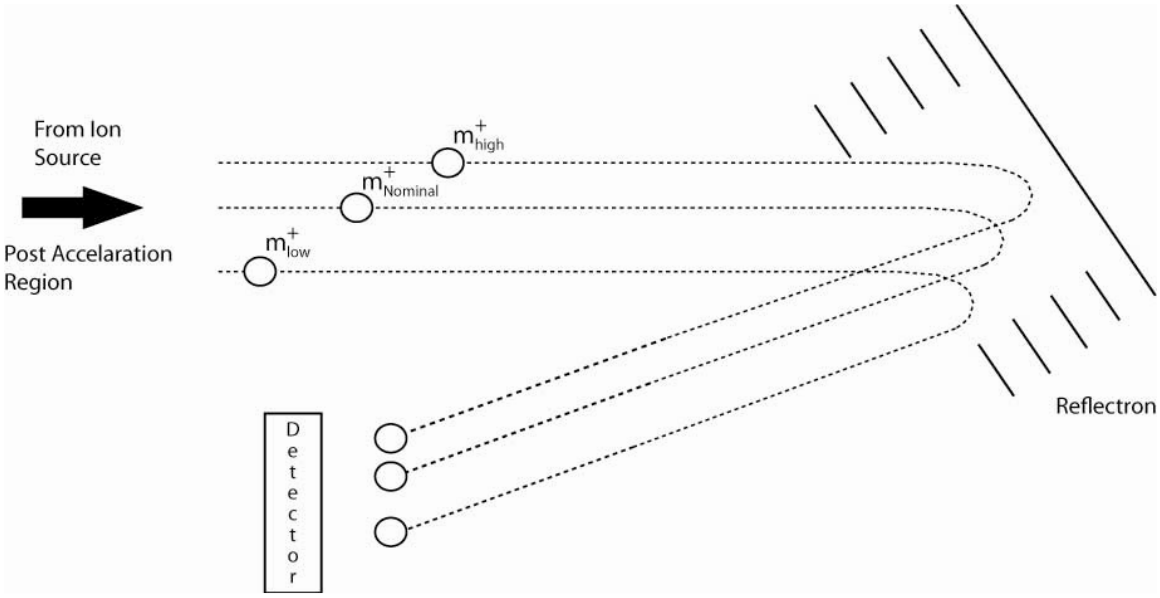

Figure 1.9. Ions reach the detector at the same time even though they have different velocities because of the distance they penetrate the reflectron.

In addition to the reflectron, the use of orthogonal acceleration also improves the resolution of a TOF m/z analyzer. The orthogonal introduction of ions, involves the sampling of an ion beam traveling in a direction perpendicular to the axis of the drift tube of the TOF. This reduces the initial velocity spread in the flight tube direction, since the ion source introduces ions with a velocity in the orthogonal direction (Figure 1.10).

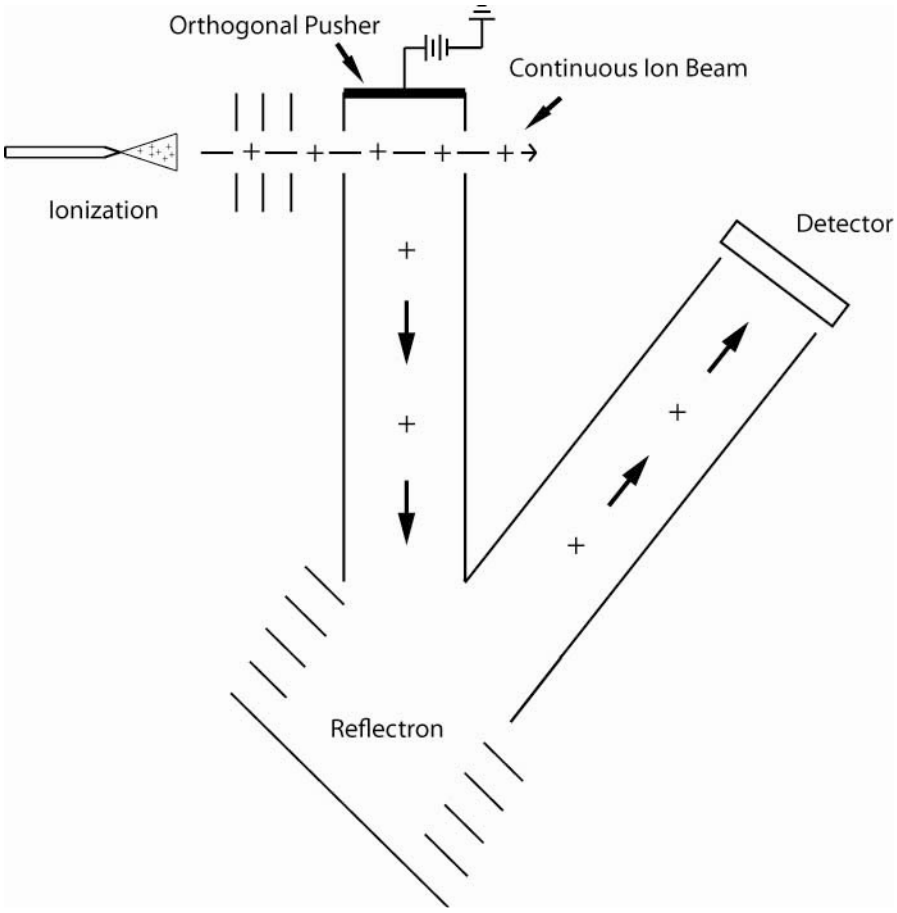

Figure 1.10. Illustration of an orthogonal acceleration TOF

1.2.5. Cell Cultures and In-Vitro Modeling of TBI

Cell culture technology is a useful tool in understanding normal and pathophysiological processes in organisms. Cell culturing is the process by which cells are isolated from tissue and are grown under controlled conditions. These cell cultures provide in vitro models that offer a powerful framework for investigating mechanisms in a simplified and controlled manner. For neuronal studies, 3-D cell cultures represent behavior in a more physiologically-relevant state as compared to monolayer (2-D) cell cultures [35]. 3-D cell cultures incorporate cell-cell and cell-extracellular matrix (ECM) interactions that may be constrained in planar cultures. The inclusion of multiple cell

types into cultures also captures the heterogeneity of in vivo tissue more accurately than monotypic cultures or cell lines. In nervous system culture models, it is important to represent such interactions as physical and metabolic coupling between neurons and astrocytes [36, 37]. The use of a more physiologically relevant cell cultures combined with an appropriate in-vitro TBI model allow for a greater chance of relevant biomarker discovery.

1.2.6. Sampling – Typical Methods and State-of-the Art

Mass spectrometric methods have opened new research opportunities in the identification of various cellular processes. The identification of biomolecules using MS techniques has become prevalent, and ESI, which can ionize large biomolecules without fragmentation, allows for fast in-line analysis of biological samples [38]. Unfortunately, sample complexity and the high salt content of the extracellular environment complicates analysis with ESI-MS. Biological samples induce clogs at the emitter tip, the high salt concentrations suppress analyte ionization, and the complexity of the sample creates a spectrum with indiscernible peaks [38].

Current methods of analyzing biological samples for marker proteins, involve a multi step process. Proteins must first be extracted from cerebral tissue by homogenizing the tissue in order to dissociate the cells, and treated with a buffer to lyse cell membranes. Samples must then be depleted of common contaminants by using filters to remove particles that interfere with liquid chromatography (LC). It is also important to remove salts, ionic detergents, lipids, and nucleic acids before conducting protein analysis [23]. Dialysis or filtering are used to lower salt concentrations to levels that will not interfere with the analysis [39, 40]. Salt concentrations interfere with sodium dodecyl sulfate (SDS) treatments, two dimensional polyarcylamide gel electrophoresis (2D-PAGE) and MS. Gel electrophoresis is a powerful tool in separating proteins in tissue samples. Proteins that are coated in SDS migrate based on their nominal mass through pores in the

polyacrylamide gel when subjected to an electrical field. 1D and 2D-PAGE separations are an effective method of resolving proteins before further LC separation methods [23]. After LC, samples can then be analyzed by MS and many times tandem MS (MSMS) is done and protein fragments are identified with protein databases (Figure1.11).

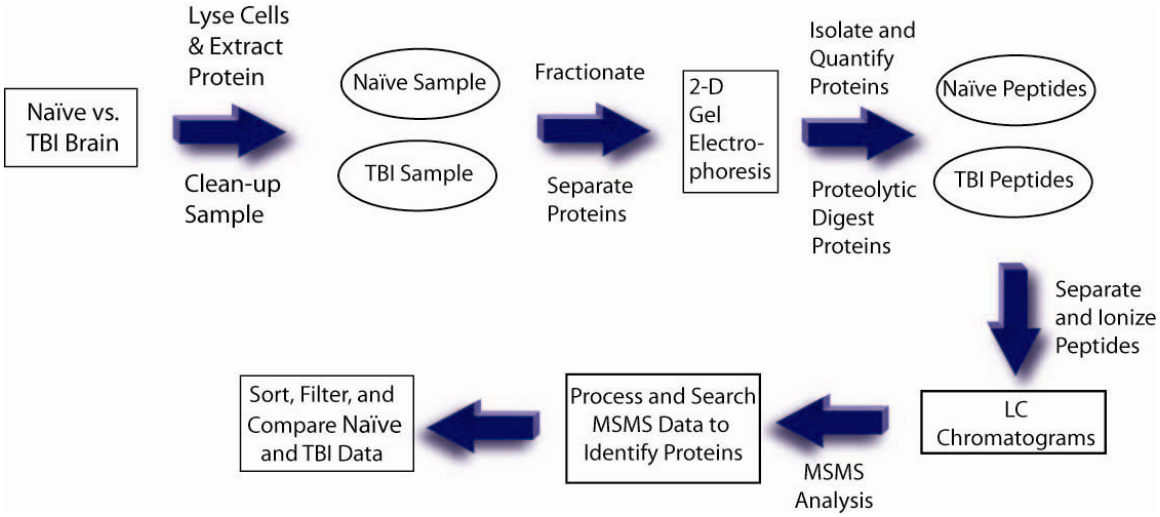

Figure 1.11. Diagram of protein identification methods [23].

The current method of protein analysis for biological samples involves multiple time consuming steps. It is of value to explore simpler alternatives that can provide improved temporal or spatial resolution when analyzing protein release in biological systems. Below is a brief introduction to alternatives to the above method.

Solid phase extraction (SPE) shares the same fundamentals as liquid LC techniques. SPE uses the principles of adsorption/distribution of analytes between mobile and stationary phases. SPE can be conducted in both off-line and in-line forms, but the most popular and simple form is off-line SPE. Off-line SPE can be used for the purification of analytes from biological liquids for quantitative analysis, desalting proteins and the enrichment of trace samples. Micro SPE cartridges allow the use of micro sized samples with the same extraction potential as regular SPE [41].

The development of new microextraction methods has been driven by the demand

of conducting analysis on smaller sample sizes, the high costs of samples, and the miniaturization of analytical techniques. There are several devices that are capable of processing small sample volumes that range from 1-100 μL. Micropipette tips packed with chromatographic sorbent allow for off-line sample microextraction. Some of these devices allow for on-line interfaces such as MD and electrodialysis.

Micropipette tips packed with chromatographic sorbent allow for facile off-line microextraction. They allow for single step desalting, concentration of analyte, and the purification of samples. They use small volumes (~10 μL) and are significantly quicker than using traditional chromatography techniques. A major disadvantage of the micropipettes is their off-line clean up nature. The ability to get temporal or spatial sample information from samples is limited.

MD utilizes the principles of dialysis, which is a separation technique that exploits a differential mass flux through a semi-permeable membrane. A hollow porous fiber can be used to exchange buffer and to desalt biological samples. This method works well in preserving small amounts of analyte that otherwise would not be detected when analyzed with MS due to the interferences. Various designs exist for MD [38].

MD has the limitation of being dependent on its mass flux. To overcome this, methods such as electrodialysis employ an electric potential in addition to the mass flux to drive dialysis through a membrane. The electric potential causes charged analytes to electromigrate through the membrane. Electrodialysis allows near quantitative transfer of analytes through the membrane, and it allows for more dialysis to occur over a shorter time period which allows for greater miniaturization. Another major benefit is the increased analyte recovery with the use of a charge selective flux.

1.3. Conclusions

It has been shown that TBI is a serious endemic that has grave health, social, and economical repercussions. Current diagnostic and clinical treatments have not been able

to make significant progress due to the lack of insight into the pathophysiological processes which occurs post injury. In order to address this need, the use of MS and other modern analytical tools have been able to identify potential TBI biomarkers. These techniques are time consuming and expensive, and a definitive marker has not been discovered. In addition to the lack of a single marker, these methods only provide limited information. There exists a need to develop a tool that would allow further analysis, such as temporal and spatial information, to better understand the complex process of TBI.

CHAPTER 2

MICRODIALYSIS-NANO-ESI MS

2.1. Microdialysis

Microdialysis (MD) is a simple and efficient method of desalting samples and exchanging buffer. MD can easily interface with electrospray ionization mass spectrometry (ESI-MS) to allow for in-line sample manipulation where it reduces the amount of salts in the solution which have a deleterious effect to the sensitivity of MS. There are many MD devices that have previously been reported but most of them are large, which requires a large amount of sample volume [38]. A small volume MD device is ideal for taking real time samples from in vitro cell cultures without causing significant alteration in the cultures. For this thesis research, a MD device was used for the in-line desalting and buffer exchange of samples taken from within neural cell culture.

2.1.1. Microdialysis Assembly

The MD device was connected to the nano-ESI emitter using a zero dead volume unit that was electrically grounded in order to create the electrolytic cell between the electrospray needle and the counter-current electrode. Using previously reported MD devices as prototypes and after many experimental trials, dimensions were established for the analysis of cell culture media that was retrieved from within a cell culture matrix. Following the design by Jakubowski et al., a 3 cm long piece of fused-silica capillary (2 μm ID, 150 μm OD) was inserted into a dry 3.5 cm long piece of regenerated cellulose hollow MD tubing (200 μm ID, 215 μm OD, Spectrum, Rancho Dominguez, CA) with a molecular weight cut off (MWCO) of 13 kDa. Into each end of the MD tubing a 10 cm long piece of fused silica capillary (50 μm ID, 150 μm OD) was inserted. Using super

glue (Locklite QuickTite Super Glue, Manco, Inc., Avon, OH, USA) the fused-silica capillary was sealed with the MD tubing and it was left to dry. The dry MD fiber was inserted into a 5 cm long Teflon tubing (762 μm ID, 1.59 mm (1/16") OD) and PEEK Tees were connected to both ends of the Teflon tubing using 10-32 PEEK fingertight nut and ferrule. The MD unit was secured using 10-32 Peek fingertight nut with a 190 μm ID Kel-F ferrule which tightened into the Tee connection on both ends. 10-32 Peek fingertight nuts with 1/16" ferrules were used to connect Teflon tubing for buffer inlet and outlet lines. A schematic of the MD unit can be seen in Figure2.1. Both the buffer flow rates and sample flow rates were varied to examine the MD unit's performance.

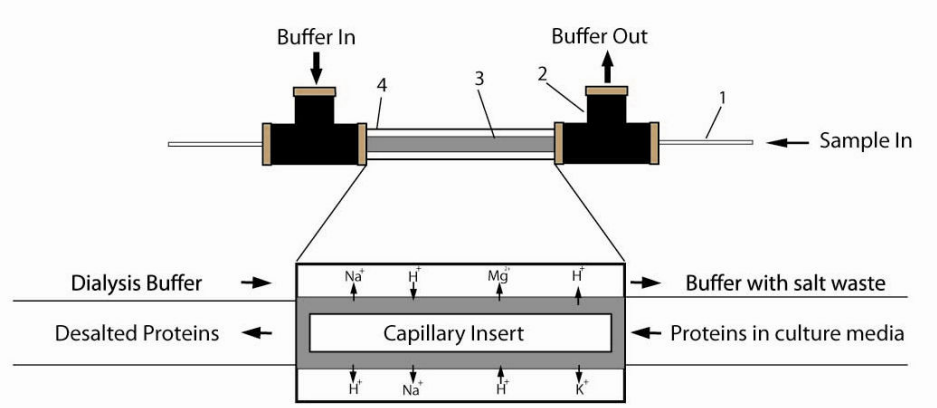

Figure 2.1. Schematic of MD unit. (1) Fused silica capillary, 50 μm ID, 150 μm OD, (2) Tee fitting connecting dialysis buffer inlet/outlet, teflon tubing, and fused silica capillary, (3) hollow fiber inside teflon tubing, (4) Teflon Tubing. The close up inset illustrates the exchange of salt cations across the dialysis membrane.

2.1.2. Microdialysis Theoretical Analysis

This MD design is a counterflow, concentric tube dialysis chamber which can be analyzed with a simple model based on the principles of mass transfer. Understanding the theoretical limits of the MD unit allowed for the determination of the appropriate size and flow rates that were used in the experimental portion.

The MD unit can be analyzed by using concepts developed for modeling mass

transfer under conditions of internal, laminar flow. For internal flow in a tube of circular cross section the Reynolds number (2.1) dictates whether the flow is laminar or turbulent.

$$Re = \frac{u_m \varphi_h}{\nu} \tag{2.1}$$

where u_m is the mean fluid velocity over the tube cross section, ν is the kinematic viscosity, and φ_h is the tube's hydraulic diameter. The hydrodynamic entry length ($x_{fd,h}$) for fully developed flow can be obtained from

$$\left(\frac{x_{fd,h}}{d_h}\right)_{lam} \approx 0.05Re \tag{2.2}$$

Using Equations (2.1) and (2.2) we find that for the MD unit under the experimental flow conditions $x_{fd,h} << L$, (where L is the length of the MD unit) and hence the flow in the MD device can be considered fully developed.

When analyzing the mass transfer of a species, e.g., species s, from one media to another across a membrane, i.e. media A and media B, (Figure 2.2) the concentration in each fluid stream can be described using a cross sectional average, and the mass flux of a species across the membrane at a given position, n_s'', can be calculated using an effective mass transfer coefficient, h_m. It was assumed that there was no pressure driven flux in the system due to small pressure differences in the MD system. At steady state, with no chemical reactions, and no adsorption of species within membrane, the mass flux of species s is

$$n_s'' = h_m(C_{s,A} - C_{s,B}) \tag{2.3}$$

where $C_{s,A}$ is the concentration of species s in media A, and $C_{s,B}$ is the concentration of species s in media B.

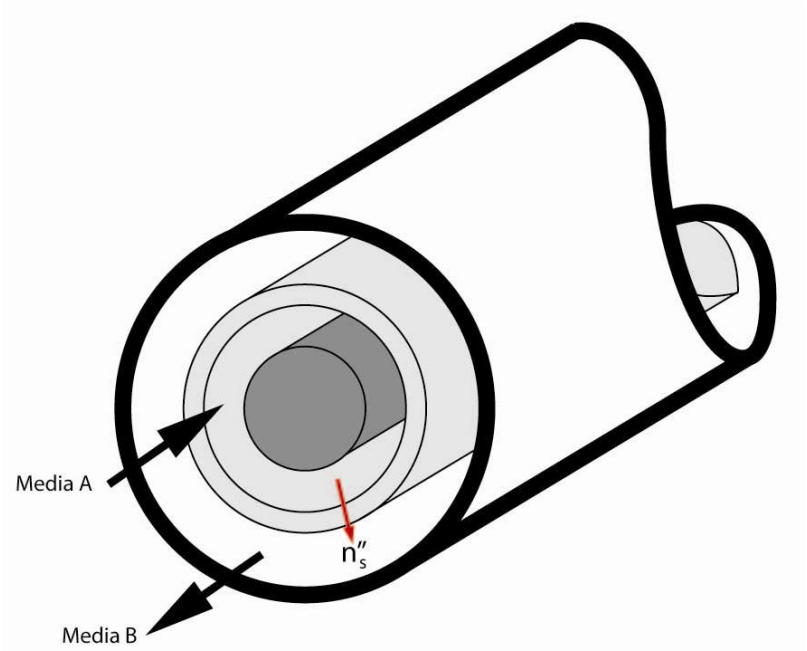

Figure 2.2. Illustration of the mass transfer of species *s* from Media A to Media B through a membrane.

The total rate of species transfer (n_s) over the membrane of surface area A_s is then obtained by integrating the local flux (n_s'') over the entire suface to obtain

$$n_s = \bar{h}_m A_s \Delta C_{s,\mathrm{lm}} \tag{2.4}$$

where $A_s = d\pi L$ and d is the membrane diameter. The log mean concentration difference, $\Delta C_{s,lm}$, is

$$\Delta C_{s,\mathrm{lm}} = \frac{\Delta C_{s,2} - \Delta C_{s,1}}{\ln\left(\frac{\Delta C_{s,2}}{\Delta C_{s,1}}\right)} \tag{2.5}$$

where $\Delta C_s = C_{s,A} - C_{s,B}$, and the subscript *2* is at the outlet of the system and subscript 1, is at the inlet of the system. At steady state and in the absence of chemical reactions, global mass conservation requires that

$$n_s = \dot{Q}(C_{s,1} - C_{s,2}) \tag{2.6}$$

where $\dot{Q}$ is the volume flow rate of the fluid stream. The overall mass transfer coefficient, $\bar{h}_m$, can be calculated from

$$\bar{h}_m = \frac{1}{\frac{1}{h_i} + R_m + \frac{1}{h_o}} \tag{2.7}$$

where h_i and h_o are the average mass transfer coefficients for interior and exterior portions of the dialysis fiber, respectively, and R_m is the resistance to mass transfer from the membrane wall. The average mass transfer coefficients can be obtained from Incopera and DeWitt (table 8.2) [42] which has the correlation for Sherwood numbers of

$$Sh_o = 4.438\left(\frac{\varphi_{o,fiber}}{\varphi_{i,teflon}}\right)^{-0.43} \tag{2.8}$$

$$Sh_i = 4.7048\left(\frac{\varphi_{insert}}{\varphi_{i,fiber}}\right)^{0.0565} \tag{2.9}$$

where $\varphi_{o,fiber}$ is the outer diameter of the fiber, $\varphi_{i,Teflon}$ is the inner diameter of the Teflon tube, φ_{insert} is the outer diameter of the capillary insert, and $\varphi_{i,fiber}$ is the inner diameter of the fiber. Equations (2.8) and (2.9) are valid under fully developed laminar flow in a

circular tube annulus with one surface that is impenetrable and the other surface with a constant concentration.

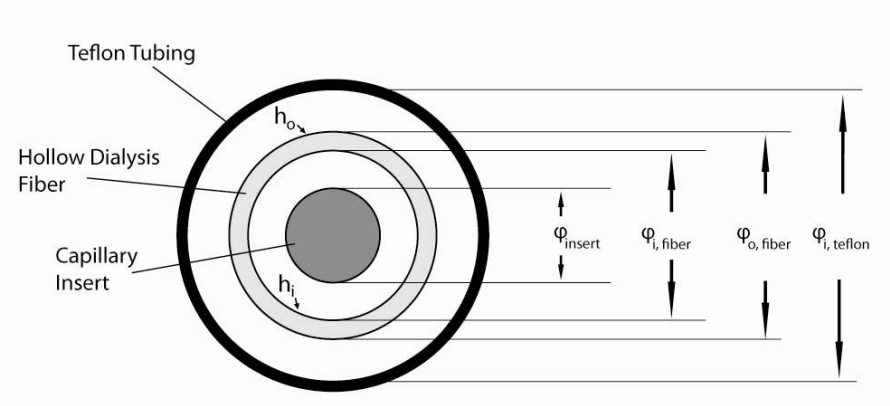

Figure 2.3. Cross section of the MD unit. h_o is defined to be on the OD of the dialysis fiber and h_i is defined as the ID of the dialysis fiber.

Then using the definition of the Sherwood number,

$$\overline{Sh}_D = \frac{\bar{h}_m \varphi_h}{D_s} \tag{2.10}$$

where D_s is the diffusion coefficient of species *s,* h_o and h_i can be calculated by

$$h_o = Sh_o \frac{D_s}{\varphi_{h,o}} \tag{2.11}$$

where $\varphi_{h,o} = \varphi_{i,teflon} - \varphi_{o,\,fiber}$

$$h_i = Sh_i \frac{D_s}{\varphi_{h,i}} \tag{2.12}$$

where $\varphi_{h,i} = \varphi_{i,fiber} - \varphi_{o,\ insert}$. The transport resistance of the membrane can be estimated as [43]

$$R_m = \frac{ln\left(\frac{\varphi_{o,fiber}}{\varphi_{i,fiber}}\right) A_{s,fiber}}{2\pi L D_s \alpha_m} \tag{2.13}$$

where α_m is the available volume fraction to analytes in the membrane and can be estimated as 0.012 from experimental results.

The mass transfer analysis of each fluid stream separately and the mass transfer rate across the membrane, yield three equations that describe system's total mass transfer:

$$n_{s,media} = \dot{Q}_{media}(C_{s,media,1} - C_{s,media,2}) \tag{2.14}$$

$$n_{s,buff} = \dot{Q}_{buff}(C_{s,buff,1} - C_{s,buff,2}) \tag{2.15}$$

$$n_s = \bar{h}_m A_s \Delta C_{s,\mathrm{lm}} \tag{2.16}$$

Combining Equations (2.14) - (2.16) yields an equation for the ratio of concentration of media post MD to the concentration of the media before MD as a function of the system parameters A_s,$\bar{h}_m$, $\dot{Q}_{media}$, and ζ.

$$\frac{C_{s,media,2}}{C_{s,media,1}} = \frac{(1+\zeta)}{\zeta + \exp\left(\frac{A_s \bar{h}_m (1+\zeta)}{\dot{Q}_{media}}\right)} \tag{2.17}$$

where $\zeta = \frac{\dot{Q}_{media}}{\dot{Q}_{buff}}$.

2.1.3. Microdialysis Theoretical Model Results

Using Equation (2.17) the expected behavior of a MD unit was investigated under conditions of varying flow rates and of different fiber lengths in order to design an initial configuration that would perform effectively. Figure 2.4 shows how the ratio of $C_{s,media,2}$ to $C_{s,media,1}$, i.e. MD unit performance, varies with respect to the two non dimensional parameters that govern the behavior of the MD unit ($\frac{\dot{Q}_{media}}{A_s \bar{h}_m}$ and ζ).

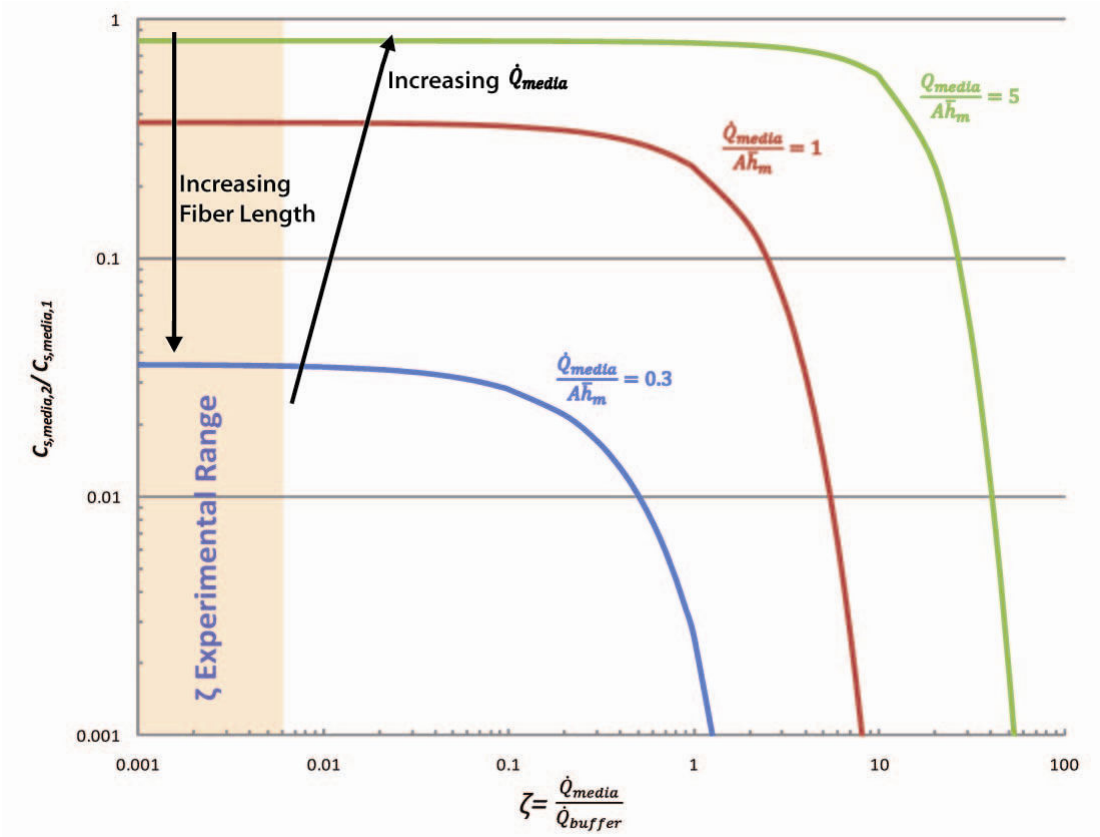

Figure 2.4. Theoretical MD performance with respect to ζ at various values of $\frac{\dot{Q}_{media}}{A_s \bar{h}_m}$. This figure takes into account the effects of increasing fiber length and varying the sample and dialysis buffer flow rate.

Only $\dot{Q}_{media}$, $\dot{Q}_{buff}$, and L were varied in the theoretical study since $\bar{h}_m$, h_i, and h_o are dictated by the diameters of the system. These could not vary due to the manufacture's specific dimensioning of fiber, silica capillary and teflon tubing OD and

ID. The diffusion coefficient, D_s, was set to $1.6x10^{-9}$ m^2/s which is the diffusion coefficient for NaCl [44].

The above analysis provides meaningful insight into the flow rates and length ranges of a MD unit for efficient removal of salts from a media sample. In addition to referring to the theoretical trends, other factors that need to be considered include the flow rate necessary for stable nano-ESI, shortest possible transit time, and practical limitations in assembly.

2.2. Microdialysis Testing

In order to validate the theoretical results, a device was built based on the MD assembly section with various lengths and flow rates.

2.2.1. Microdialysis Experimental Assembly

Samples of 500mM and 300 mM NaCl in DI water were used to examine the effectiveness of the MD unit. Sample and buffer flow rates were controlled using syringe pumps (KD Scientific, Holliston, MA), and the dialyzed sample were collected at the outlet of the MD unit in a sample vial and was analyzed with an osmometer (Vapro 5520, Vescor Biomedical Systems, Logan, UT). An osmometer measures the osmotic pressure of an aqueous solution by measuring the vapor pressure of the liquid, and from osmotic pressure, the concentration of dissolved species can be determined.

2.2.2. Microdialysis Experimental Results

The MD unit's performance was examined by varying both sample flow rates and dialysis buffer flow rates, and MD unit length. Below, Figure 2.5 - Figure 2.8, are the results of these experiments. A two sample T-test was conducted to determine whether statistical differences existed between the different experimental conditions.

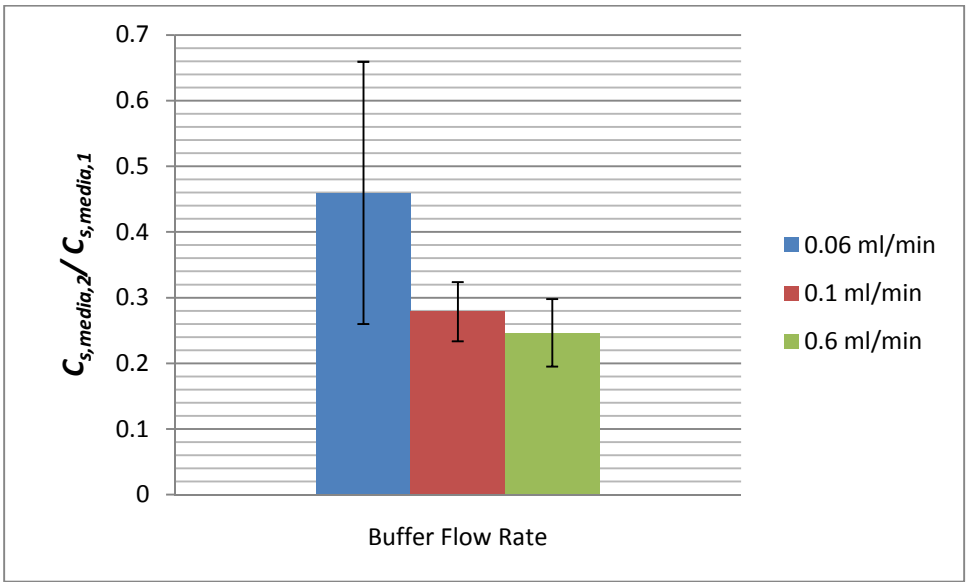

Figure 2.5. Experimental MD performance with respect to a varying buffer flow rate. The dialysis buffer of DI water was set to flow rates that varied from 0.06 ml/min, 0.1 mL/min, and 0.6 mL/min. The MD unit's length was 1 cm and the sampled of 300 and 500 mM NaCl were set to a flow rate was 60 µl/hr. There was no statistical significant difference in varying the dialysis buffer flow rate. Sample size of n = 3 for each buffer flow rate.

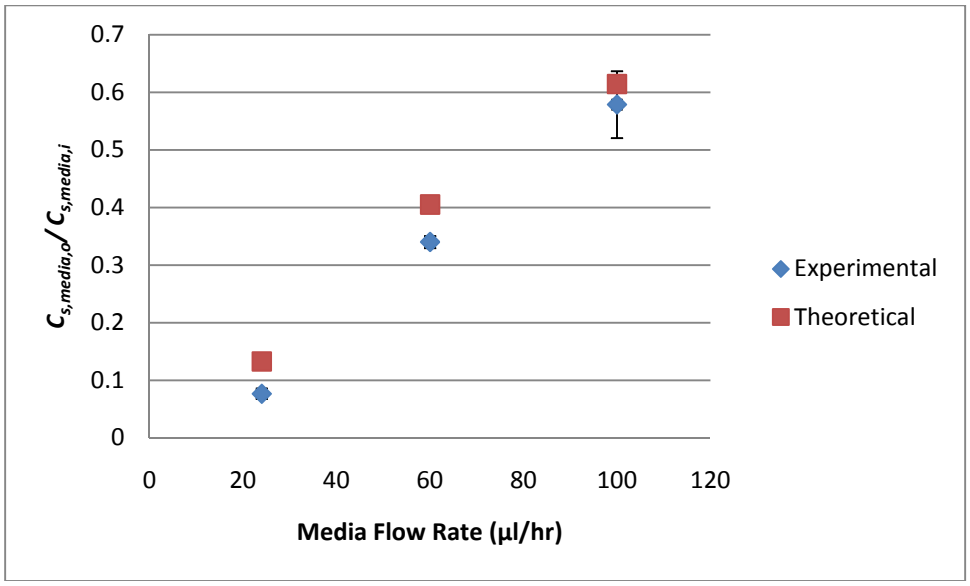

Figure 2.6. Experimental MD performance with respect to a varying sample flow rate for a length of 1cm. The sample of 300mM of NaCl was set to flow rates that varied from 24 µL/hr, 50 µL/hr, and 100 µL/hr. The dialysis buffer of DI water was set to a flow rate of 0.3 ml/min. The experimental values followed the theoretical trend for varying sample flow rate. Sample size of n = 3 for each experimental media flow rate. The theoretical data are based on an empirical fit for membrane resistance.

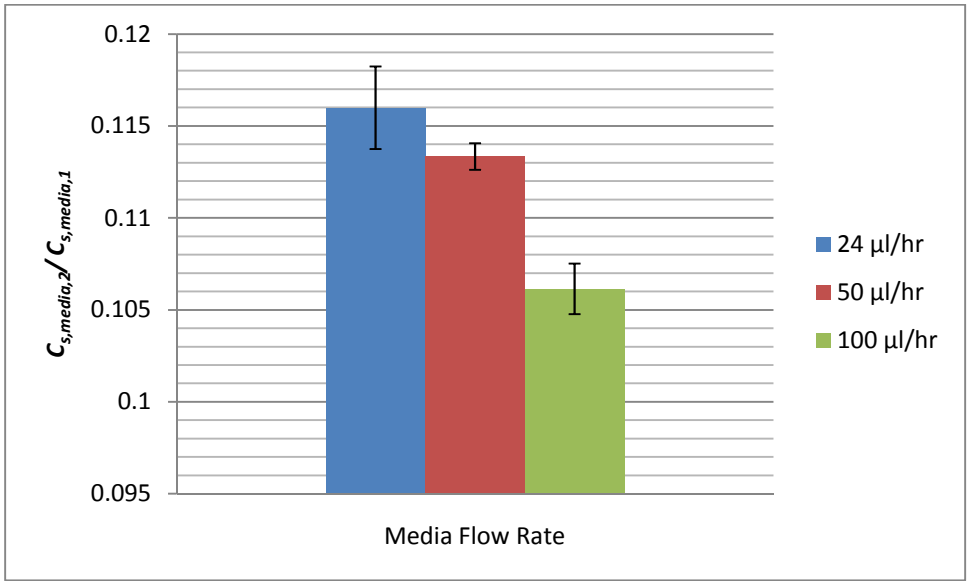

Figure 2.7. Experimental MD performance with respect to a varying sample flow rate for a length of 2cm. The sample of 300mM of NaCl was set to flow rates that varied from 24 µL/hr, 50 µL/hr, and 100 µL/hr. The dialysis buffer of DI water was set to a flow rate of 0.3 ml/min. There was no statistical significant difference in varying the sample flow rate. Sample size of n = 3 for each media flow rate.

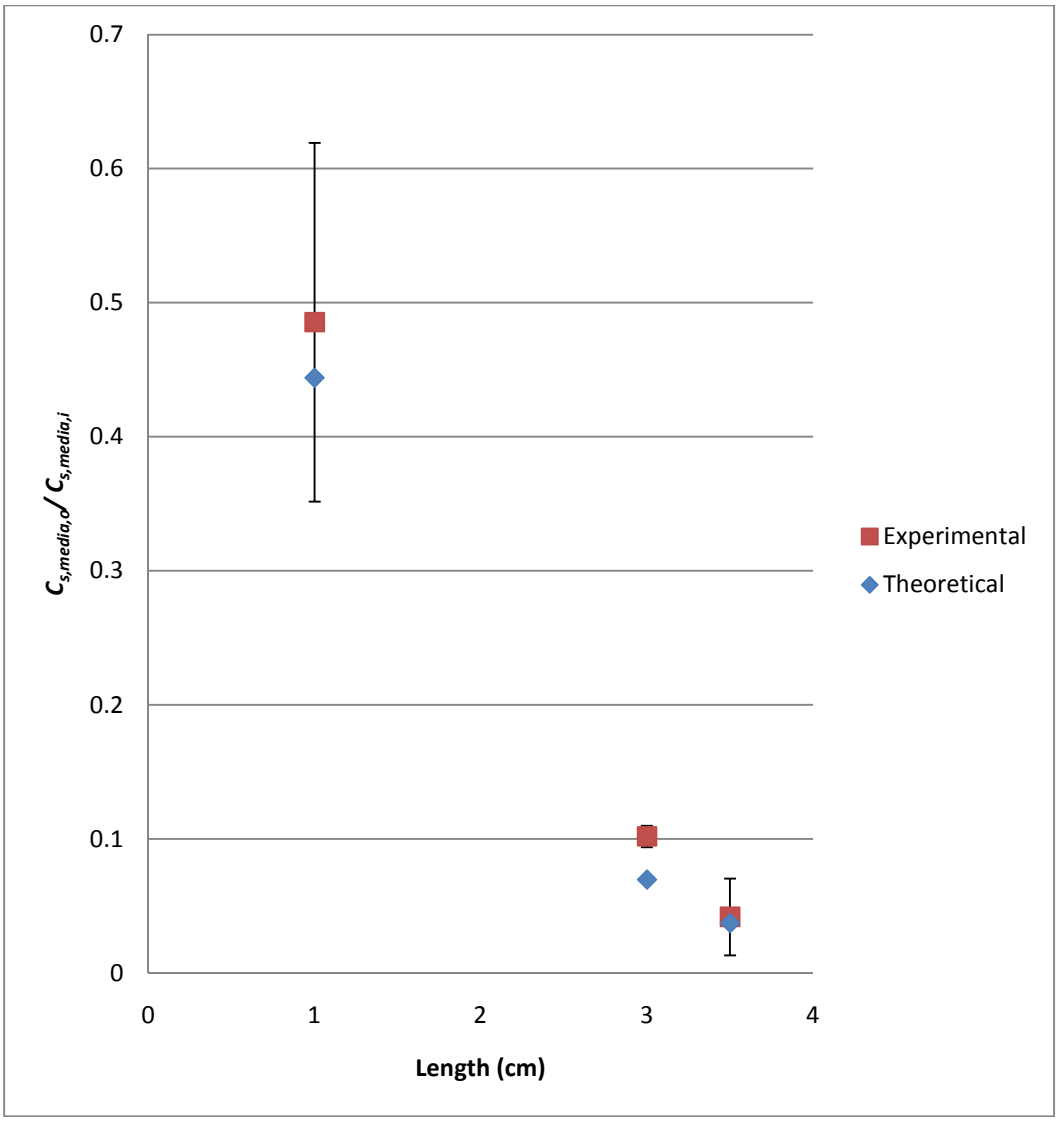

Figure 2.8. Experimental MD performance with respect to a varying MD unit length. Samples of 300 and 500mM of NaCl were set to a flow rate of 60 µL/hr. The MD unit's length varied from 1, 3, and 3.5 cm and the dialysis buffer of DI water was set to a flow rate of 0.06 mL/min. There was a significant difference between each MD unit's length and performance. Sample size of n = 3 for each experimental MD unit length. The theoretical data are based on an empirical fit for membrane resistance.

The experimental values varied from the theoretical values; however, both the dialysis buffer flow rate and length variations followed similar trends as in the theoretical results. The theoretical results for varying dialysis buffer flow rate showed little change in the MD unit's performance. The experimental results showed a similar trend in little

variation in the MD unit's performance based on changing the dialysis buffer flow rate. There were inconsistencies when the sample flow rate was varied at different experiments. Figure 2.6 demonstrates that the experimental MD unit behaves similarly to the theoretical model, but Figure 2.7 shows that varying the sample flow rate had no effect on the MD unit's performance. These inconsistencies are most likely due to irregularities in the MD unit's assembly, and there may also be fiber to fiber performance differences that lead to different mass transfer resistances. As the mass transfer membrane resistance decreases, the sample flow rate's influence on performance minimizes.

Although some experiments demonstrated that sample flow rate may benefit the amount of salt that is removed from samples, ultimately nano-ESI will dictate the sample flow rate [45]. Under typical nano-ESI conditions the sample flow cannot be varied enough to affect the MD unit's performance.

The results from the theoretical model demonstrated that increasing length improved the MD unit's performance. Similarly increasing length showed to be the design parameter which provided significant changes in the MD unit's performance in the experimental section. Originally the membrane resistance to mass transfer was calculated using the estimation from Tong et al. It was found that experimental results were significantly different from the theoretical results. From the experimental results it was concluded that our estimation of α_m was more than an order of magnitude less. With α_m set to 0.012, the theoretical model can accurately predict the performance of the MD unit.

2.3. MD nano-ESI Experiments

With the establishment of an optimum set of design parameters for the MD unit, the device was tested by running samples through the MD unit in an off-line setting and the collected samples were then run through a micrOTOF MS (Bruker Daltonics,

Billerica, MA), which is an orthogonal acceleration TOF MS. The MD unit's ability to remove salt and retain proteins was demonstrated through these experiments. Testing to determine the optimum buffer and nano-ESI emitter for the most consistent and steady signal was conducted by using the in-line MD nano-ESI setup. Characterization of the system was done by using various concentrations of cytochrome-c (Cyt-C), equine heart, Sigma Aldrich, St. Louis, MO) in various concentrations of salt solution and media solutions. Cyt-C is a small (12 kDa) heme protein that is associated with the inner membrane of the mitochondrion. It is a highly soluble protein and has been found to be released extracellularly in neuronal cultures post apoptosis [46, 47].

2.3.1. MD Bruker ESI Analyte Retention Experiments

Initially samples were passed through the MD unit at flow rates of $\dot{Q}_{media}$ = 50 µl/hr and a $\dot{Q}_{buff}$ = 150 µL/hr. The media sample consisted of 20 µM Cyt-C in a 10% methanol, 1% acetic acid buffer, and the buffer was 10% methanol, 1% acetic acid solution. Samples were collected off-line and run through the Bruker ESI ion source instead of the nano-ESI emitter. This was done to asses protein losses when the sample went through the MD fiber. Initially the 20 µM Cyt-C in a 10% methanol, 1% acetic acid buffer was analyzed with the Bruker ion source without MD (Figure 2.9).

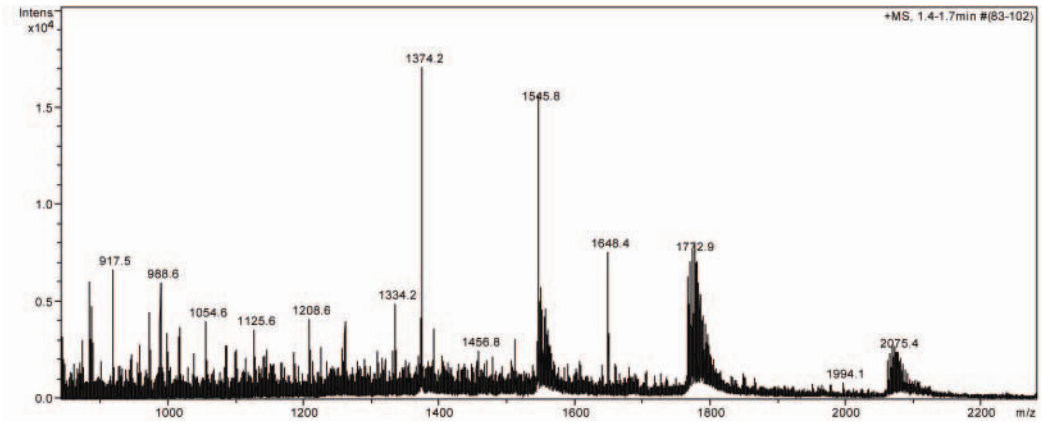

Figure 2.9. Spectrum of 20 µM Cyt-C in a 10% methanol, 1% acetic acid buffer using the Bruker ion source with no MD.

Using the same MS settings as the experiment in Figure 2.9, the MD unit was incorporated into the MS experiment in an off-line manner. Samples were flowed through the MD unit and collected in a vile at the end of the MD unit. A 10% methanol, 1% acetic acid dialysis buffer was used in the MD unit. Figure 2.10 shows the resulting MS spectrum of the experiment.

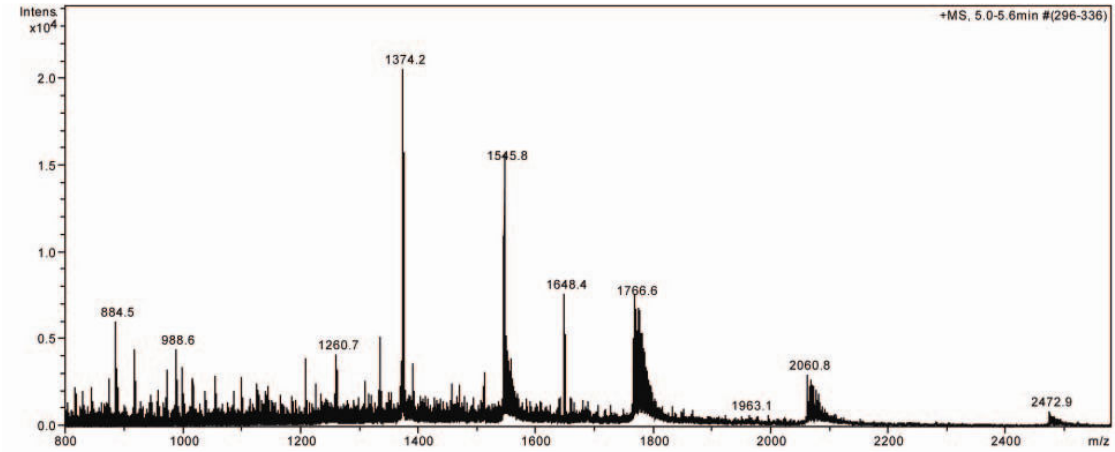

Figure 2.10. Spectrum of 20 µM Cyt-C in a 10% methanol, 1% acetic acid buffer using the Bruker ion source with off-line MD. MD length was 1 cm.

A simple comparison of the peak intensities of Figure 2.9 and Figure 2.10 qualitatively indicate that there was no apparent loss in Cyt-C due to dialysis, and when comparing the two spectra it can be seen that the post MD spectrum shows a greater Cyt-

C intensity. Furthermore, when examining the protein's charge states, there was also a reduction in the amount of sodium adducts in post MD sample as seen in Figure 2.11.

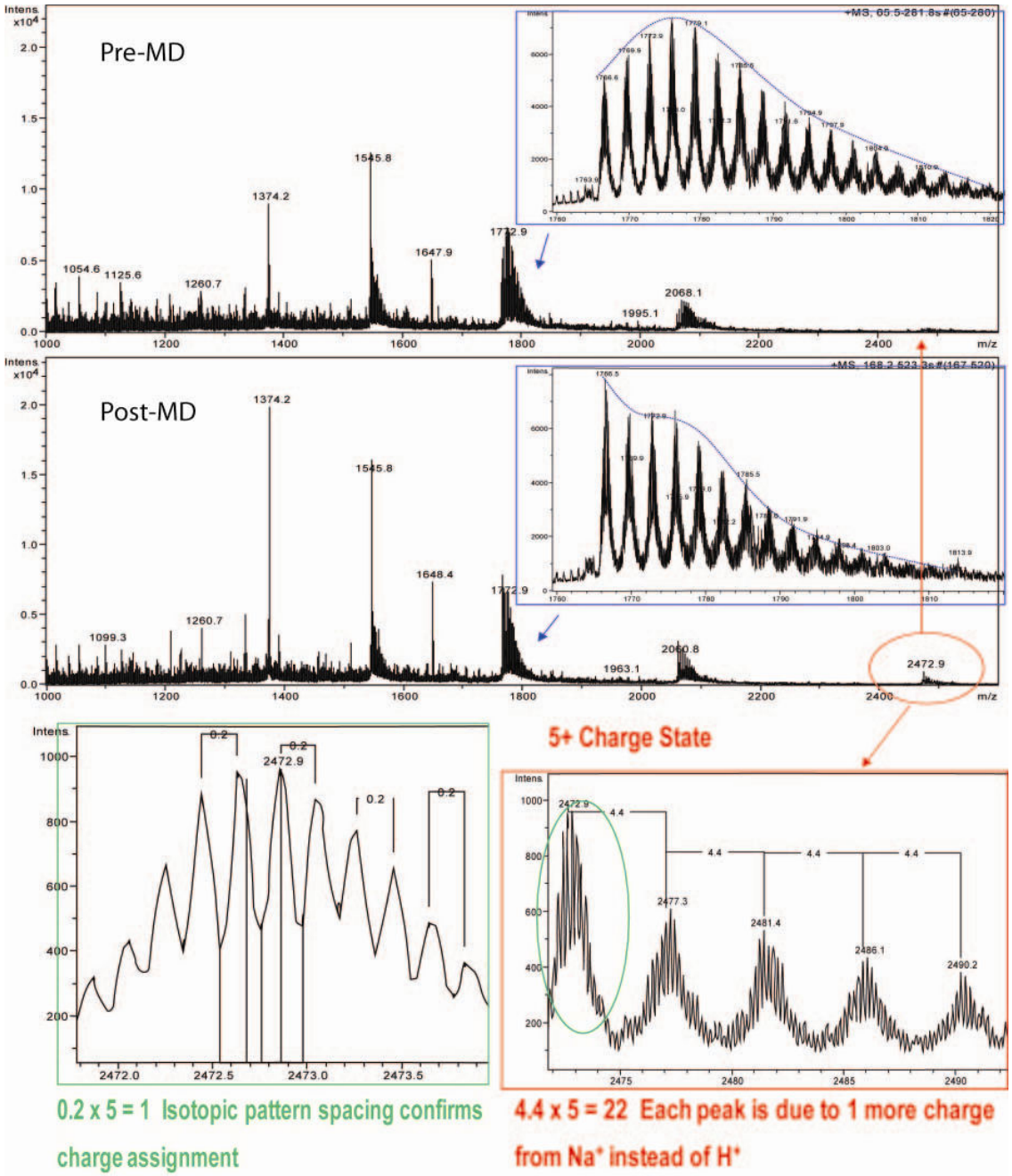

Figure 2.11. Comparison between the pre-MD and post-MD MS analysis. There was a reduction in the number of adducts to each charge state in the post-MD experiment. Further examination of the charge states shows that there are Na^+ adducts instead of H^+.

2.3.2. In-line MD nano-ESI Performance Experiments

The MD membrane's performance in reducing the amount of salt adducts and its ability to retain proteins was demonstrated in the off-line experiments with the Bruker ESI ion source. The MD unit's performance as an in-line device was evaluated in the following experiments. The MD unit was assembled in-line with a nano-ESI emitter and stationed in front of the MS. Figure 2.12 shows the MD unit connected to the nano-ESI emitter (New Objective, Woburn, MA) by a grounded metallic union.

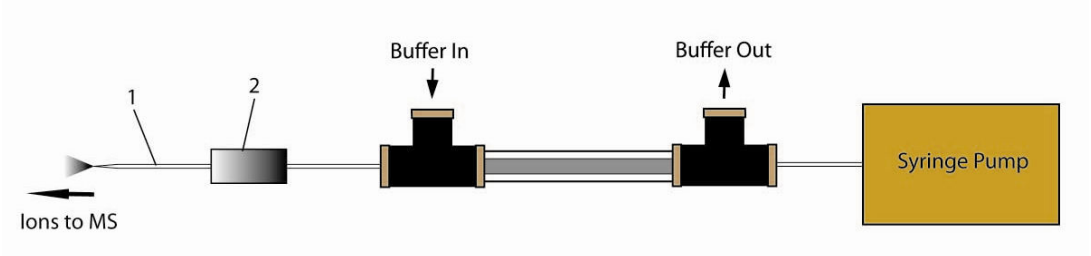

Figure 2.12. Schematic of in-line MD-nano-ESI. (1) nano-ESI Emitter and (2) grounded metallic union.

For the in-line MD-nano-ESI experiments the buffer flow rate was held constant at $\dot{Q}_{buff}$ = 150 µL/hr. The sample flow rates were held at 30 -50 µL/hr in order to maintain a stable MS signal. In these experiments media flow rate, and various dialysis buffer mixtures of Methanol, acetic acid, and ammonium acetate were examined. In addition, two different types of nano-ESI emitters were used, a 50 µm ID, 360 µm OD, 8 µm Tip ID emitter and a 75 µm ID, 360 µm OD, 15 µm Tip ID emitter. Cyt-C was dissolved in various NaCl solutions or NEUROBASAL (Invitrogen, Carlsbad, CA) cell culture media. Each experiment was examined for signal consistency, run length, and signal intensity.

2.3.3. MD-nano-ESI Performance Experimental Results

The effectiveness of the MD unit's ability to clean samples during in-line MD nano-ESI is illustrated below.

A 20 μM Cyt-C in a 10% methanol 1% acetic acid solution with no added salt underwent dialysis through a membrane of a 1cm length, and a dialysis buffer of 10% methanol and 1% acetic acid (Figure 2.13). The results indicate a higher intensity compared to the results presented in Figure 2.10, likely due to the use of a nano-ESI emitter and a large reduction in the amount of sodium adducts to the individual charge states.

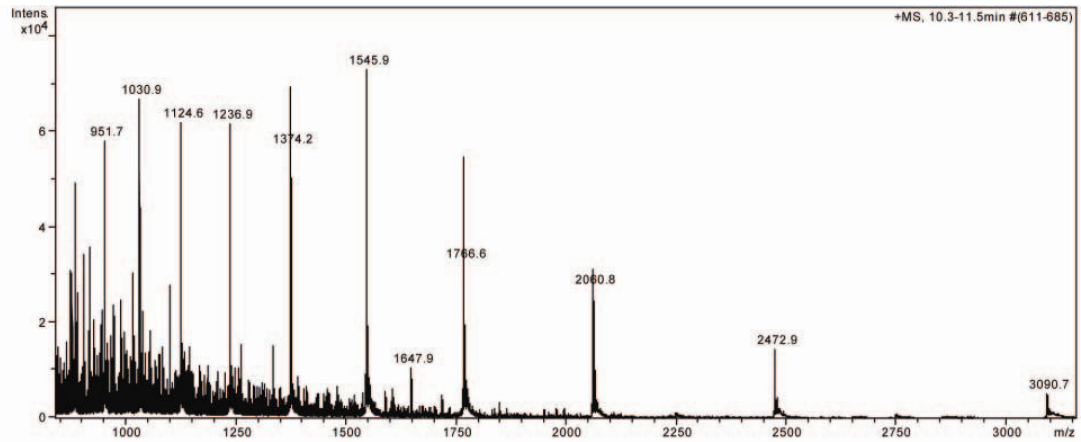

Figure 2.13. MD nano-ESI 20 μM Cyt-C in a 10% methanol 1% acetic acid solution with no added salt. MD unit's length was 1 cm.

Samples of 20 μM Cyt-C were in solutions of NaCl, 300-500mM, that mimic salt levels in cell culture media. In addition to the NaCl in the Cyt-C solutions, the sample buffer solution of 10% methanol and 1% acetic acid was eliminated and replaced with pure DI water. Typically ESI is done with an organic solvent and acid buffer mixture. Instead of including the buffer in the initial sample, the dialysis buffer would provide the necessary solvent through the MD step. Figure 2.14 illustrates the suppressive nature of high salt concentration samples on the detection of analyte in the MS spectrum. There

was no sign of Cyt-C, but adducts of NaCl could be found throughout the spectrum due to the high salt content of the sample.

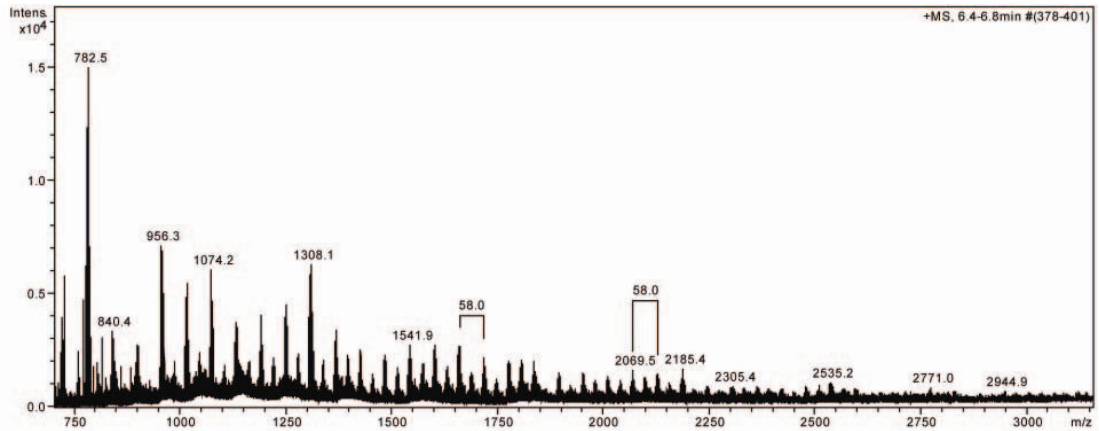

Figure 2.14. A sample of 20 µM Cyt-C in a 500 mM NaCl solution was flowed through the in-line MD nano-ESI device without any dialysis buffer flowing.

Figure 2.15 shows the improvements of incorporating the dialysis buffer into the in-line MD step.

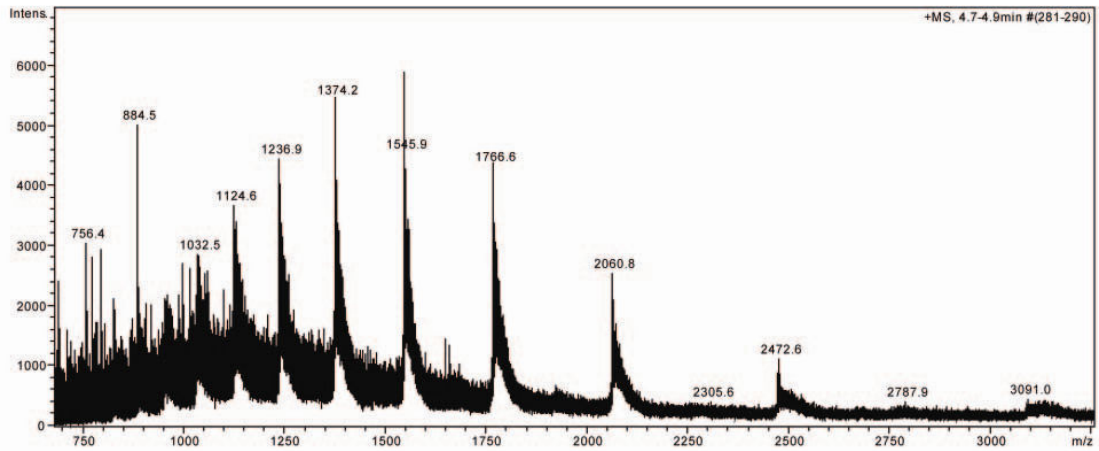

Figure 2.15. 20 µM Cyt-C in a 250 mM NaCl solution with in-line MD. Dialysis buffer of 10% methanol and 1% acetic acid. MD unit's length was 1 cm.

Another factor that led to improved MS results was the incorporation of a low pressure cross flow nebulizer gas Figure 2.16. When incorporated with MD-nano-ESI, there were improvements in peak intensities and the duration of experiments. The use of

a sheath flow or nebulizer gas has been reported to improve liquid break up in higher flow rate ESI [31]. Although nano-ESI is traditionally operated without nebulizer gas [26], it consistently increased the intensity of Cyt-C peaks for high salt concentration and cell culture media samples. Although not thoroughly examined, high salt concentration samples consistently benefitted from a low pressure nebulizer gas perpendicular to the spray, as seen in Figure 2.17 and Figure 2.18, perhaps due to facilitating desolvation as reported with traditional ESI.

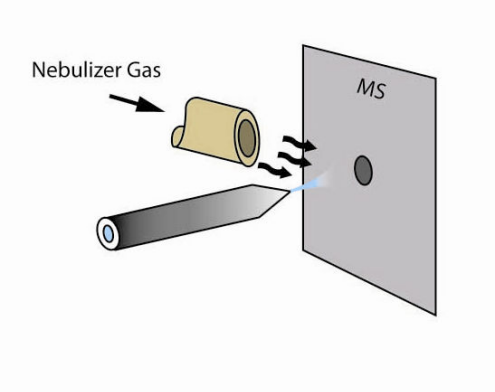

Figure 2.16. Schematic of nano-ESI with a perpendicular low pressure nebulizer gas cross flow of nitrogen.

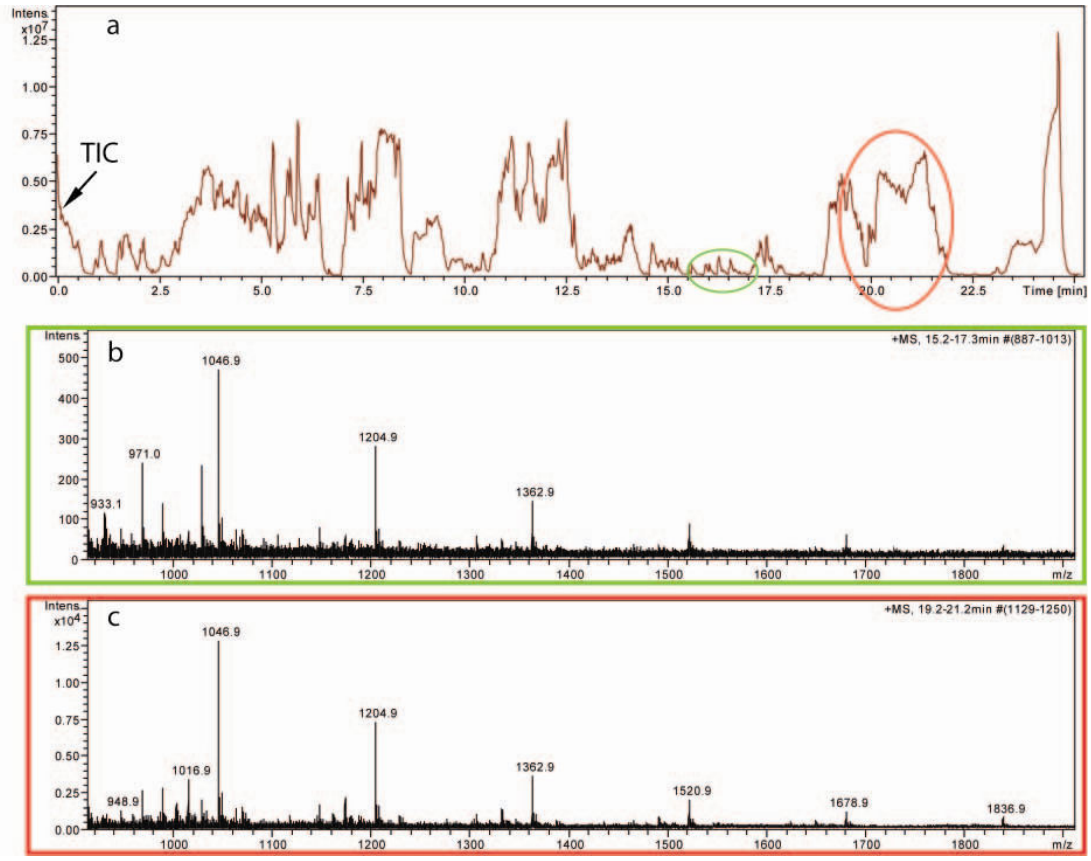

Figure 2.17. Experiment with intermittent low pressure nebulizer gas cross flow application. (a)Total Ion Chromatogram (TIC) of a blank DI water sample from a model cell culture chamber with intermittent nebulizer gas. The areas with higher chromatogram intensity had low pressure nebulizer gas applied to the tip of the emitter. (b) Averaged spectrum of time point with no nebulizer gas application. (c) Averaged spectrum of time point with nebulizer gas. Spectrum (c) has a much higher intensity than spectrum (b).

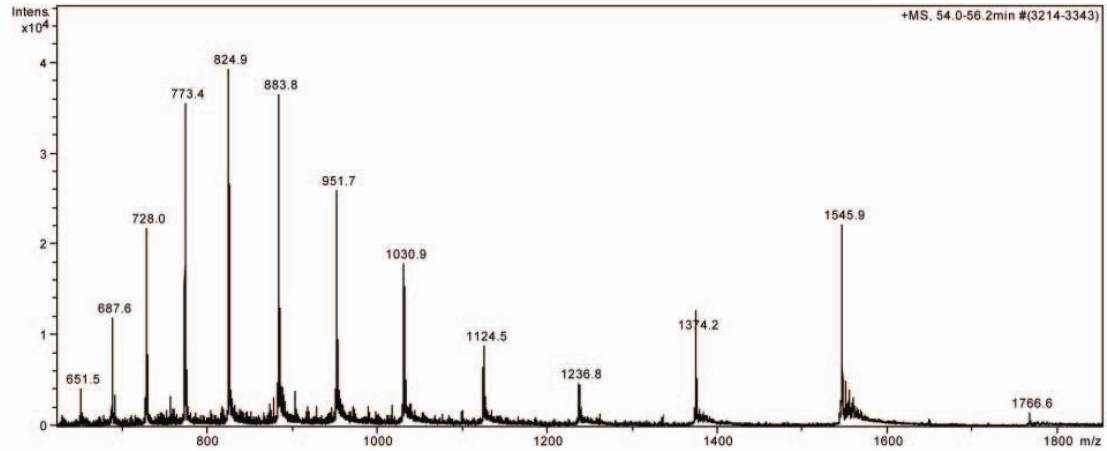

Figure 2.18. 20 µM Cyt-C in a 250 mM NaCl solution with a MD unite length of 2.4cm and the use of a nebulizer cross flow. Dialysis buffer of 10% methanol and 1% acetic acid.

In addition to characterizing the effectiveness of the MD unit's ability to remove NaCl from Cyt-C samples, the MD-nano-ESI device was tested with Cyt-C mixed in fresh neural cell culture media. Figure 2.19 illustrates how the high salt levels of culture media suppress the Cyt-C signal.

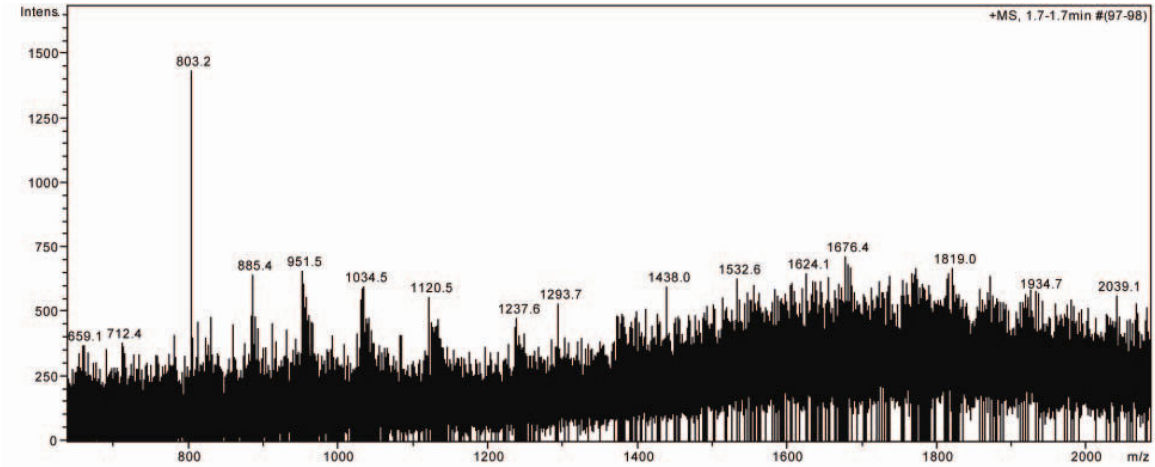

Figure 2.19. 20 µM Cyt-c in a neuronal cell culture media solution with no MD

When the MD unit and the perpendicular cross flow nebulizer gas were incorporated, the Cyt-C could clearly be distinguished from the cell culture media with an excellent peak intensity corresponding to Cyt-C (Figure 2.20).

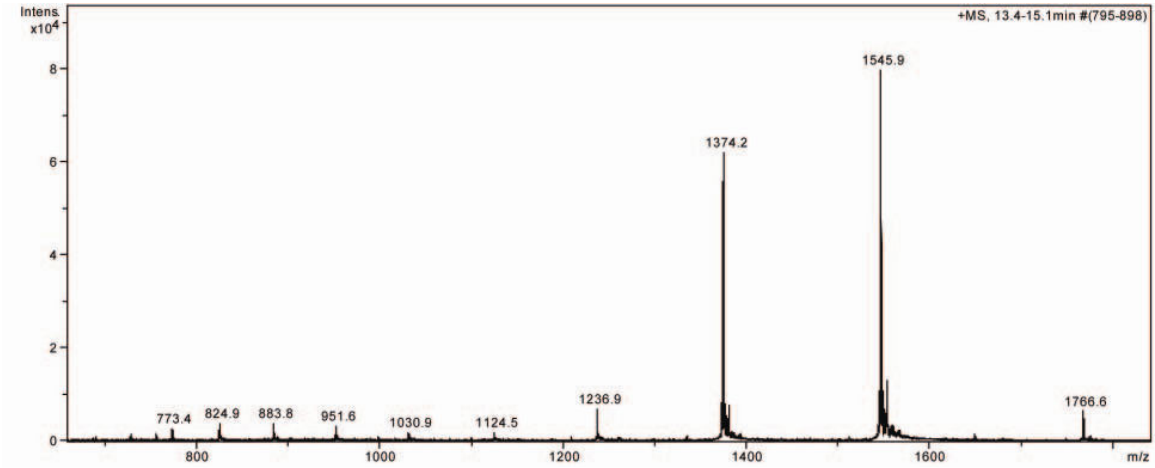

Figure 2.20. 20 µM Cyt-C in neuronal cell culture media solution with a MD unit length of 2.4cm and the use of a nebulizer cross flow.

Some of the key issues that were encountered when running high salt concentration Cyt-C samples with MD nano-ESI included analyte suppression due to salt contamination, inconsistent signal, and limited run time due to clogging at the emitter tip. By varying the MD unit length, changing the dialysis buffer's solvents, and modifying the spray tip conditions these issues were overcome. The most consistent, adduct free spectra and clog free MS runs were obtained by lengthening the MD unit to 3.5 cm, using a dialysis buffer consisting of only 1% acetic acid, using a 75 µm ID, 360 µm OD, 15 µm Tip ID emitter, and using a low pressure nebulizer gas cross flow across the emitter tip (Figure 2.21).

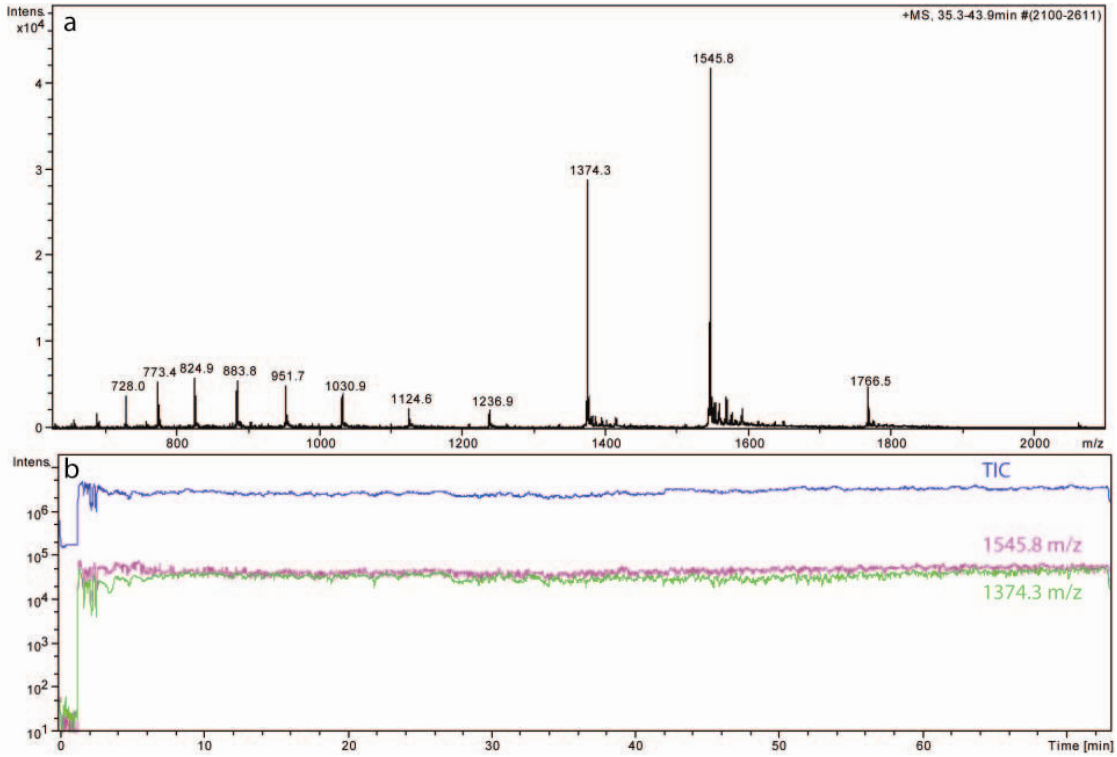

Figure 2.21. Typical performance of a MD-nano-ESI device. 10 µM Cyt-C in neuronal cell culture media solution with a MD unit length of 2.4cm and the use of a nebulizer cross flow and a 1% acetic acid dialysis buffer.(a) Averaged spectrum of the sample.(b) Chromatogram demonstrating steady signal obtained with MD-nano-ESI MS.

2.4. Discussion

The MD unit experimental testing demonstrated that salt content can effectively be removed. Theoretical analysis of the unit based on principles of mass transfer predicted that both increasing the length of the MD unit and decreasing the sample flow rate would improve the salt removal. Experimental results demonstrated that increasing the MD unit's length provided significant improvements in the reduction of salt content in solutions. A length of 3.5 cm provided the greatest reduction while not greatly increasing the volume of the system.

The MD unit's capability of desalting samples while in-line with nano-ESI MS was clearly demonstrated. Samples that previously provided poor MS spectra and created emitter clogging, could now be effectively sampled and analyzed with the MS when first passed through the MD unit. The MD unit removed the deleterious effects of high salt concentration samples, reduced clogging issues, and increased the sensitivity of nano-ESI. The addition of a low flow rate nebulizer gas cross flow of nitrogen, also improved the peak intensities and reduced the occurrence of clogs. The nebulizer gas seems to improve desolvation of high salt concentration samples, and it has also eliminated the issue of salt precipitation at the tip of the emitter by blowing away droplets that contain few or no ions away from the tip. Ultimately the MD unit provides an effective method of analyzing high salt and complex samples that could otherwise not be analyzed by MS.

CHAPTER 3

SAMPLING PROBE AND 3-D CELL CULTURE MODEL OF LOCALIZED INJURY

The effectiveness of MD-nano-ESI MS was shown in Chapter 2, but samples were introduced directly to the system using a syringe loaded with the sample. In order to characterize and demonstrate the system's potential as a novel method of TBI biomarker discovery, the system's performance was examined in the context of cell cultures. The goal of this chapter is to demonstrate a sampling probe's ability to determine temporal and spatial information about a localized model injury. A model cell culture chamber and model of injury were developed and examined in order to demonstrate the probe's detection capabilities. The model was studied through theoretical concepts and experiments. In addition, the probe was inserted into 3-D neural cultures and samples were drawn with no adverse effects on the culture.

3.1. Local Marker Release Injury Model

A model to characterize the sampling probe's effectiveness in monitoring a localized release of a marker chemical was developed. This model represents a number of experimental possibilities, such as a local cellular release of biomolecules to the porous cell culture extracellular space (ECS) that may be used as markers for normal or pathological cell states. The model consisted of small polycarbonate cylinder with a 3.175mm ID and a 9.524mm OD (1/8" ID, 3/8" OD) with a length of 1cm. Two 10-32 Flat-Bottom NanoPorts (Upchurch Scientific, Oak Harbour, WA) were affixed to both top and bottom of the polycarbonate cylinder with Quick Set (JB Weld, Sulphur Springs, TX). Two 300μm holes were drilled on the side of the chamber and silica capillaries (150 μm OD, 50 μm ID) were inserted and affixed with Quick Set. Figure 3.1 shows a

schematic of the model injury chamber, and Appendix A gives a detailed protocol for the construction of the chambers.

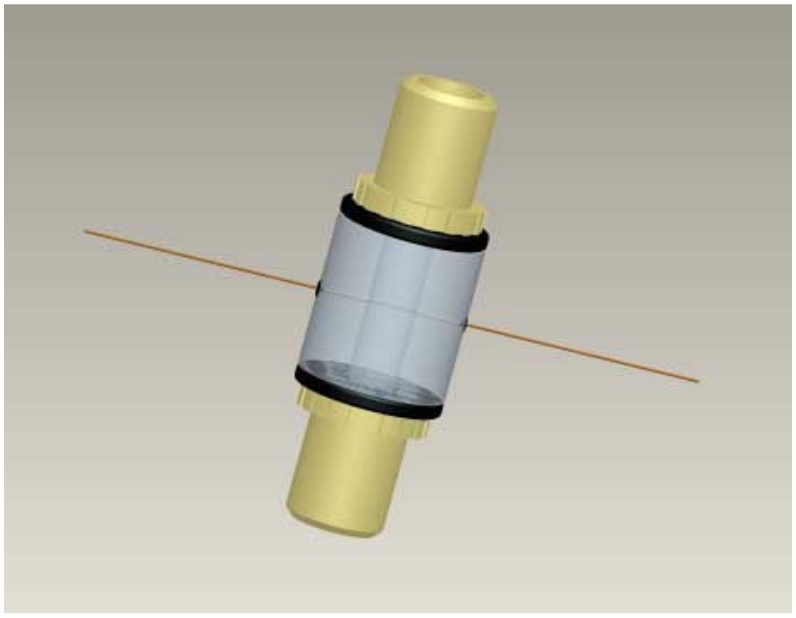

Figure 3.1. Model cell culture chamber constructed out of an extruded polycarbonate cylinder with NanoPorts and silica capillaries affixed to it.

The chamber was filled with agarose in order to represent the porous matrix used in cell culturing. Agarose is a gelatinous substance that is used in biological cell culture procedures, and its porosity can be adjusted based on its concentration. A 0.6% agarose concentration was used to obtain properties such as porosity and tortuosity similar to those found in the brain [48, 49]. The full experimental arrangement involves the connection of one silica capillary to the MD-nano-ESI device, and the other capillary connected to a plugged metallic union. At the bottom end of the chamber a silica capillary (150 μm OD, 50 μm ID) was connected to the NanoPort using a 190 μm ID Kel-F ferrule. The top NanoPort was connected to a syringe using a PEEK tubing (125 μm ID, 1/16" OD) and was secured using 10-32 Peek fingertight nut with a 1/16" ferrule that flows a bulk flow fluid. Figure 3.2 illustrates a schematic of the model injury experiment which was placed in front of the MS.

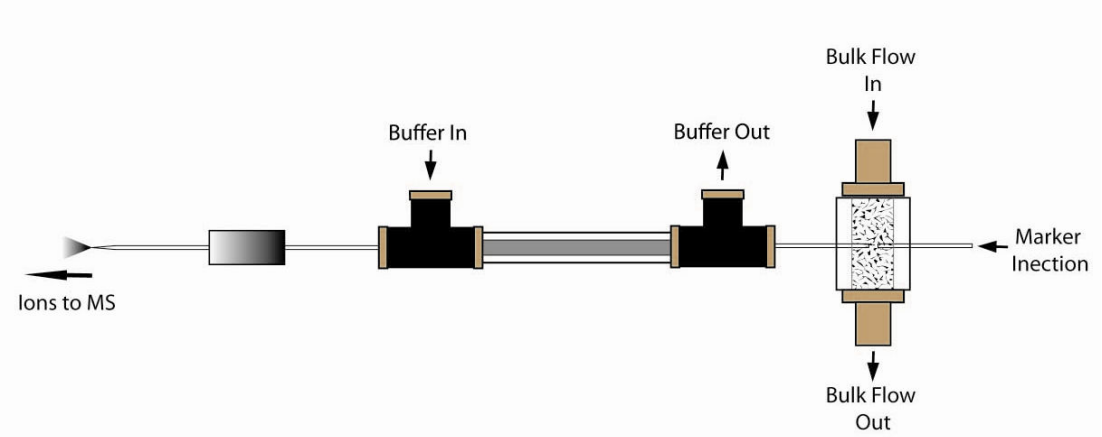

Figure 3.2. Schematic of the model cell culture connected in-line with the MD-nano-ESI device. Samples were continually collected and analyzed with MS. Flow is driven by the bulk flow into the chamber.

A syringe pump (KD Scientific, Holliston, MA) was used to flow a bulk liquid through the agarose matrix and out to the sampling probe and the bulk flow outlet at uniform flow rates. This was done to recreate conditions of 3-D cell cultures under conditions of bulk perfusion flow. Once a steady signal was achieved with the MD-nano-ESI MS analysis, the plug on the injection line was exchanged with a 10μL Hamilton syringe and 8 μL of a marker was injected into the system. The syringe was then removed and the line was immediately plugged. The injection creates a small sphere of marker within the agarose matrix. The sphere undergoes diffusion and advection overtime, which alters the concentration in the solution sampled by the probe. This injury model was studied both theoretically and experimentally.

3.2. Local Marker Release Model Theory

The model of a localized injury can be analyzed based on the principles of mass transport in porous matrix. The resulting theoretical description provides a prediction of marker transport in agarose with bulk flow.

3.2.1. Theoretical Model

Diffusion can be described by Fick's law of diffusion, Equation ((3.1)

$$\boldsymbol{j} = -D\nabla c \tag{3.1}$$

where $\boldsymbol{j}$ is the mass flux, D is the diffusion coefficient , and c is the mass concentration. A partial differential equation describing transient diffusion can be derived from the *continuity equation*, for a concentration $\boldsymbol{c(r}, t)$ at position $\boldsymbol{r}$ and time t, and is coupled to a flux $\boldsymbol{j(r}, t)$ and a source density $s(\boldsymbol{r}, t)$.

$$\frac{\partial c}{\partial t} + \nabla \cdot \boldsymbol{j} = s \tag{3.2}$$

A relationship between the flux ($\boldsymbol{j}$), and the concentration ($\boldsymbol{c}$) can be achieved from Fick's law, Equation (3.1), and incorporation of an advection term, $\boldsymbol{v}$,

$$\boldsymbol{j} = -D\nabla c + \boldsymbol{v}c \tag{3.3}$$

Combining equations (3.2) and (3.3) give the transient advection diffusion equation

$$\frac{\partial C}{\partial t} = D\nabla^2 C - \boldsymbol{v} \cdot \nabla C + s \tag{3.4}$$

Mass transport in porous matrix is affected by the presence of two phases, the permeable and the impermeable. A porous matrix creates a discontinuous concentration profile, which means Equation (3.4) cannot be applied. In order to overcome the discontinuities, volume averaging is used. The entire volume that is being considered is defined by V, and the representative ECS, which is the phase where diffusion will occur, will be defined by V_o. With these two terms, the parameter of *volume fraction* (porosity), α, is defined by

$$\alpha = \frac{V_o}{V} \tag{3.5}$$

For porous matrix, the mass flux, Equation (3.3) becomes

$$\boldsymbol{j} = -D^*\nabla c + \boldsymbol{v}^* c \tag{3.6}$$

where $D^* = D/\lambda^2$, λ is the tortuosity of the porous matrix, and $\boldsymbol{v}^* = \boldsymbol{v}/\alpha$. Inserting the expression for the mass flux in a porous matrix into the advection diffusion equation and dropping the source term yields [50].

$$\frac{\partial C}{\partial t} = D^*\nabla^2 C - \boldsymbol{v}^* \cdot \nabla C \tag{3.7}$$

In the case of the local release injury model, a finite quantity of marker is injected into the system and it fills an initial volume in the porous matrix [51]. For the case of porous matrix, we assume that the marker uniformly fills a sphere with a radius of

$$b = \left(\frac{3U}{4\pi\alpha}\right)^{1/3} \tag{3.8}$$

where U is the volume of the fluid injected into the porous matrix. We analyze an idealized conceptualization in which this uniform sphere is instantaneously placed in a uniform steady flow, $\boldsymbol{v}^* = u$. We neglect the effect of the presence of the walls and treat the domain as unbounded, with vanishing concentration far from the injection site. The resulting model is solved through application of a coordinate transformation [52]. The advection term is removed by transforming to a translating coordinate system: $\eta = z - ut$. The transformed boundary and initial conditions posses a spherical symmetry, and hence the resulting transient diffusion equation is cast in a spherical coordinate system, with radial coordinate r (requiring the addition of the constraint that the solution remain bounded at the origin). The solution in the transformed coordinate system is

$$C = \left(\frac{C_f}{2}\right)\left[\operatorname{erf}(f_+) - \operatorname{erf}(f_-) + \frac{2}{\lambda r}\sqrt{\frac{Dt}{\pi}}\left[\exp(-f_+^2) - \exp(-f_-^2)\right]\right] \tag{3.9}$$

where C_f is the concentration of the injected volume and $f_\pm = (r \pm b)\lambda/2\sqrt{Dt}$. When returned to the original coordinate system, the solution retains cylindrical symmetry, and can be still written as in Equation (3.9) with $r = \left(\sqrt{(z-ut)^2 + \rho^2}\right)$ and $f_\pm =$

$(r \pm b)\lambda/2\sqrt{Dt}$, where ρ is the radial coordinate in a cylindrical coordinate system. Figure 3.3 demonstrates the coordinate system in the model injury chamber.

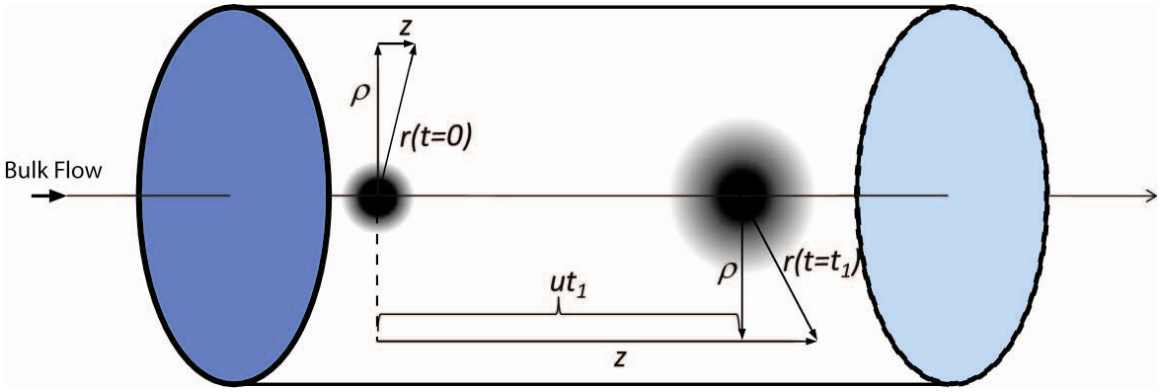

Figure 3.3. Schematic demonstrating the coordinate system for the model cell culture.

3.2.2. Model Results

Using Equation (3.9) the theoretical results of the injury model were examined with a small bulk flow and an instantaneous injection of Cyt-C. The incorporation of both the effects of diffusion and advection must be considered. This is indicated by the system's Péclet number, which is given by Equation (3.10).

$$Pe = \frac{uL_s}{D} = Re \cdot Sc \tag{3.10}$$

where u is the velocity of the fluid, L_s is the characteristic length, and D is the mass diffusion coefficient. The Péclet number is the ratio of the rate of advection of a physical quantity by the diffusion of the same quantity. For the injury model, Table 3.1 shows the flow conditions and the chamber dimensions.

Table 3.1. Model injury conditions and dimensions.

Bulk Flow rate ($\dot{Q}_{bulk}$)	60 μL/hr
Marker Injection Capillary ID ($\varphi_{i,cap}$)	50 μm
Chamber ID ($\varphi_{i,chaber}$)	3.175 mm
Cyt-C Diffusion Coefficient [53]	1.50×10^{-10} m^2/s

The equivalent velocity of the system was calculated by Equation (3.11)

$$u_e = \frac{\dot{Q}_{bulk}}{\alpha A} = u \tag{3.11}$$

where $A=\pi\ (\varphi_{i,chaber})^2/4$, *and* α is the porosity of the agarose which is 0.98 [54]. For the conditions given in Table 3.1 $u_e = 2.14 \times 10^{-6}$ m/s. Laminar flow can be assumed due to the low Reynolds number of 6.81×10^{-3}, which was calculated from equation (2.1), with a ν of 1×10^{-6} m^2/s. In addition the flow can be assumed to be fully developed by equation (2.2). A tortuousity of 1.6 was used for all of the calculations [55].

The Peclet number was calculated to be 0.714 using equation (3.10), when L_s is equal to the ID of the injection capillary. Since the Péclet number is ~ 1, it can be concluded that the transport of the Cyt-C in the injury model is driven by both diffusion and advection. In addition the capillaries for the sampling probe and the marker injection were both assumed to have no effect on the diffusion of marker, and it was also assumed that the walls of the chamber were far enough away from the marker injection site for their effects to be neglected. These assumptions were made for ease and generality of

analysis. Figure 3.4 shows the solution to equation (3.9) at various time points along the axial (z) direction of the chamber.

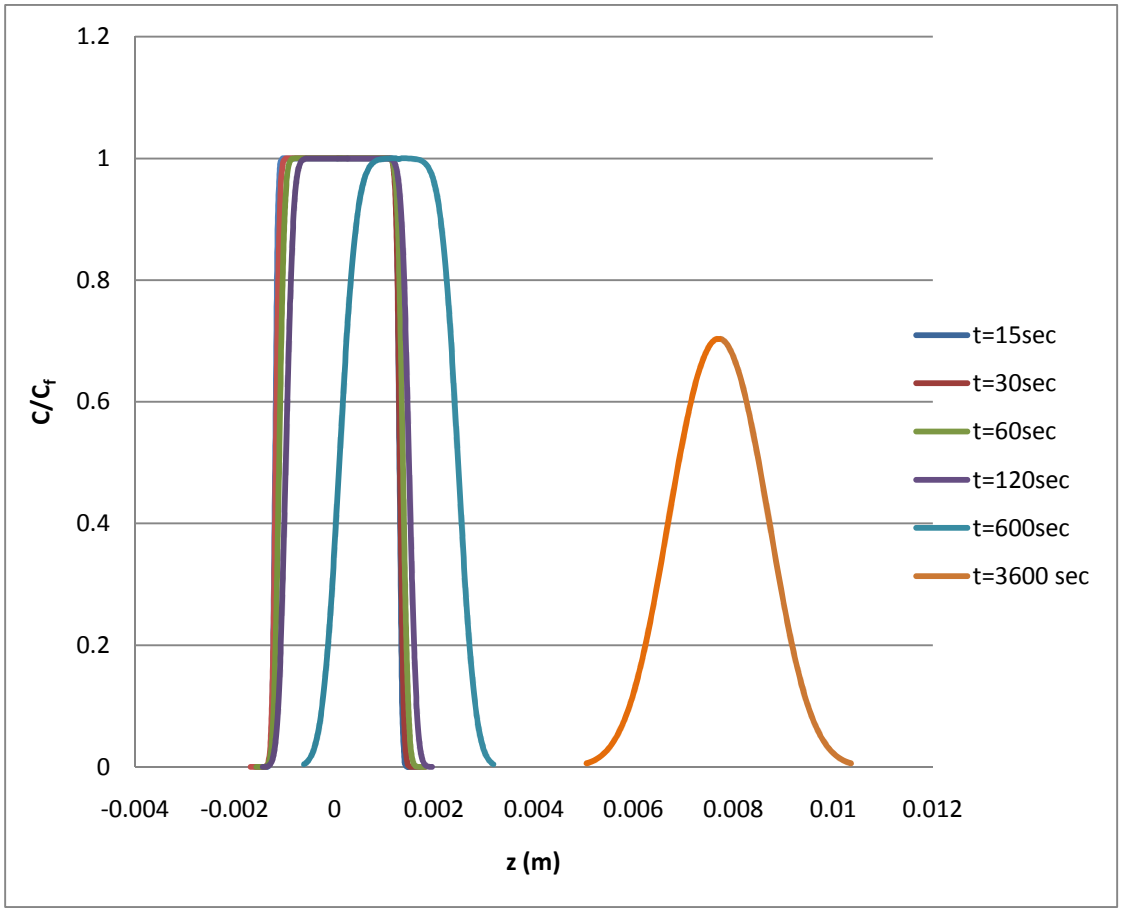

Figure 3.4. C/C_f with respect to axial position in a chamber filled with 0.6% agarose porous matrix at various time points. The injection of 8 µL origin is at z=0 and each series shows the concentration profile of the Cyt-C in the z-direction at different time points.

Figure 3.5 shows the change in concentration at a given point with respect to time using Equation (3.9).

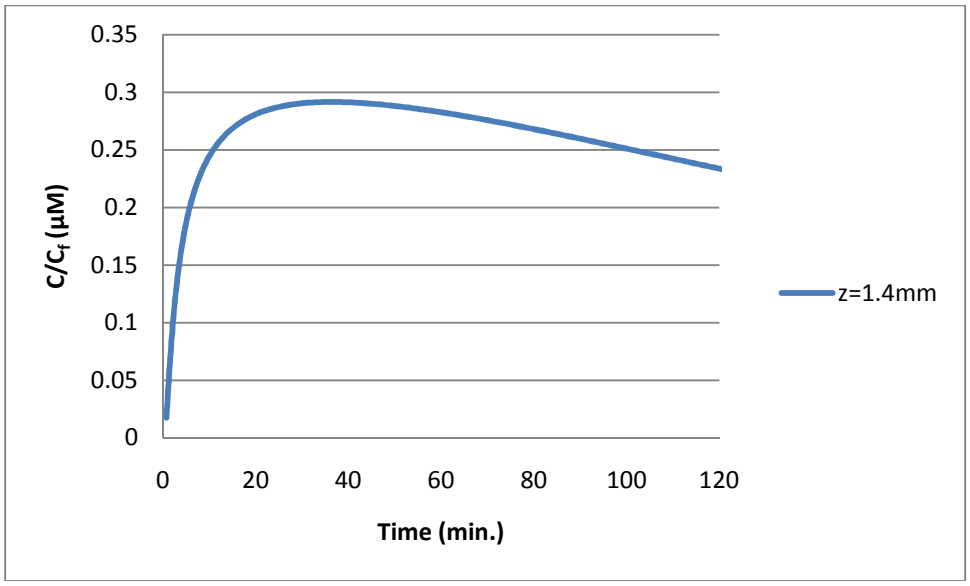

Figure 3.5. C/C_f with respect to time for a 8 μL injection of Cyt-t into 0.6% agarose porous matrix at a fixed distance of 1.4mm downstream of the injection point.

The theoretical analysis provides a simplified model of the transport of Cyt-C within porous matrix under the influences of both diffusion and advection. Estimates of the time it will take Cyt-C to reach the sampling probe at various positions in the chamber, and the concentration profile of the marker injection in chamber can be made with the above analysis.

3.3. Injury Model and Probe Experiments

Experiments were conducted under similar conditions to those analyzed using the theoretical model. Visualization experiments were conducted with dye before moving onto analysis with MS.

3.3.1. Dye Injection Study

Experiments were first conducted to observe the injection of a dye marker into a porous matrix. 0.25% Bromophenol blue was used as the marker in order to provide easy visualization of the injection and has been previously used to study molecule transport through the brain [48]. These experiments were conducted in modified planar chambers, which improved the visibility of the injected marker under a digital microscope (VHX-500F, Keyence, Osaka, Japan). The exact dimensions for the planar chambers can be found in Appendix B. The dimensions were chosen so that the planar chambers maintained equivalent flow conditions as the cylindrical chambers. Figure 3.6 shows a schematic of a planar chamber.

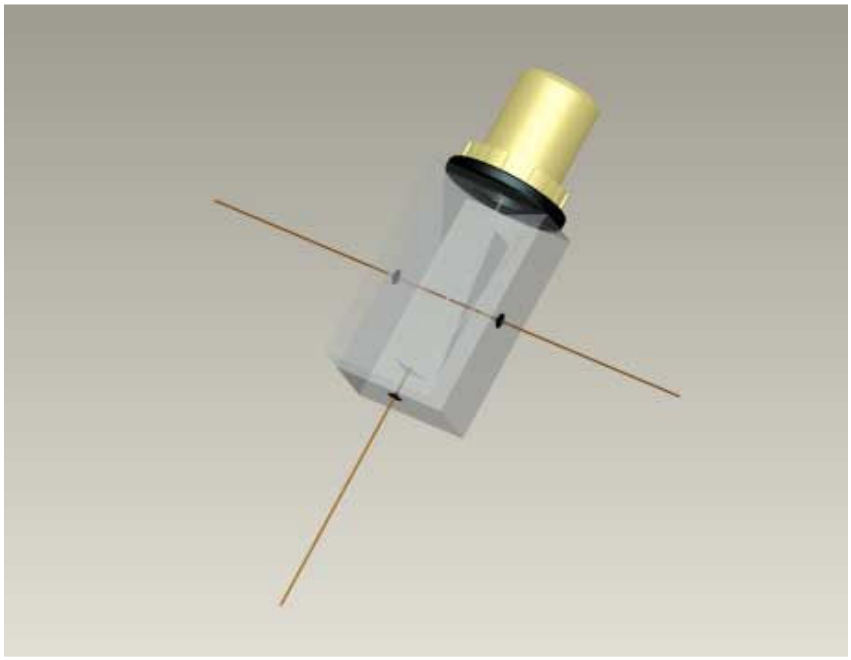

Figure 3.6. Schematic of the planar chamber. The cylindrical cell culture chamber was modified to this planar version for dye injection studies.

The porous matrix of 0.06% agarose was used to fill the chamber, and a sampling probe and injection capillary were inserted into its sides (50 μm ID, 150 μm OD, silica

capillaries), a silica capillary (50 μm ID, 150 μm OD) was inserted into the bottom of the chamber, and a NanoPort was affixed to the top of the chamber for the bulk flow. A flow rate of 60 μL/hr was used as the bulk flow and a volume of 5μL of Bromophenol blue was injected into the system. Figure 3.7 shows the injection study experiment.

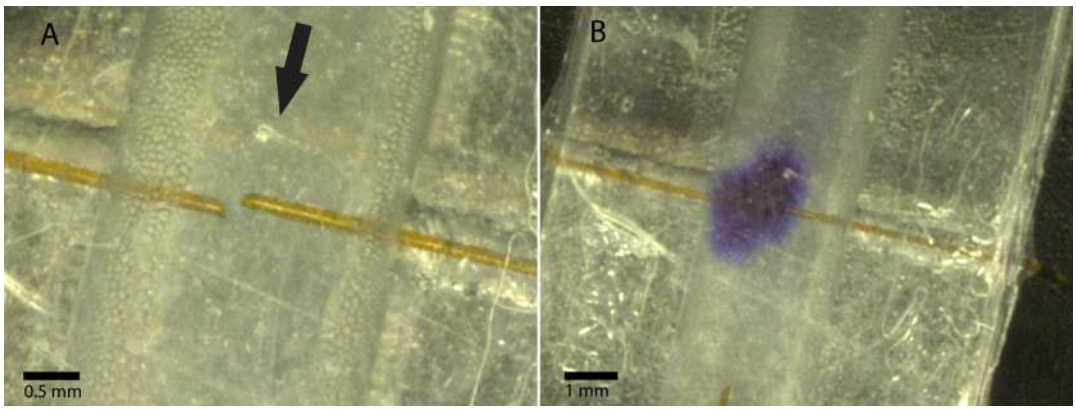

Figure 3.7. Dye injection experiments. The arrow denotes the direction of the 60 μL/hr bulk flow. The capillary on the left side of the chamber is the injection capillary. (A) Image of planar chamber filled with 0.6% agarose before injection. (B) Image of planar chamber immediately after 5 μL of dye was injected.

From Figure 3.7(B), the radius of the injection was approximated to be 1.01mm. According to Equation (3.8), the theoretical results the radius should be 1.07mm for an injection of 5 μL in a porous matrix of 0.98 porosity. Other observations that were seen during the dye experiments included the occasional release of air bubbles prior to the introduction of dye as seen in Figure 3.8.

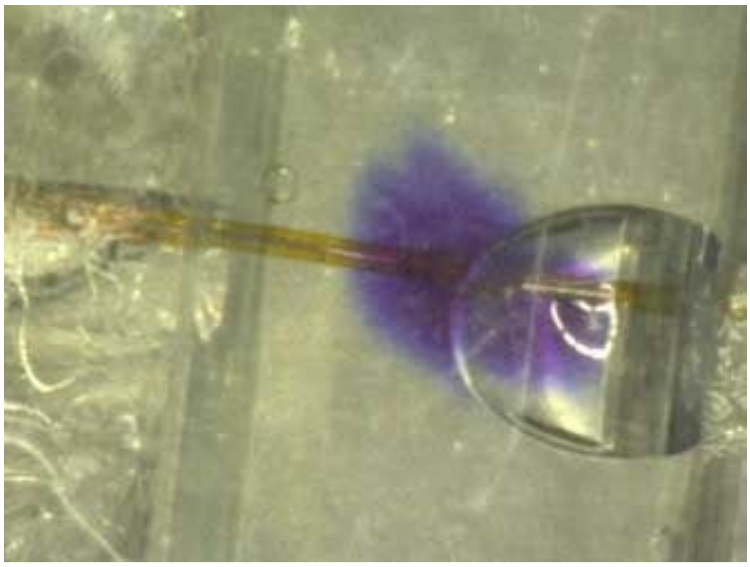

Figure 3.8. Image of an air bubble released before dye exited the injection capillary.

It was also observed that the transport of the marker downstream of the injection point is not entirely uniform as the model predicts. Figure 3.9 shows the continuous injection of a marker at a set flow rate of 30 μL/hr over 8.5 minutes. It was observed that downstream of the droplet, a stream of dye has moved away from the droplet. This may be due to the heterogeneity of the porous matrix where some areas may permit a larger velocity which allows for a quicker transport of dye through the matrix.

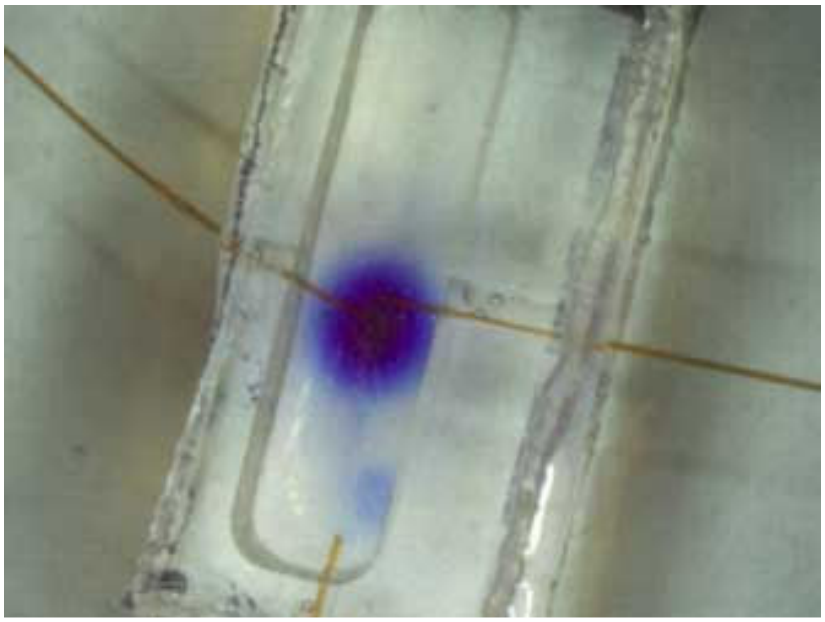

Figure 3.9. Image of dye at 8.5 minutes after initial introduction. A stream of dye can be seen coming off of the droplet. The dye was continuously introduced into the chamber at a flow rate of 30 μL/hr.

The dye experiments provided a visual understanding of the type of transport an injection of a marker will undergo during experimental MD-nano-ESI MS analysis. Ideally the marker transport would behave similarly to the theoretical model previously discussed. It was determined from the dye experiments that the theoretical model may be too simple to accurately predict the transport of marker molecules through a porous matrix. Factors such as air bubbles in the injection capillary, and irregularities in the porous matrix may alter the transport of molecules through the porous matrix. In addition the assumption that the effects from the chamber walls and capillaries could be neglected was most likely inaccurate and should be incorporated into the model for future studies. These discrepancies between the theoretical model and the behavior of the model injury become more evident in the MS experimental results.

3.3.2. Experimental Assembly

The injury model and the MD-nano-ESI probe were assembled as described in section 3.1. Cyt-C was injected into the chamber and the MD-nano-ESI-MS probe continually sampled and analyzed liquid taken from within the porous matrix. The bulk flow through the chamber was set to 60 μL/hr and initially the injection capillary was plugged. Before injecting the sample, the injection capillary is unplugged and the marker is introduced via 10 μl syringe. Immediately after the injection the capillary is plugged.

3.3.3. Agarose Experimental Results

Different concentrations and probe placements were examined to demonstrate the probe's capability of deciphering between different concentrations and probe placement locations in agarose. Model chambers were made with the injection capillary within 100μm to the sampling probe capillary. Figure 3.1 shows a schematic of the chamber model with adjacent capillaries. This is well within the spherical space of the injected marker and one can expect similar results to the dye experiments of Figure 3.7.

Another set of chambers were constructed where the two capillaries were offset by 1.4mm in the z-direction of the cylindrical chamber. The sampling probe was place downstream of the injection probe. Figure 3.10 shows a schematic of the chamber model with offset capillaries.

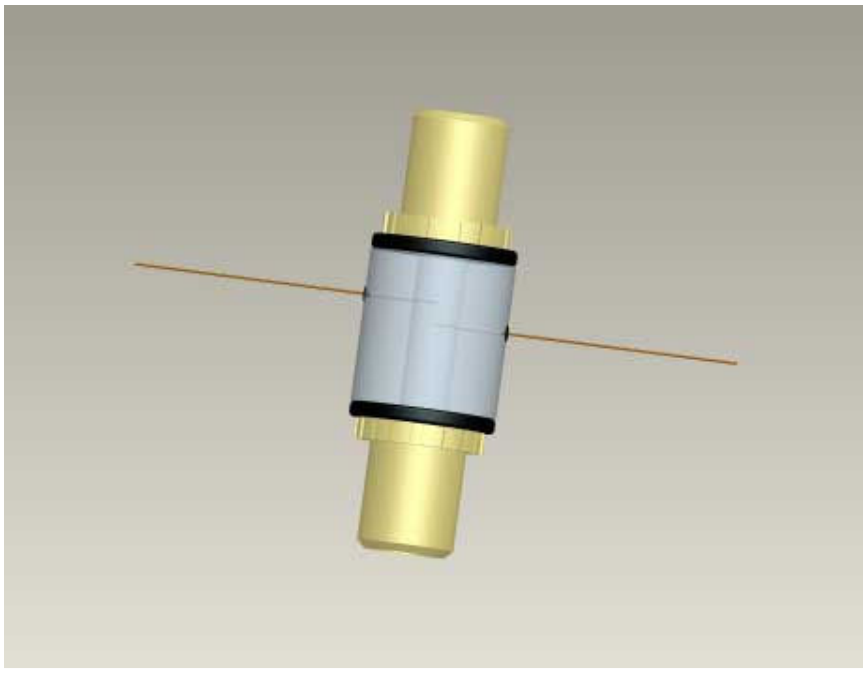

Figure 3.10. Schematic of model injury chamber with the sampling probe offset by 1.4mm downstream of the injection capillary.

Two different concentrations were used for both adjacent and offset probe placements: 30μM and 5μM of Cyt-C. For each concentration, 8 μL of marker was injected into the porous matrix. The probe continuously sampled and the MS provided chromatograms and spectra for the samples. Below in Figure 3.11 and Figure 3.12 are the results for both the adjacent set of experiments compared to the offset experiments.

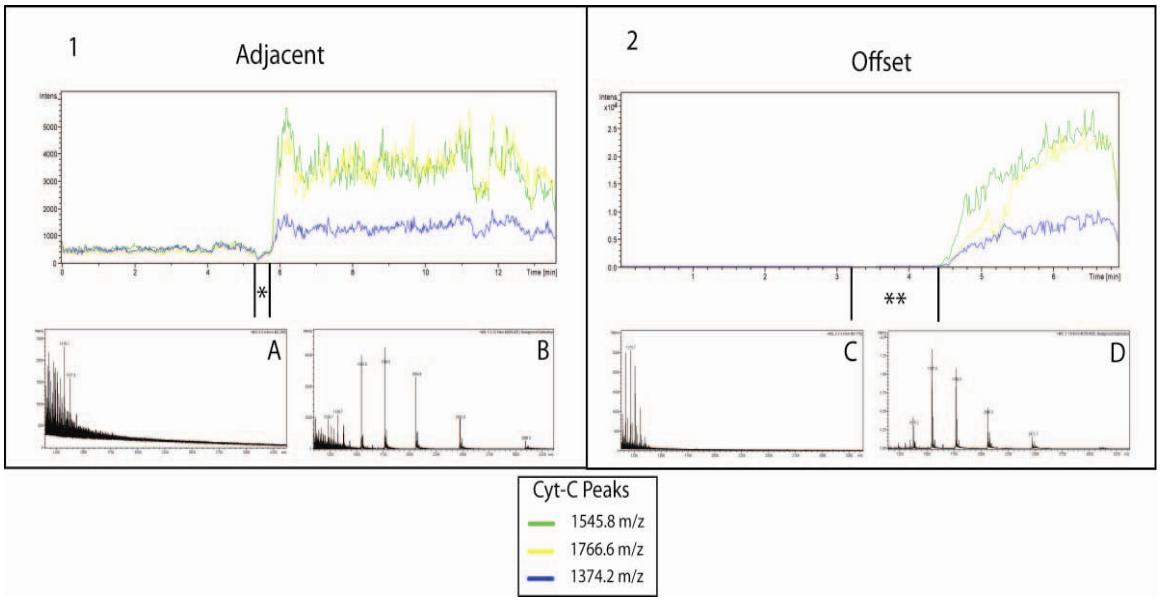

Figure 3.11. MS chromatograms and spectra from continuous in-line analysis with MD-nano-ESI of 8 µL injections of 30 µM Cyt-C. (**1**) A model chamber with adjacent sampling probe showed a nearly immediate detection of Cyt-C. The wait time (*) was less than 30 seconds. (A) is an averaged spectrum of the chromatogram before the injection. (B) is an averaged spectrum of the chromatogram post marker injection, with spectrum A subtracted out as background noise. (**2)** A model chamber with 1.4mm offset capillaries showed a delay (**) of approximately 72 seconds and a more gradual increase in intensity on the chromatograms. (C) is an averaged spectrum of the chromatogram before the injection. (D) is an averaged spectrum of the chromatogram post marker injection, with spectrum C subtracted out as background noise.

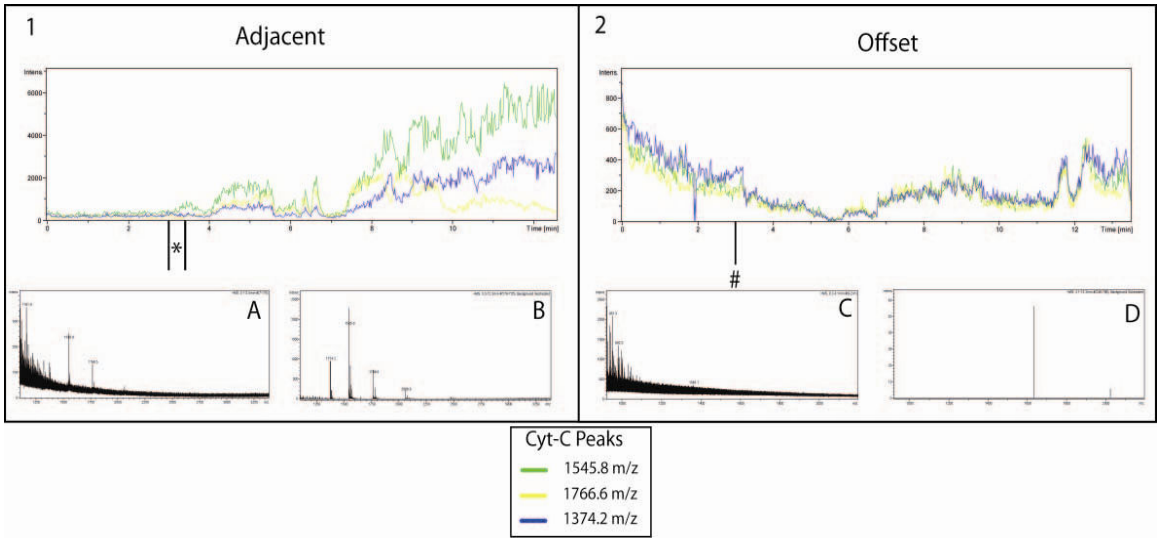

Figure 3.12. MS chromatograms and spectra from continuous in-line analysis with MD-nano-ESI of 8 µL injections of 5 µM Cyt-C. (**1**) A model chamber with adjacent sampling probe showed a nearly immediate detection of Cyt-C. The wait time (*) was less than 30 seconds. (A) is an averaged spectrum of the chromatogram before the injection. (B) is an averaged spectrum of the chromatogram post marker injection, with spectrum A subtracted out as background noise. (**2)** A model chamber with 1.4mm offset capillaries, and an injection (#) at 3 minutes. There was no detection of Cyt-C with the probe throughout the entire experiment. (C) is an averaged spectrum of the chromatogram before the injection. (D) is an averaged spectrum of the chromatogram post marker injection, with spectrum C subtracted out as background noise.

Although the adjacent probes show a slight delay, this can be accounted for by the volume of the MD-nano-ESI device. The injection also introduces a slight increase of pressure into the system which affects the performance of the nano-ESI emitter. The sampling probe's experimental results were comparable to the theoretical results. The adjacent probes showed a nearly immediate increase in the signal for Cyt-C. The 30µM Cyt-C injections showed a delay of 72 seconds which was quicker than the theoretical delay of 90 seconds for the same concentration and volume of Cyt-C to become detectable on the MS. This quicker response may have been due to the irregularities observed in the dye experiments. An air bubble may have displaced Cyt-C further downstream for the quicker detection time, or a stream of Cyt-C may have flowed off of the initial droplet similar to Figure 3.9. In addition, it is very difficult to determine the

relative concentrations measured by the MS. One can observe that the adjacent probe spectrum shows a lower peak intensity than the offset probe placement. According to the theoretical predictions the concentration at the offset probe should be about 5 times less than the adjacent probe concentration. This may be due to inconsistencies in the nano-ESI conditions. Small variations in the experiments may have lead to different Cyt-C ionization efficiencies and hence the different peak intensities. It is difficult to verify experimentally with MS the concentration which is being sampled.

The lower concentration experiments with 5 μM Cyt-C also showed a slight delay in the adjacent capillary chamber which agreed with the 30 μM concentration injury model and the theoretical analysis. The offset probe chamber showed no increase or detection of Cyt-C. The theoretical analysis showed 5 μM of Cyt-C at a volume of 8μL would reach the emitter, but its concentration would never reach above 1.46 μM of Cyt-C which was not detectable under these experimental conditions. The lower concentration did show lower peak intensity when compared to the 30 μM sample but, once again, it is difficult to decipher information regarding concentration from only the Cyt-C peak intensities.

3.4. Matrigel Experimental Results

Similar to the experiments in the previous section, chambers were filled with Matrigel (BD Biosciences, Sparks, MD) instead of agarose and the sampling probe was placed within 100 μm of the injection capillary. These experiments were conducted in order to determine whether MD-nano-ESI MS could detect Cyt-C from within a more biologically complex porous matrix. All experimental variables were the same as the agarose experiments other than the Matrigel. Figure 3.13 shows the results of MD-nano-ESI MS analysis from within Matrigel.

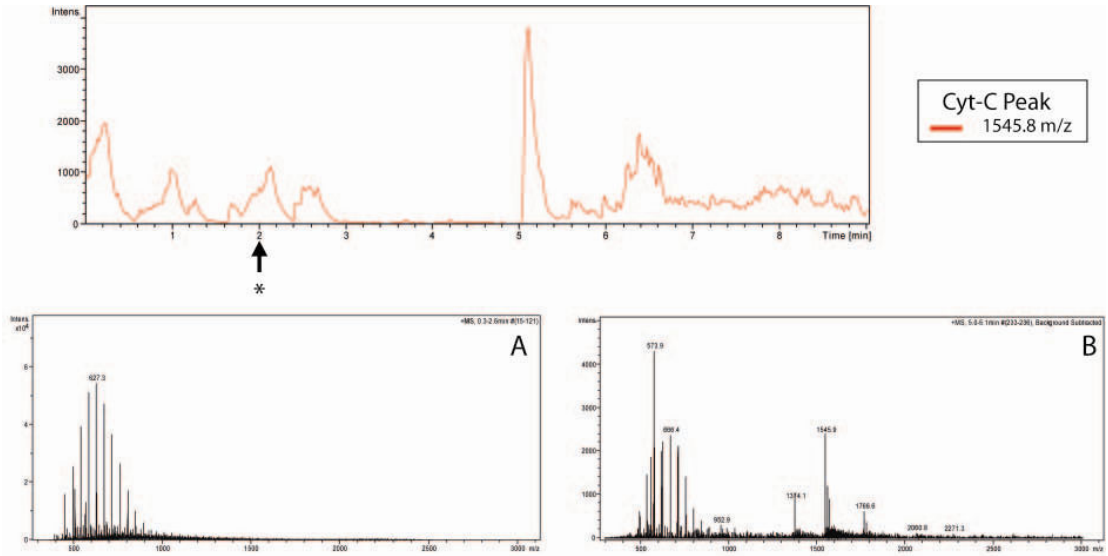

Figure 3.13. MS chromatogram and spectra from continuous in-line analysis with MD-nano-ESI of 8 µL injection of 30 µM Cyt-C in a Matrigel filled chamber. The injection (*) occurred at 2 minutes and signal was lost from 3-5 minutes. Spectra (A) is an averaged spectrum of chromatogram before the injection. At 5 minutes, when signal was regained, Cyt-C peaks were apparent. Spectrum (B) is an averaged spectrum of the chromatogram from 5-5.5 minutes with the spectrum (A) subtracted out as background.

Cyt-C detection with MD-nano-ESI was successful, but detection was delayed from a loss of signal post injection. Maintaining a steady nano-ESI signal was more difficult in the Matrigel experiments, there was an increase in the amount and intensity of back ground noise peaks, and there was more Cyt-C suppression. This is all due to the increase in the complexity of the porous matrix. The MD unit's effectiveness to clean samples prior to nano-ESI proved to be insufficient to provide consistent results for sampling within Matrigel.

3.5. In-Vitro Probe Placement and Sampling

Mixed primary cortical neural cultures in Matrigel were plated in the model cell culture chambers at a density of 4000 cells/μL. A porous piece of polyethylene was inserted into the bottom of the chamber in order to provide the cultures a uniform surface. The cultures were examined to determine if the probe had any adverse effects on the culture. It was determined that the probe inserted into the culture had no effect on the cells in the culture in terms of acute cell death. In addition a bulk flow of NEUROBASAL media was perfused through the cultures to determine if sample collection through the probe would cause cell death or create discrepancies in the cultures. Figure 3.14, Figure3.15, and Figure 3.16 show mixed neural cultures in the chambers under different conditions. To determine how cells reacted to probe placement and perfusion a live/dead was conducted on the cultures using calcein AM and ethidium homodimer-1 (Sigma Aldrich, St. Louis, MO). Live/dead cell viability staining is an easy and sensitive method of determining whether cells were able to withstand probe insertion and perfusion. Calcien AM is cleaved by esterases in live cells to yield cytoplasmnic green fluorescence, and membrane-impermeant ethidium homodimer-1 labels nucleic acids of membrane-compromised cells with red fluorescence. The treated cultures are placed under EPI fluorescence light under an upright microscope (Nikon Eclipse 80i, Melville, NY), and images were captured with a MicroFIRE microscope camera (Optronics, Goleta, CA).

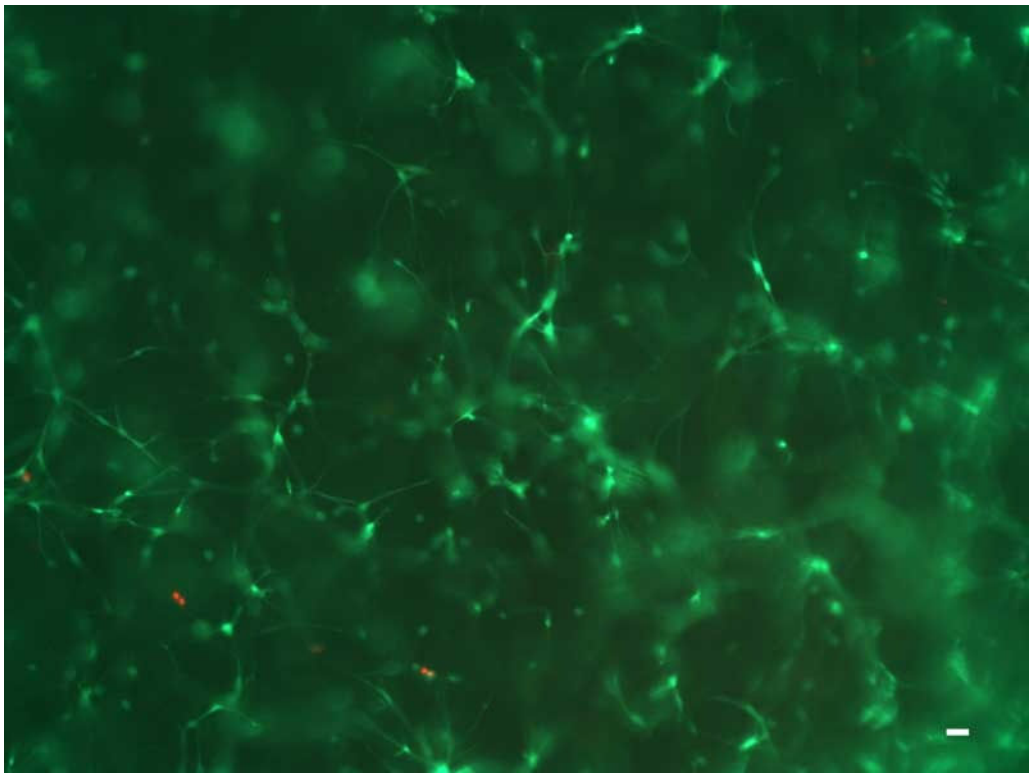

Figure 3.14. Four day old mixed neural cultures in Matrigel plated in a model cell culture with no probe or perfusion. Scale bar is 25 μm.

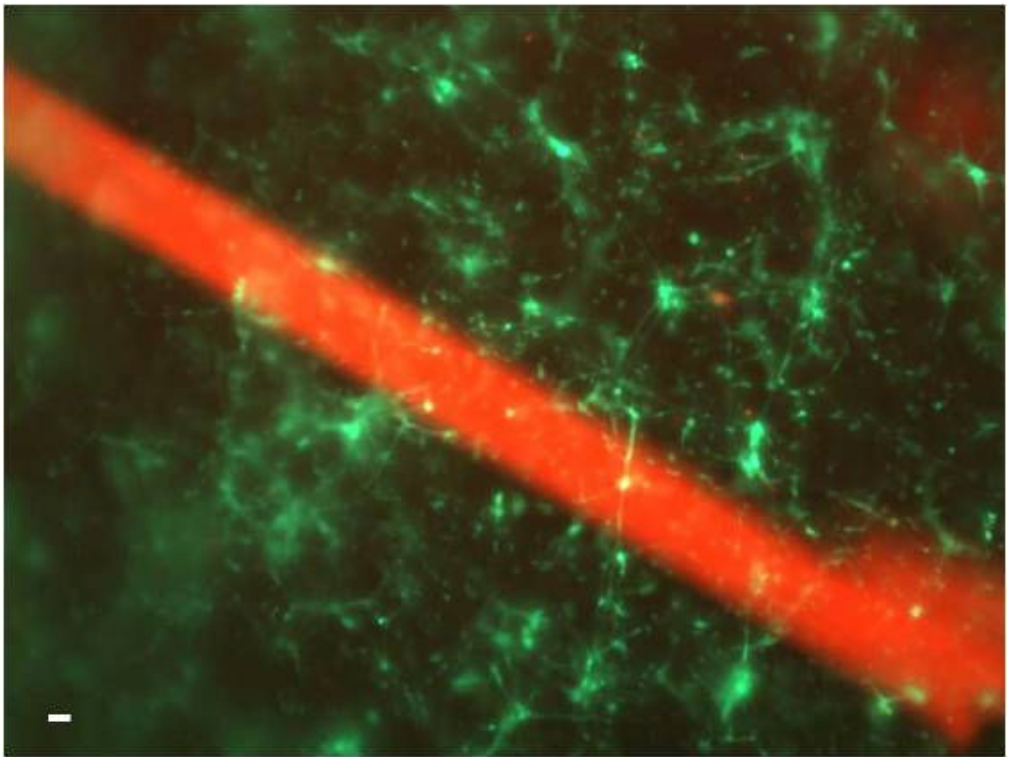

Figure 3.15. Four Day old mixed neural cultures in Matrigel plated in a model cell culture with probe and no perfusion. Scale bar is 25 μm. The sampling probe is the large red line across the image.

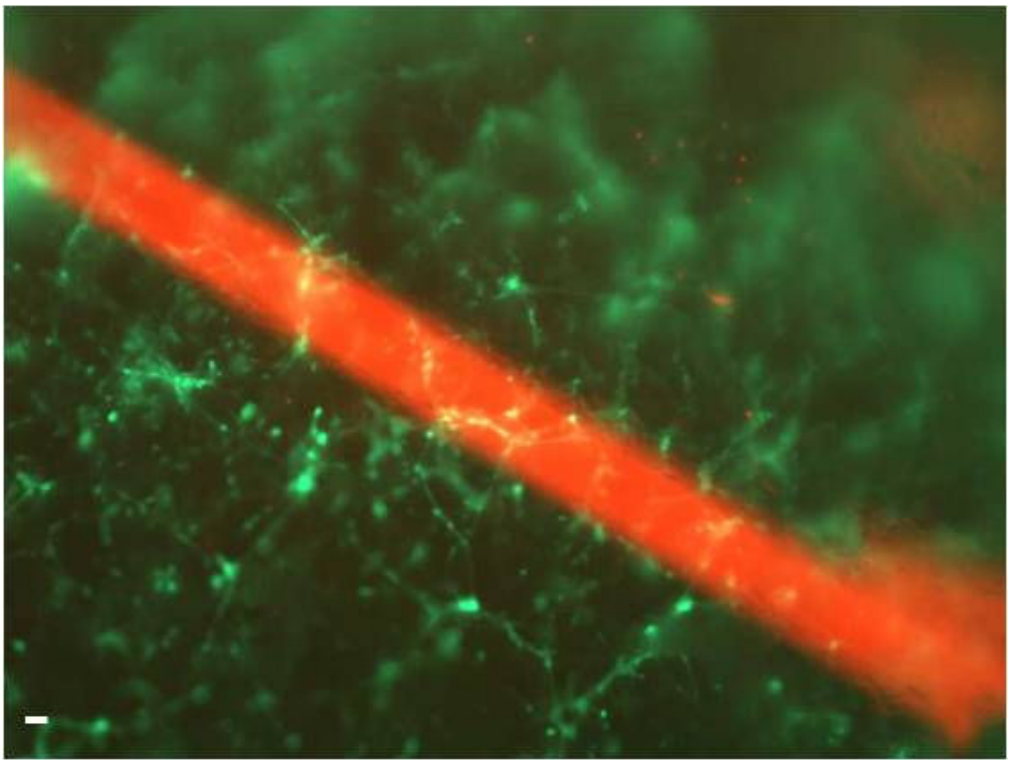

Figure 3.16. Four day old mixed neural cultures in Matrigel were perfused with fresh NeruoBasal media for 15 minutes and liquid was allowed to flow through the sampling probe. Cultures were placed back in incubator overnight and a live dead was conducted. Scale bar is 25 μm. The sampling probe is the large red line across the image.

The live dead staining on the cell cultures showed that introduction of the probe and sampling had no adverse effects on the cell cultures. All three cultures had similar amounts of dead cells (red fluorescence) and cell growth appeared to be similar. This demonstrates that using the probe for sampling will have little effect on the cells and should not affect experimental results in the short term. In addition, it was shown that the probe was capable of obtaining samples without clogging for the fifteen minutes of the perfusion.

3.5.1. Cell Culture Local Injection Experimental Results

As demonstrated in the previous section, sampling from within cell cultures with a small silica capillary was possible with no noticeable effects to the cells and no clogging. Mixed 3-D neural cultures in Matrigel were plated into chambers, and the sampling probe was placed within 100 µm of the injection capillary. These experiments were conducted in order to determine whether MD-nano-ESI MS could detect Cyt-C from within a neural cell culture. All experimental variables were the same as the agarose and matrigel experiments. Figure 3.17 shows the results of the MD-nano-ESI MS analysis within mixed 3-D neural cultures.

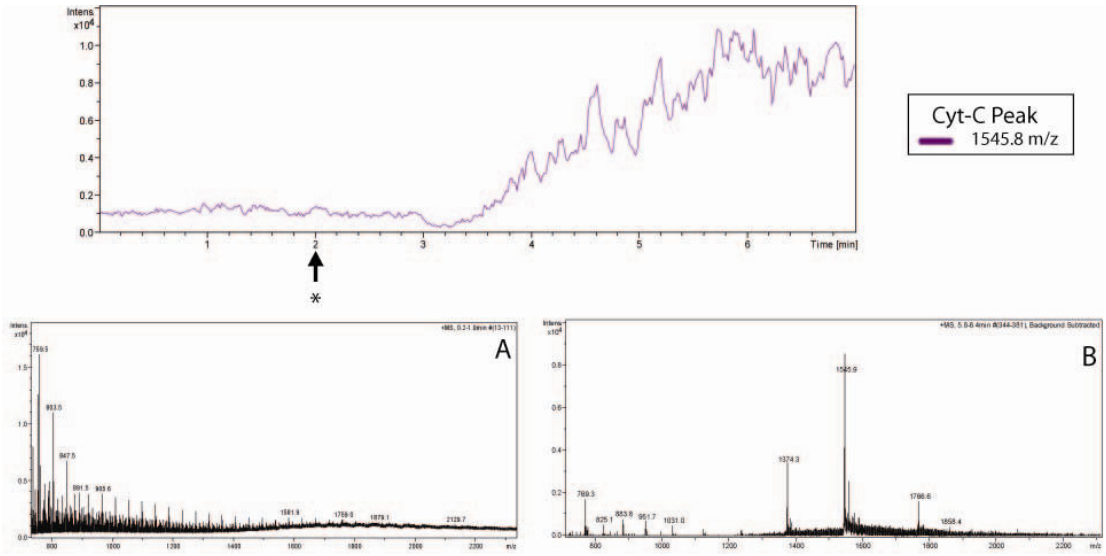

Figure 3.17. MS chromatogram and spectra from continuous in-line analysis with MD-nano-ESI of 8 µl injection of 30 µM Cyt-C in a chamber filled with a mixed 3D neural cell culture. The injection (*) occurred at 2 minutes. Spectra (A) is an averaged spectrum of the chromatogram before the injection. At 3.5 minutes, Cy-C peaks were apparent within the spectrum. Spectrum (B) is an averaged spectrum of the chromatogram from 7 minutes and on with the spectrum (A) subtracted out as background.

Cyt-C detection with MD-nano-ESI was successful and was much more consistent than the previous acellular Matrigel experiments. This may have occurred due

to a remodeling of the matrix by the cells. The MD unit's effectiveness to clean samples prior to nano-ESI proved to allow the detection of Cyt-C from within a live cell culture.

3.6. Discussions

A model injury was developed by injecting a finite amount of volume into a porous matrix. With these experiments the probe's capabilities to decipher information about different concentrations and probe placements were observed by studying the MS chromatograms and spectra. A simple theoretical model based on the diffusion equation with a bulk flow was developed to understand the effects of diffusion and advection in the transport of Cyt-C through the cell culture model. In order to understand whether the simplifications made in the model were valid experimentally, planar cell culture models were developed and a dye was injected into the porous matrix. The dye was observed under a microscope and irregularities such as air bubbles and non uniform transport of dye downstream were observed. These deviations demonstrated that the transport of dye in the model cell culture was not as simple as predicted by the model. A model that could take into account factors such as air bubbles, porous matrix heterogeneity, and other irregularities would be able to better predict the transport of Cyt-C through porous matrix.

Even though the Cyt-C transport through the matrix does not perform exactly like the model predicted, the agarose sampling experiments demonstrated that differences between probe placements can be detected through MS analysis. With a higher Cyt-C concentration, both adjacent and offset samplings were able to detect Cyt-C in the MS. The lapse in time between the marker injection and its detection with the MS was quicker experimentally than what was predicted theoretically. This discrepancy could be accounted for by the observations made with the dye experiments. Lower concentrations of Cyt-C were detected with the adjacent probe placement, but the offset placement showed no detection by the MS. This result agreed with the theoretical results.

Concentration information could not be inferred from the peak intensities from spectra. This is due to the lack of sample to sample repeatability which causes differences in nano-ESI efficiency. To accurately measure concentration an internal MS standard for Cyt-C would have to be used in order to obtain accurate concentration information.

The probes ability to sample and detect Cyt-C from more biologically complex samples was demonstrated by the Matrigel injury model experiments. Cyt-C was successfully detected, but maintaining constant signal, eliminating background signal, and eliminating analyte suppression effects was difficult to accomplish with the current MD-nano-ESI device. Increasing the performance of the MD unit by increasing the length, using different dialysis membranes, or even multiple in-line MD units with different molecular weight cut offs could improve the performance of the system. The highly complex composition of the Matrigel matrix which includes, laminin, collagen IV, and entactin, and the addition of growth factors all lead to the increase in ion suppression and background peaks. Cells were successfully cultured and sampled with the probe with no adverse effects to the cells. Sampling with in-line MD-nano-ESI MS demonstrated that the system was capable of detecting a marker from a cell culture. In addition the experiments demonstrated a cleaner spectrum was capable of being obtaining from the cell culture when compared to the acellular Matrigel experiments. This may have been due to the cells remodeling the matrix, and the Matrigel used in the cell cultures was half as dense as the one used in the acellular experiments. The results in the last experiment, gives promise to future experiments of monitoring actual biological processes within cell cultures.

CHAPTER 4

CONCLUSIONS AND RECOMMENDATIONS

4.1. Conclusions

The MS sampling probe that was developed and analyzed in this thesis demonstrated its ability to detect small concentrations of biological markers within cell culture matrix with little sample preparation. By incorporating the method of in-line MD, analyte that was previously undetectable with MS analysis, due to the nature of cell culture media and matrix, can now be detected with nano-ESI MS with no other manipulation. When incorporated in-line with a sampling probe, the system was capable of being incorporated into cell culture matrix and detected small volume injections of a marker analyte. In addition experiments demonstrated that through sampling from closer to the source of a marker improved temporal resolution and sensitivity are achieved.

Various MD unit designs were studied for their effectiveness in reducing the salt content in samples. An effective fiber length was determined to be 3.5cm, which provided a good compromise between salt removal capability and impact on response time. At this length the MD unit provided over an order of magnitude reduction in sample salt content while increasing response time by mere seconds. The theory governing the mass transfer of salts out of samples and into the dialysis buffer accurately predicts the MD unit's performance. In accordance with the experimental results, the theoretical model showed that MD fiber length was the variable which allowed for the most improvement in the MD unit's performance. Experimentally, varying sample flow rate showed inconsistent results and the buffer flow rate, in agreement with the theoretical analysis, had no effect on MD unit performance. It was ultimately beneficial that flow rate had little effect on MD performance since nano-ESI ionization performance is heavily affected by sample flow rate.

Samples with Cyt-C in high salt solutions and cell culture media were analyzed via MS using in-line MD-nano-ESI. The MD step allowed for the detection of Cyt-C using nano-ESI. Previous experiments with no MD step demonstrated that Cyt-C was either masked by the high salt solutions or the solutions repeatedly created clogs at the emitter tip. The in-line MD step allowed for the continuous analysis of samples from within cell culture media, maintain a clog free emitter for an indefinite amount of time with a steady signal. It was also determined that a low pressure cross flow of nebulizer gas across the emitter tip increased peak intensity, removed background noise spectra, and stabilized MS signal. It is believed that the nebulizer gas improved droplet desolvation at the tip of the nano-ESI emitter, which provided increased ionization efficiency.

A set of experimental variables were determined for in-line MD-nano-ESI analysis of biomolecules in cell culture media. The counter-flow dialysis buffer was determined to be 1% acetic acid at a flow rate of 150 µL/min, and a sample flow rate of 30 µL/hr provided stable nano-ESI spray MS analysis. A nano-ESI MS emitter with a 75 µm ID and 15 µm tip ID was determined to provide consistent results, and the larger tip ID minimized clogging while maintaining the benefits of working in the nano-ESI regime. Table 4.1 summarizes the design parameters for MD nano-ESI.

Table 4.1. Final design parameters for MD-nano-ESI MS.

Design Parameters	
MD Fiber Length	3.5 cm
Dialysis Buffer	1% Acetic Acid
Dialysis Buffer Flow Rate	150 µL/min
Emitter	360 µm OD, 75 µm ID, 15 µm Tip ID

The MD-nano-ESI device was stationed in front of the MS, so that the emitter tip was within 1mm of the MS capillary cathode. The MS was set to positive ion mode and the appropriate MS settings are summarized in Table 4.1.

Table 4.2. Final experimental MS settings.

MS Settings	
End Plate Offset	0V
Capillary	-1300 V
Nebulizer	0.2 bar
Dry Gas	1.5 l/min
Dry Temp	160° C
Capillary Exit	300 V
Skimmer 1	50.0 V
Hexapole 1	23.0 V
Hexapole RF	600.0 Vpp
Skimmer 2	23.0 V
Lens 1 Transfer	113.0 µs
Lens 1 Pre Puls Storage	2.0 µs

The goal of the research was to develop a probe that could be imbedded into cell cultures and actively monitor changes in chemical biomarker levels over time, and examine spatial concentration gradients. The problem of analyzing biological samples with little manipulation was solved by incorporating the MD unit in-line with nano-ESI. The probe's capability to sample and analyze biomolecules from within porous cell culture matrix was examined by the use of model cell cultures and creating a model injury.

First, samples were examined in a 0.6% agarose matrix, which replicated physical properties of porosity and tortuosity of the brain. Small volume injections of Cyt-C were introduced into the system to recreate a localized release of a marker in a cell culture. Sampling probes were placed either adjacent or downstream to the injection capillary. The experimental results showed that sampling and analyzing using MD-nano-ESI from a probe imbedded within cell culture matrix was possible. In addition, noticeable

differences were observed when different concentrations and probe placements were examined.

Similar results were obtained with the adjacent probe injury model at the two different Cyt-C concentrations. For both the 30 μM and 5μM injections, a delay of less than 30 seconds was encountered post injection. Most of this delay can be accounted for by the volume of the probe and MD-nano-ESI system. When the sampling probe was placed downstream by 1.4mm the experiment with the 30 μM Cyt-C injection showed a delay of 72 seconds before the first signs of Cyt-C was detected by the mass spec. With the 5 μM Cyt-C injection at the same offset probe position, the mass spec was not able to detect any Cyt-C.

A theoretical model describing the effects of transient diffusion and advection of small molecules injected into a porous media was developed. The results of the model are in agreement with the experimental results of the adjacent probe placement. For the offset probe experiment of the 30 μM sample, experimental results showed detection quicker than the theoretical results predicted. Dye injection experiments had demonstrated that the transport of molecules through the porous media does not exactly follow the theoretical results. Factors such as air bubbles and non-homogeneous transport through the porous media were not taken into account in the model. Though it can be concluded that the model is too simple to accurately predict the transport of Cyt-C through porous media, it can provide useful insight. The theoretical model did accurately predict that the 5 μM Cyt-C injection would not be detectable by the mass spec at any time point. The maximum concentration with the probe at 1.4mm downstream was still too low for the mass spec to detect at the given sampling conditions. The theoretical analysis provided a basic understanding of the transport of Cyt-C through a porous matrix but a more involved model is necessary in order to predict the transport of molecules in the cell culture model with better detail and accuracy.

In addition to using agarose, a more biologically relevant and complex matrix of Matrigel was plated into the chamber and Cyt-C was injected and sampled. Matrigel has similar properties of porosity and tortuosity as agarose, but it also includes biological extracellular components such as laminin, collagen, and entactin. In addition, it also contains growth factors to promote cell growth in a 3-D culture. The sampling probe was placed adjacent to the injection capillary, and analyzed using MD-nano-ESI MS. Cyt-C was successfully detected by the MS. Although Cyt-C was detected, it was much more difficult to maintain a steady MS signal and there was more background noise and signal masking when sampling from Matrigel.

Mixed 3-D neural cell cultures were plated in the chambers with the sampling probe. Cell cultures were examined to determine whether the probe or sampling from the probe caused any adverse effects to the cells. For both cultures that were sampled and not sampled from, there was no significant difference from control chambers which contained no probe and had undergone no perfusion. In addition it was shown that coupling in-line MD-nano-ESI MS allowed the detection of Cyt-C from within mixed 3-D neural cultures.

Ultimately the results reported in this thesis shows promise for further developing and optimizing the sampling probe for in-line MD-nano-ESI MS analysis of cell cultures. As samples progressively became more complex, the analysis became increasingly more difficult. Emitter clogging, inconsistent signal, analyte masking, and background noise typically plagued the analysis of biological samples, but with the incorporation of a single in-line MD step, analysis could effectively be conducted from within cell culture matrix. This system will allow researchers to actively monitor neural cell cultures during normal physiological activities and monitor changes during injury experiments. The probes ability to be placed in various positions in a chamber, allows for localized TBI studies to be conducted and monitor the spatial effects which occur in a culture over time. In-line

MD-nano-ESI MS has the potential to offer researchers unique insights into the complex biological processes which occur during TBI.

4.2. Recommendations for Future Work

This research has shown the method of MD-nano-ESI MS's effectiveness to sample proteins within a cell culture matrix. The experiments highlighted above were simplified with respect to sampling from live cell cultures. The future of this method is dependent on being able to manipulate samples directly from in-vitro neuronal cultures with no off-line sample manipulation.

First to accurately predict the transport of a marker through the porous space of a cell culture an improved model should be developed. A model that takes into account the heterogeneity of porous media and a non uniform flow rate would allow for a more accurate transport prediction. Also, factors such as air bubbles and actual cells should be accounted for in the model. Disregarding wall effects or capillary effects cannot be done in this new model. This would allow researchers to accurately predict what concentration can be expected to be sampled at the probe.

Experiments also demonstrated that deciphering accurate information regarding Cyt-C concentration was not achievable in the current experimental protocol. It is necessary to incorporate an internal standard to the experiments. A standard at a given concentration with similar ionization characteristics to the marker should be introduced into the sample prior to ionization. This could be done with an in-line introduction of the standard right before the MD step. For equine heart Cyt-C, researchers have used bovine heart Cyt-C as an internal standard. This would provide accurate information regarding marker concentration.

One variable that could easily be manipulated is the MD unit. Various methods could be explored to increase the efficiency of salt removal, such as increasing the length

of the MD unit, and using different fiber materials to reduce the membrane resistance to mass transfer. Other forms of salt removal can be used such as an ultrarapid desalting method using a microchannel laminar flow device [56]. This device does not employ a dialysis membrane, but instead uses a two-layered laminar flow geometry that depends on the differential diffusion of macromolecular analytes and low molecular weight contaminants. In addition to a single MD unit, another MD unit incorporated in-line with a different molecular weight cut off fiber could be used to further separate macromolecules before analysis with the MS.

Moving away from the multiple parts and components of the current MD unit, a single capillary could be used as the probe, microdialysis fiber and emitter. Hydrofluoric acid can be used to etch pores in the silica capillary [57] for the MD unit, and a silica capillary puller can be used to pull the emitter tip. This would allow for easier and quicker fabrication, and this would lower the total volume of the system and provide a quicker signal response with the MS. Another form of improving fabrication would be the miniaturization of the probe into a microfabricated unit. Using these manufacturing techniques would also increase repeatability between devices and would reduce experimental variability.

The use of tandem MS (MSMS) would allow for further sample manipulation and analysis. The use of a quadrapole MS in-line with a TOF (Q-TOF) would allow researchers to filter out unwanted ions in the first MS step and analyze the rest of the ions in the second MS. Samples could undergo a fractionalization after the first MS, and the detected peaks in the second MS could be put through MS data base and software can search for potential proteins. This would be similar to proteomic work but with less sample prep work.

Once an optimized in-line sample manipulation device is created further in vitro TBI experiments should be conducted. Studies should be conducted with the probe inserted into the culture so that continuous sampling can be conducted. A panel of

potential markers, similar to the ones discussed in Chapter 1, can be monitored with MSMS. Changes in these markers concentrations can be actively monitored from before injury and at specific times post injury. These recommendations should provide a direction for future research to improve the capabilities of the MD-nano-ESI device and create a better understanding of TBI.

APPENDIX A

CYLINDRICAL MODEL INJURY CHAMBER ASSEMBLY PROTOCOL

Machining

1. Use a rod of extruded polycarbonate with and 1/8” ID and 3/8” OD.
2. Cut extruded polycarbonate to a length of 1 cm.
3. Remove any burr left on the edges of the cylinder.
4. Drill two holes with 300μm diameters through the side of the cylinder.
5. Remove burr from holes.
6. Remove chips with compressed air and DI water.
7. Dry the chambers by placing them in a 50°-70° oven for 10 minutes.

Figure A.1(A&B) show the hole configuration for aligned and offset configurations.

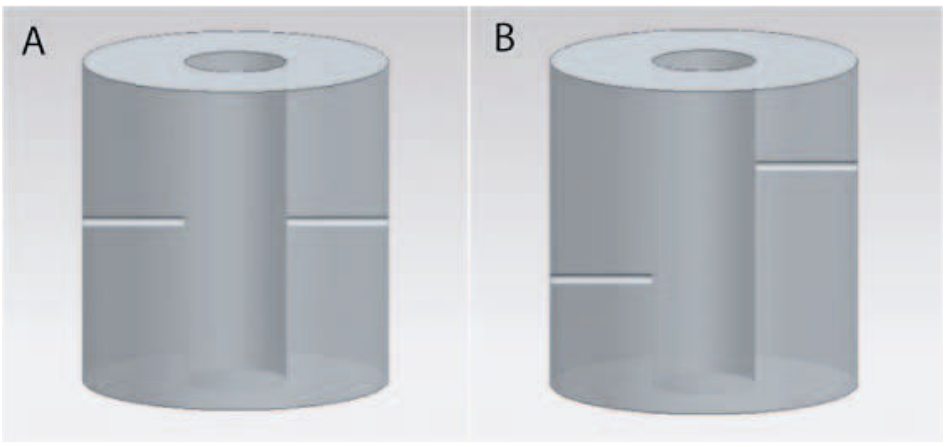

Figure A.1. (A) Aligned hole configuration. (B) Offset hole Configuration

Attaching NanoPorts

1. Apply Quick Set (JB Weld, Sulphur Springs, TX) to the rim of a 10-32 Flat-Bottom NanoPort (Upchrch Scientific, Oak Harbour, WA)
2. Attach the NanoPort to the top of the cylinder (Figure A.2)

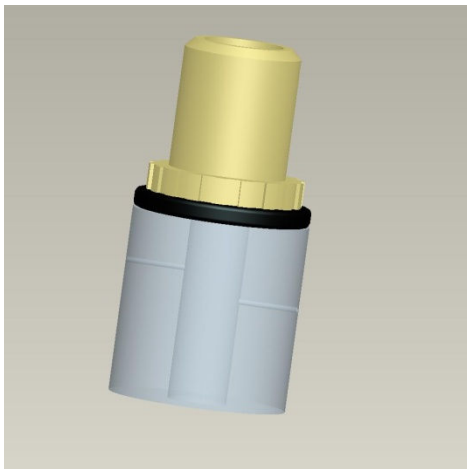

Figure A.2. NanoPort attached to the top of a cylinder using Quick Set

3. Repeat step 1 and attach the other NanoPort to the bottom of the cylinder (Figure A.3)

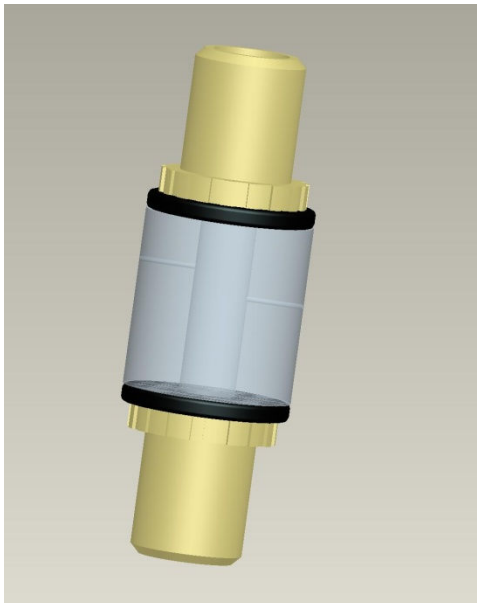

Figure A.3. Cylinder with two NanoPorts attached to the top and bottom of the cylinder

Adding Capillaries

1. Cut 150 μm OD 50 μm ID silica capillary using diamond tip pen to a length of 10 cm.
2. Add small dab of Quick Set to end of capillary just below the end of the silica capillary (Figure A.4).

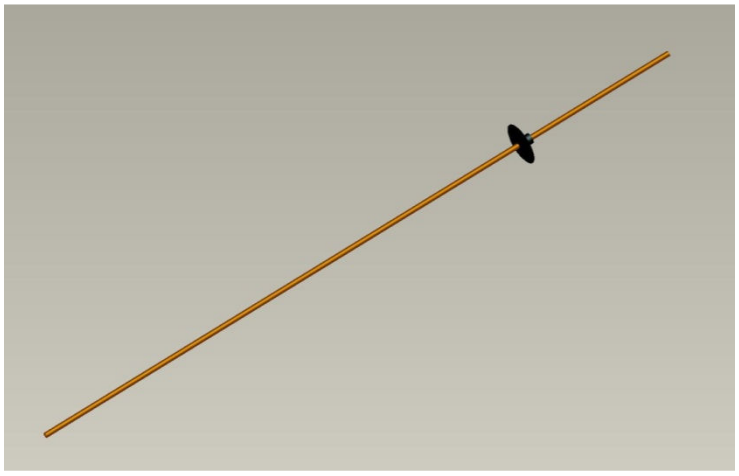

Figure A.4. Small dab of Quick set at the tip of a silica capillary

3. Insert capillary into chamber until capillary end is at the midpoint of the chamber (Figure A.5).

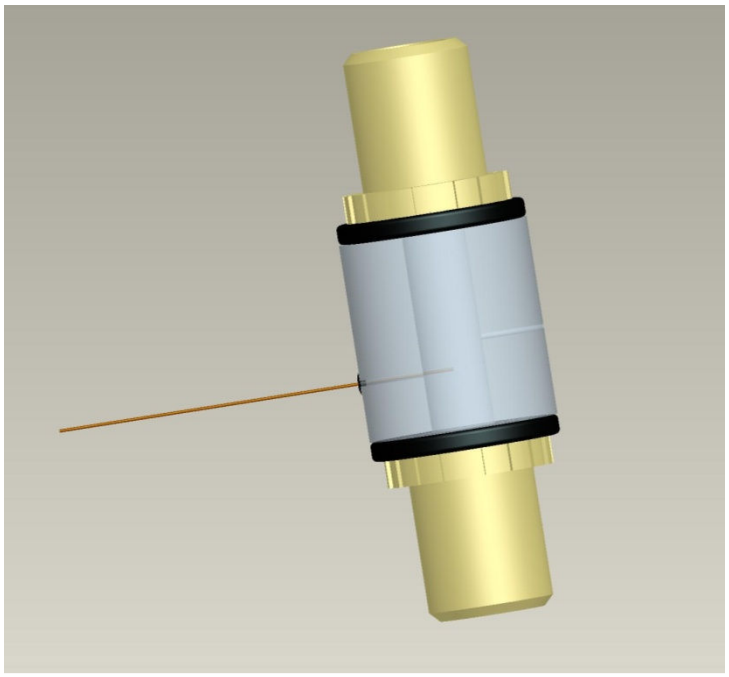

Figure A.5. Inserted silica capillary affixed with Quick Set

4. Repeat steps 1-3 and attach the silica capillary to the other drilled hole (Figure A.6)

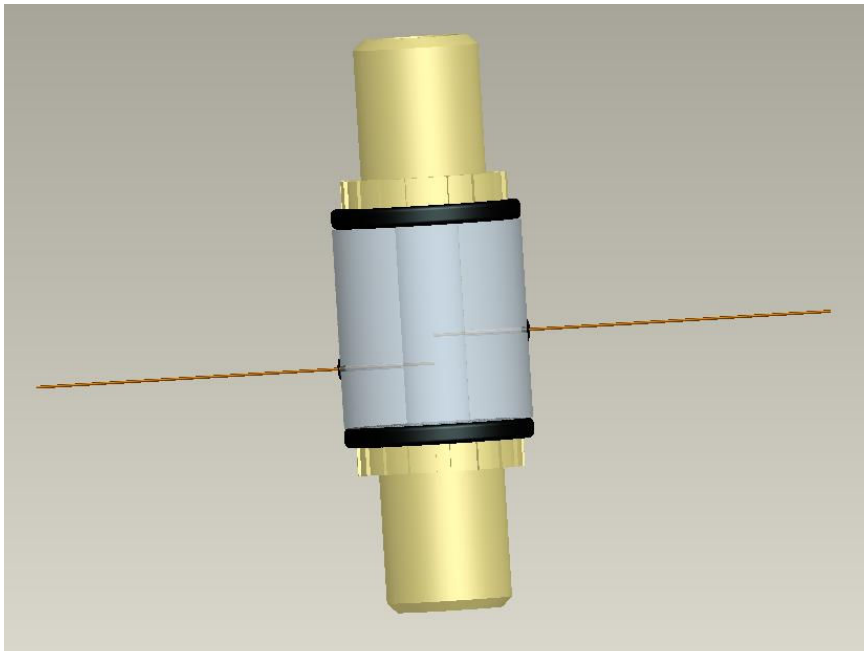

Figure A.6. Assembly with both capillaries affixed with Quick Set.

5. Allow Quick Set to cure for 30 minutes.

6. Plug one of the NanoPorts and attach a syringe pump with DI water and check for leaks.

APPENDIX B

PLANAR MODEL INJURY CHAMBER ASSEMBLY PROTOCOL

Machining:

8. Use clear polycarbonate
9. Machine the bottom of the planar chamber according to Figure B.1.

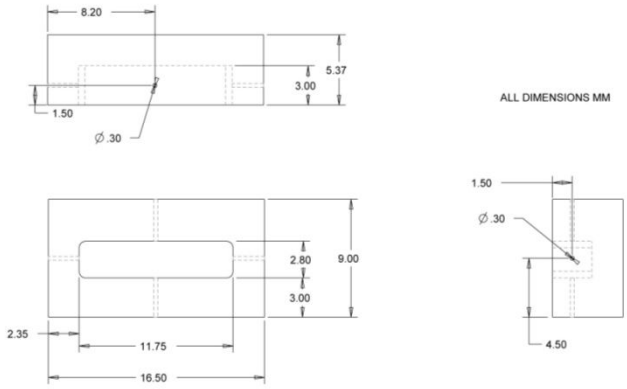

Figure B.1. Dimensions for the bottom of the chamber

10. Machine the top of the planar chamber according to Figure B.2

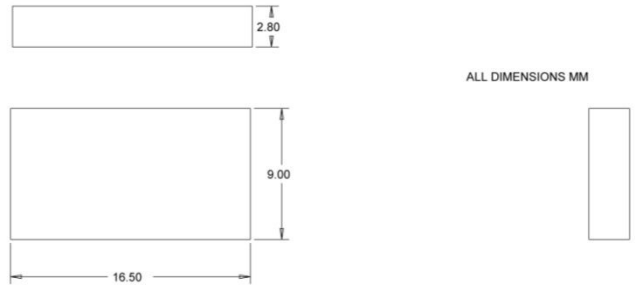

Figure B.2. Dimensions for the top of the chamber

11. Remove any burr left on the edges after machining.

12. Remove chips with compressed air and DI water.

13. Dry the chambers by placing them in a 50°-70° oven for 10 minutes.

Chamber Assembly

4. Apply a thin layer of SYLGARD 186 silicone elastomer (Dow Corning, Midland, MI) to the highlighted surface in Figure B.3.

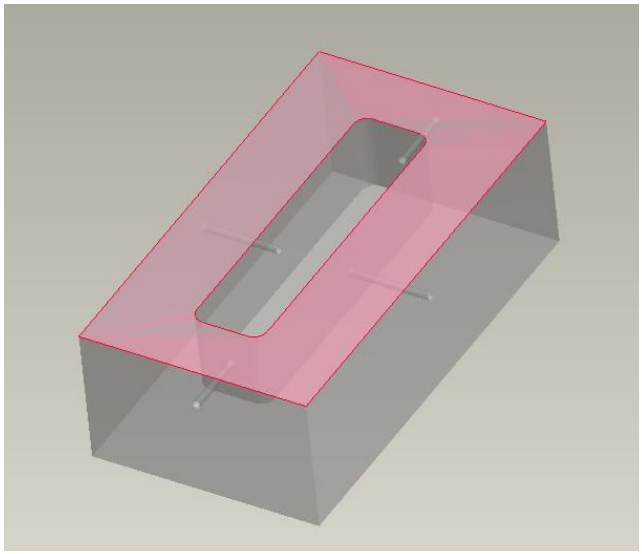

Figure B.3. Highlighted surface of the bottom part to apply thin layer of SYLGARD 186.

5. Align top of chamber with the bottom part and press together Figure B.4.

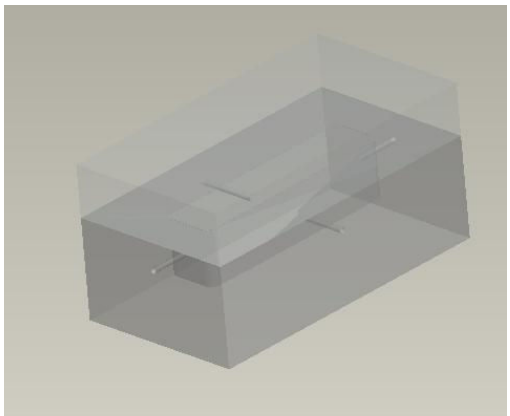

Figure B.4. Top and bottom assembly with all four sides aligned and pressed together.

6. Clamp top and bottom assembly together with a binder clip and place into a 70°C oven for 10 minutes.
7. Add a 10-32 Flat-Bottom NanoPort to the top of the assembly with Quick Set (Figure B.5).

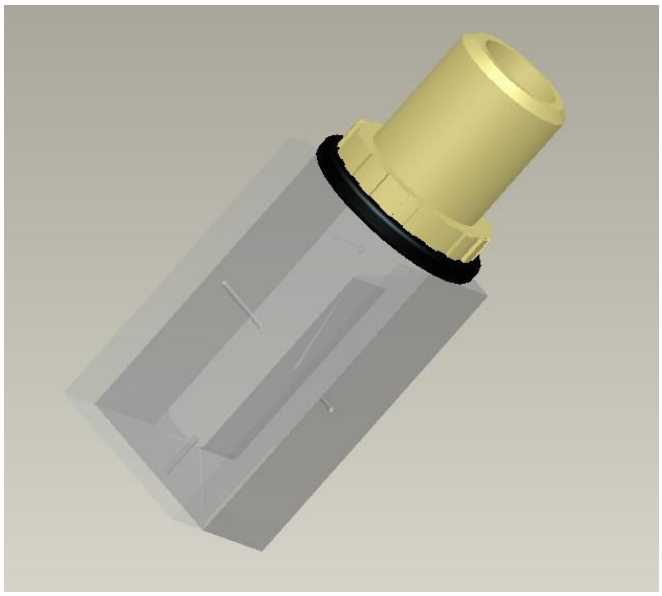

Figure B.5. Nanoport affixed to the top of the chamber with Quick Set.

8. Cut 150 µm OD 50 µm ID silica capillary using diamond tip pen to a length of 10 cm (2x).
9. Apply Quick Set to each capillary just below the end Figure A.4 and insert each 10cm capillary into a side hole (Figure B.6)

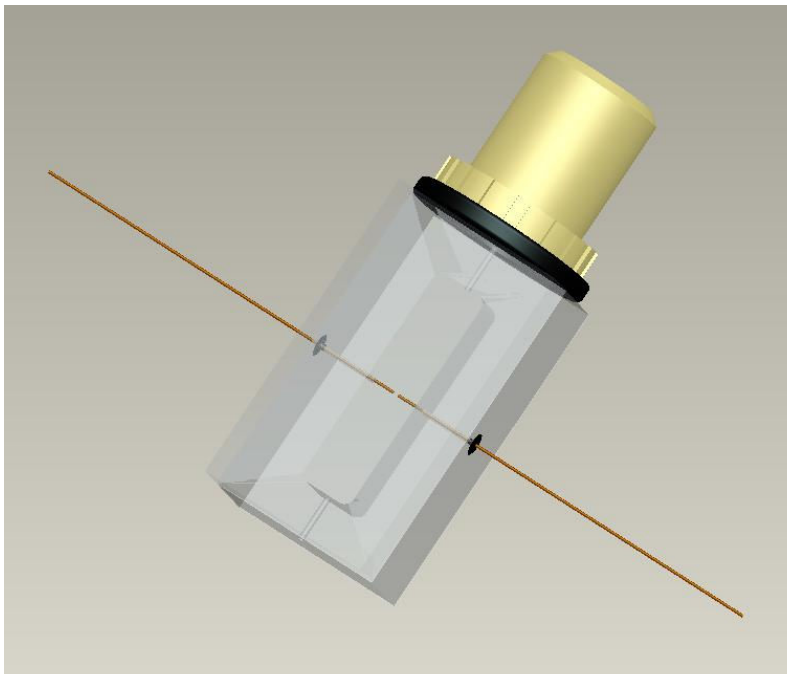

Figure B.6. Assembly with silica capillaries inserted into the sides.

10. Cut 150 µm OD 50 µm ID silica capillary using diamond tip pen to a length of 5 cm and insert into the bottom hole (Figure B.7).

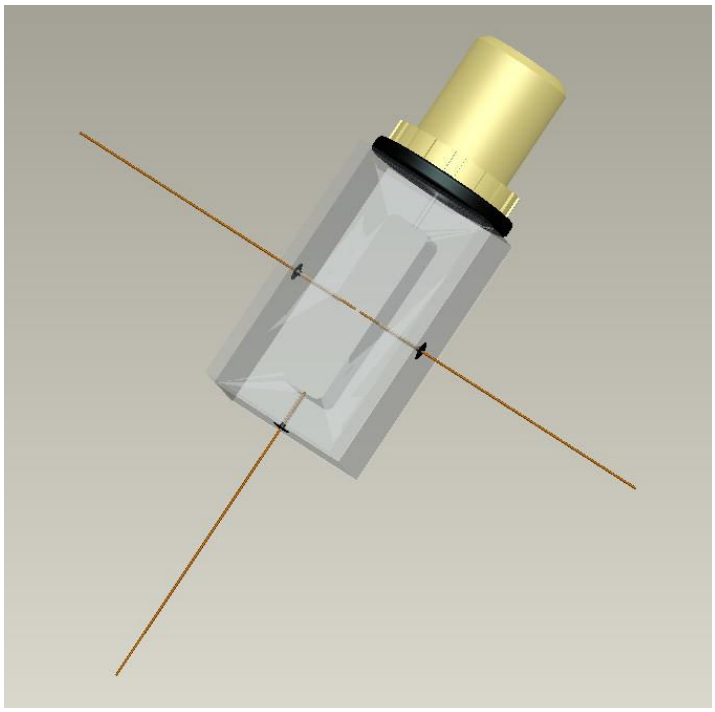

Figure B.7. Inserted silica capillary affixed with Quick Set into the bottom hole.

REFERENCES

[1] S. I. Svetlov, *et al.*, "Biomarkers of Blast-Induced Neurotrauma: Profiling Molecular and Cellular Mechanisms of Blast Brain Injury," *Journal of Neurotrauma,* vol. 26, pp. 913-921, 2009.

[2] A. J. Atkinson, *et al.*, "Biomarkers and surrogate endpoints: Preferred definitions and conceptual framework*," *Clin Pharmacol Ther,* vol. 69, pp. 89-95, 2001.

[3] M. Faul, *et al.*, "Tramatic Brain Injury in the United States: Emergency Department Visits, Hospitalizations and Death 2002-2006," W. L Xu, Ed., ed. Atlanta (GA): Centers for Disease Control and Prevention, National Center for Injury Prevention and Control, 2010.

[4] K. E. Saatman, *et al.*, "Classification of Traumatic Brain Injury for Targeted Therapies," *Journal of Neurotrauma,* vol. 25, pp. 719-738, 2008.

[5] M. Balestreri, *et al.*, "Predictive value of Glasgow coma scale after brain trauma: change in trend over the past ten years," *Journal of Neurology, Neurosurgery & Psychiatry,* vol. 75, pp. 161-162, January 1, 2004 2004.

[6] E. Kövesdi, *et al.*, "Update on protein biomarkers in traumatic brain injury with emphasis on clinical use in adults and pediatrics," *Acta Neurochirurgica,* vol. 152, pp. 1-17, 2010.

[7] T. A. G. M. Huisman, *et al.*, "Diffusion-Weighted Imaging for the Evaluation of Diffuse Axonal Injury in Closed Head Injury," *Journal of Computer Assisted Tomography,* vol. 27, pp. 5-11, 2003.

[8] NINDS, "Traumatic Brain Injury: Hope Through Research," N. I. o. Health, Ed., ed. Bethesda: NIH, 2002.

[9] M. F. Stiefel, *et al.*, "Reduced mortality rate in patients with severe traumatic brain injury treated with brain tissue oxygen monitoring," *Journal of Neurosurgery,* vol. 103, pp. 805-811, 2005.

[10] J. Beaudeux, *et al.*, "Pathyophysiologic aspects of S-100beta protein: a new biological marker of brain pathology," *Ann Biol Clin,* vol. 57, pp. 261-272, 1999.

[11] F. Michetti and D. Gazzolo, "S100B Protein in Biological Fluids: A Tool for Perinatal Medicine," *Clin Chem,* vol. 48, pp. 2097-2104, December 1, 2002 2002.

[12] H. Haimoto, *et al.*, "Differential distribution of immunoreactive S100-alpha and S100-beta proteins nonnervous human tissue," *Lab Invest.,* vol. 57, pp. 489-98, 1987.

[13] A. Leviton and O. Dammann, "Brain damage markers in children. Neurobiological and clinical aspects," *Acta Pædiatrica,* vol. 91, pp. 9-13, 2002.

[14] P. Johnsson, *et al.*, "Neuron-specific enolase increases in plasma during and immediately after extracorporeal circulation," *Ann Thorac Surg,* vol. 69, pp. 750-754, March 1, 2000 2000.

[15] R. P. Berger, *et al.*, "Identification of Inflicted Traumatic Brain Injury in Well-Appearing Infants Using Serum and Cerebrospinal Markers: A Possible Screening Tool," *Pediatrics,* vol. 117, pp. 325-332, February 1, 2006 2006.
[16] R. P. Berger, *et al.*, "Serum Biomarker Concentrations and Outcome after Pediatric Traumatic Brain Injury," *Journal of Neurotrauma,* vol. 24, pp. 1793-1801, 2007.
[17] U. Missler, *et al.*, "Measurement of Glial Fibrillary Acidic Protein in Human Blood: Analytical Method and Preliminary Clinical Results," *Clin Chem,* vol. 45, pp. 138-141, January 1, 1999 1999.
[18] D. C. Rueger, *et al.*, "Purification of a brain-specific astroglial protein by immunoaffinity chromatography," *Analytical biochemistry,* vol. 89, pp. 360-71, 1978.
[19] L. E. Pelinka, *et al.*, "GFAP Versus S100B in Serum after Traumatic Brain Injury: Relationship to Brain Damage and Outcome," *Journal of Neurotrauma,* vol. 21, pp. 1553-1561, 2004.
[20] S.-M. Lucas, *et al.*, "The role of inflammation in CNS injury and disease," *British Journal of Pharmacology,* vol. 147, pp. S232-S240, 2006.
[21] S. R. Goodman, *et al.*, "Brain spectrin: Of mice and men," *Brain Research Bulletin,* vol. 36, pp. 593-606, 1995.
[22] T. Hayakata, *et al.*, "Changes in Csf S100b and Cytokine Concentrations in Early-Phase Severe Traumatic Brain Injury," *Shock,* vol. 22, pp. 102-107, 2004.
[23] A. K. Ottens, *et al.*, "Neuroproteomics in neurotrauma," *Mass Spectrometry Reviews,* vol. 25, pp. 380-408, 2006.
[24] T. Watson and D. Sparkman, *Introduction to Mass Spectrometry, 4th Edition: Instrumentation, Applications, and Strategies for Data Interpretation*: John Wiley & Sons, Ltd, 2007.
[25] J. F. d. l. Mora, *et al.*, "Electrochemical processes in electrospray ionization mass spectrometry," *Journal of Mass Spectrometry,* vol. 35, pp. 939-952, 2000.
[26] M. Wilm and M. Mann, "Analytical Properties of the Nanoelectrospray Ion Source," *Analytical Chemistry,* vol. 68, pp. 1-8, 1996.
[27] M. Dole, *et al.*, "Molecular Beams of Macroions," *The Journal of Chemical Physics,* vol. 49, pp. 2240-2249, 1968.
[28] L. L. Mack, *et al.*, "Molecular Beams of Macroions. II," *The Journal of Chemical Physics,* vol. 52, pp. 4977-4986, 1970.
[29] J. V. Iribarne and B. A. Thomson, "On the evaporation of small ions from charged droplets," *The Journal of Chemical Physics,* vol. 64, pp. 2287-2294, 1976.
[30] B. A. Thomson and J. V. Iribarne, "Field induced ion evaporation from liquid surfaces at atmospheric pressure," *The Journal of Chemical Physics,* vol. 71, pp. 4451-4463, 1979.
[31] R. B. Cole, "Some tenets pertaining to electrospray ionization mass spectrometry," *Journal of Mass Spectrometry,* vol. 35, pp. 763-772, 2000.
[32] J. B. Fenn, *et al.*, "Electrospray Ion Formation: Desorption Versus Desertion," in *Biochemical and Biotechnological Applications of Electrospray Ionization Mass Spectrometry*. vol. 619, ed: American Chemical Society, 1996, pp. 60-80.

[33] J. B. Fenn, "Ion formation from charged droplets: roles of geometry, energy, and time," *Journal of the American Society for Mass Spectrometry,* vol. 4, pp. 524-535, 1993.
[34] J. Fernandez de la Mora, "Electrospray ionization of large multiply charged species proceeds via Dole's charged residue mechanism," *Analytica Chimica Acta,* vol. 406, pp. 93-104, 2000.
[35] J. W. Fawcett*, et al.*, "Dopaminergic neuronal survival and the effects of bFGF in explant, three dimensional and monolayer cultures of embryonic rat ventral mesencephalon," *Experimental Brain Research,* vol. 106, pp. 275-282, 1995.
[36] M. Tsacopoulos and P. Magistretti, "Metabolic coupling between glia and neurons," *J Neurosci,* vol. 16, pp. 877-885, 1996.
[37] M. Tsacopoulos, "Metabolic signaling between neurons and glial cells: a short review," *Journal of Physiology-Paris,* vol. 96, pp. 283-288.
[38] J. A. Jakubowski*, et al.*, "Online microdialysis-dynamic nanoelectrospray ionization-mass spectrometry for monitoring neuropeptide secretion," *Journal of Mass Spectrometry,* vol. 40, pp. 924-931, 2005.
[39] A. Peyrl*, et al.*, "Proteomic characterization of the human cortical neuronal cell line HCN-2," *Journal of Chemical Neuroanatomy,* vol. 26, pp. 171-178, 2003.
[40] L. Jiang*, et al.*, "Comparison of protein precipitation methods for sample preparation prior to proteomic analysis," *Journal of Chromatography A,* vol. 1023, pp. 317-320, 2004.
[41] M. Gilar*, et al.*, "Advances in sample preparation in electromigration, chromatographic and mass spectrometric separation methods," *Journal of Chromatography A,* vol. 909, pp. 111-135, 2001.
[42] F. Incopera*, et al.*, *Foundamentals of Heat and Mass Transfer 6th ed.*: John Wiley & Sons, Inc., 2007.
[43] S. Tong and F. Yuan, "An equivalent length model of microdialysis sampling," *Journal of Pharmaceutical and Biomedical Analysis,* vol. 28, pp. 269-278, 2002.
[44] A. N. Campbell and B. G. Oliver, "Diffusion coefficients of sodium and lithium chlorates in water, at 25°," *Canadian Journal of Chemistry,* vol. 47, pp. 2681-2685, 1969.
[45] I. Marginean*, et al.*, "Electrospray Characteristic Curves: In Pursuit of Improved Performance in the Nanoflow Regime," *Analytical Chemistry,* vol. 79, pp. 8030-8036, 2007.
[46] C. J. Ma*, et al.*, "meso-Dihydroguaiaretic acid attenuates the neurotoxic effect of staurosporine in primary rat cortical cultures," *Neuropharmacology,* vol. 50, pp. 733-740, 2006.
[47] B. Ahlemeyer*, et al.*, "Release of cytochrome c into the extracellular space contributes to neuronal apoptosis induced by staurosporine," *Brain Research,* vol. 934, pp. 107-116, 2002.
[48] Z.-J. Chen*, et al.*, "Intraparenchymal drug delivery via positive-pressure infusion: experimental and modeling studies of poroelasticity in brain phantom gels," *IEEE Transactions on Biomedical Engineering,* vol. 49, pp. 923-929, 2002.
[49] Z.-J. Chen*, et al.*, "A realistic brain tissue phantom for intraparenchymal infusion studies," *Journal of Neurosurgery,* vol. 101, pp. 314-322, 2004.

[50] C. Nicholson and J. M. Phillips, "Ion diffusion modified by tortuosity and volume fraction in the extracellular microenvironment of the rat cerebellum," *The Journal of Physiology,* vol. 321, pp. 225-257, December 1, 1981 1981.
[51] C. Nicholson, "Diffusion from an injected volume of a substance in brain tissue with arbitrary volume fraction and tortuosity," *Brain Research,* vol. 333, pp. 325-329, 1985.
[52] S. Socolofsky and G. Jirka. (2005). *CVEN 489-501: Special Topics in Mixing and Transport Processes in the Environment 5th Edition*.
[53] A.-K. Kontturi*, et al.*, "The Effective Charge Number and Diffusion Coefficient of Catioinic Cytochrome c in Aqueous Solution," *Acta Chemica Scandinavica,* vol. 46, pp. 348-353, 1992.
[54] W. Y. Gu*, et al.*, "New insight into deformation-dependent hydraulic permeability of gels and cartilage, and dynamic behavior of agarose gels in confined compression," *Journal of biomechanics,* vol. 36, pp. 593-598, 2003.
[55] C. Nicholson and E. Syková, "Extracellular space structure revealed by diffusion analysis," *Trends in Neurosciences,* vol. 21, pp. 207-215, 1998.
[56] WILSON*, et al.*, *Ultrarapid desalting of protein solutions for electrospray mass spectrometry in a microchannel laminar flow device* vol. 77. Washington, DC, ETATS-UNIS: American Chemical Society, 2005.
[57] Wei and E. S. Yeung, "On-Line Concentration of Proteins and Peptides in Capillary Zone Electrophoresis with an Etched Porous Joint," *Analytical Chemistry,* vol. 74, pp. 3899-3905, 2002.